

NONLINEAR VIBRATIONS OF STRAIGHT AND BUCKLED
BEAMS UNDER HARMONIC EXCITATION

by

Wu-Yang Tseng

B.S. National Taiwan University 1963

M.S. Virginia Polytechnic Institute 1965

SUBMITTED IN PARTIAL FULFILLMENT
OF THE REQUIREMENTS FOR THE DEGREE

OF

Doctor of Philosophy

at the

Massachusetts Institute of Technology

February, 1970

Signature of Author _____

Dept. of Aeronautics and Astronautics,
November 10, 1969

Certified by _____

Thesis Supervisor

Chairman, Departmental Committee of Graduate Students

Archives



thesis
Aero
1975
Ph.D.

ACKNOWLEDGEMENTS

The author wishes to express his appreciation to Professor John Dugundji for his invaluable guidance as thesis advisor, and to Professors Theodore H.H. Pian and Emmett A. Witmer for their aid and criticism throughout the theoretical development. Thanks are also due to Mr. Oscar Wallin for the design of the testing apparatus, and to Mr. Allan R. Shaw and Mr. Fred Merlis for the installation of the instrumentation.

This work was sponsored by the United States Air Force of Scientific Research under Contract No. F44620-69-C-0091, administered by Dr. Jacob Pomerantz.

ABSTRACT

A straight and a buckled beam with fixed ends, excited by the periodic motion of their supporting base in a direction normal to the beam span, were investigated analytically and experimentally.

For the straight beam case, by using Galerkin's method (one mode approximation) the governing partial differential equation reduces to the well known Duffing equation. The harmonic balance method is applied to solve the Duffing equation. Besides the solution of simple harmonic motion (SHM), many other branch solutions, involving superharmonic motion (SPHM) and subharmonic motion (SBHM), are found analytically and experimentally. The stability problem is analyzed by solving a corresponding variational Hill-type equation.

For the buckled beam case, using similar procedures as the straight beam case, the resulting equation becomes a modified Duffing equation. Solution for SHM, SPHM are again found analytically and experimentally. The importance of the second mode on these results is examined by a stability analysis. The Runge-Kutta numerical integration method is used to investigate the snap-through problem.

The results of the present analysis agree well with the experiments.

TABLE OF CONTENTS

<u>Section</u>		<u>Page</u>
1	INTRODUCTION	1
2	NONLINEAR VIBRATION OF A STRAIGHT BEAM	4
	2.1 Formulation and General Solution	4
	2.2 Specific Cases	10
	2.3 Exact Solution of Free Vibration	19
3	NONLINEAR VIBRATION OF A BUCKLED BEAM	21
	3.1 Formulation and General Solution	21
	3.2 Specific Cases	28
	3.3 Exact Solution of Free Vibration	34
	3.4 Numerical Analysis of Steady State Solutions	35
4	STABILITY CONDITION OF THE PERIODIC SOLUTIONS	36
	4.1 Stability Condition of the Periodic Solutions	36
	4.2 Stability Analysis of the Second Mode Solution	39
5	SNAP-THROUGH ANALYSIS	43
	5.1 Numerical Analysis of Snapping Phenomena	43
	5.2 Continuous SHM Snap-Through	46
6	EXPERIMENTAL INVESTIGATION	47
	6.1 Test Setup	47
	6.2 Test Procedures	47
7	COMPARISON OF THEORY AND EXPERIMENT	51
	7.1 Straight Beam Case	51
	7.2 Buckled Beam Case	52
8	CONCLUSIONS	54
	8.1 Straight Beam Case	54
	8.2 Buckled Beam Case	55
	8.3 General	56

<u>Section</u>	<u>Page</u>
APPENDIX A - NEWTON ITERATION METHOD	57
APPENDIX B - STATIC SNAP-THROUGH LOAD	59
REFERENCES	62
FIGURES	66

NOMENCLATURE

a	Dimensionless initial static deflection = W_c/h
A	Beam cross section area
A_{F_0}	Base motion amplitude
A_F	Dimensionless base motion amplitude = $A_{F_0} \omega_0/h\omega_1$ --- (Str.), = A_{F_0}/ha --- (Buck.)
A_0, A_1, A_2, A_3	Functions given by Eq. 2.21
A_{eff}	Effective forcing amplitude
b	Beam width
b_k	Coefficients of assumed solutions
B_n	Coefficient given by Eq. 2.11 --- (Str.) " " " Eq. 3.20 --- (Buck.)
c	Damping coefficient
c_k	Coefficients of assumed solutions
C_n	Coefficient given by Eq. 2.11 --- (Str.) " " " Eq. 3.20 --- (Buck.)
D_n	Coefficient given by Eq. 2.11 --- (Str.) " " " Eq. 3.20 --- (Buck.)
E	Young's modulus
E_n	Coefficient given by Eq. 2.11 --- (Str.) " " " Eq. 3.20 --- (Buck.)
$f_{s_{crl}}$	Nondimensional static first mode snap-through load
$(f_s)_B$	Nondimensional static bifurcation load
F_1	Coefficient given by Eq. 2.11 --- (Str.) " " " Eq. 3.20 --- (Buck.)

F_d	Dynamic force
F_s	Static force
$F_{s_{crl}}$	Critical static load
G_n	Coefficient given by Eq. 3.20
h	Beam thickness
H_n	Coefficient given by Eq. 3.20
I	Moment of inertia of beam
k	Integer, Also coefficient given by Eq. 3.18
K_n	Coefficients given by Eq. 2.13 --- (Str.)
	" " " Eq. 3.26 --- (Buck.)
l	Beam length
m	Mass/unit length of beam
m_1	Mode shape coefficient, see Eq. 2.7
n	Integer
N_o	Initial tension force on beam
N_x	Total tension force on beam
P_o	Fictitious compressive force on beam
P_{cr}	Critical buckling load = $4\pi^2 EI/l^2$
\tilde{q}_1, \tilde{q}_2	Generalized coordinates
q_1	Reduced first generalized coordinate = $\tilde{q}_1 \omega_o / \omega_1$
	--- (Str.)
	Reduced first generalized coordinate = $\tilde{q}_1 - 1$
	--- (Buck.)
q_{1s}	Steady state solution for q_1
r_i	Amplitude of i^{th} component = $\sqrt{x_i^2 + y_i^2}$

R	Dynamic to static force ratio
t	Time in seconds
T	Period of free vibration
ΔT	Temperature increment
W	Beam displacement
W_B	Base displacement
W_O	Initial static deflection
W_C	Initial static deflection at center = $W_O(\frac{\ell}{2})$
x	Longitudinal axis
x_k	Amplitude of $\sin k\tau$ component
y_k	Amplitude of $\cos k\tau$ component
α	Dimensionless frequency parameter = $(\omega_1/\omega_F)^2$
α_T	Thermal expansive coefficient
β	Mode shape coefficient, see Eq. 2.8 --- (Str.) " " " " Eq. 3.17 --- (Buck.)
ζ	Critical damping ratio of beam = $c/(2m\omega_1)$
η	Perturbation from steady state solution
$\theta_O, \theta_{cv}, \theta_{sv}$	Coefficients of Mathieu-Hill Eq. 4.2
ν	Integer
ξ	Dimensionless variable = x/ℓ
τ	Dimensionless time = $\omega_F t/n$
$\bar{\tau}$	Dimensionless time = $\tau/2$
ϕ_1	First vibration mode of beam, see Eq. 2.6 --- (Str.) " buckling " " " see Eq. 3.14 --- (Buck.)
ϕ_2	Second buckling mode of beam, see Eq. 3.15

ϕ	Dimensionless beam displacement = W/h --- (Str.)
	" " " = W/ah --- (Buck.)
ϕ_B	Dimensionless base displacement = W_B/h --- (Str.)
	" " " = W_B/ah --- (Buck.)
ϕ_0	Dimensionless initial static deflection = W_0/ah
ω	Nonlinear natural frequency
ω_1	First mode linear natural frequency, Eq. 2.13
	--- (Str.)
	First mode linear natural frequency, Eq. 3.23a
	--- (Buck.)
ω_2	Second mode linear natural frequency, Eq. 3.23b
ω_0	Beam natural frequency without tension, Eq. 2.13
ω_T	Induced frequency due to tension, Eq. 2.13
ω_F	Forcing frequency
Ω	Dimensionless frequency parameter = ω_F/ω_1
	(for free vibration = ω/ω_1)

SECTION 1

INTRODUCTION

Vibrations occur everywhere in a structure. The existence of vibration can bring about fatigue failure if vibrations continue for a long time. Some failures are of a different nature. When the structure is subjected to external periodic motion, it may continually increase its response until it suddenly changes its normal operating shape. For example, a thin shallow arch excited by periodic excitation of its base at some particular exciting conditions and geometrical parameters, may snap through. This is the so-called dynamic buckling. In modern design work of aircraft, spacecraft, missiles, etc., detailed knowledge of dynamic behavior is necessary in order to obtain the better system.

There are two kinds of periodic vibration; one is the so-called parametric oscillation and the other is forced vibration. The typical example of linear parametric excitation is the Mathieu equation which has been well studied.¹ Bolotin,² Weidenhammer,³ and Minorsky⁴ have dealt with nonlinear modified Mathieu equations. Bolotin,² in particular, has investigated the parametric excitation of a number of nonlinear structural systems. Recently, Dugundji and Chhatpar⁵ have investigated the parametric excitation of a pendulum and found some interesting nonlinear phenomena. The present research, however, will consider only pure forced vibration, including nonlinear effects. The physical models of the forced vibration will be,

- 1) A straight beam with fixed ends excited by the periodic motion of its supporting base.
- 2) A buckled beam with fixed ends excited by the periodic motion of its supporting base.

In the straight beam case, using the first vibration mode approximation, the governing equation of motion becomes the well-known Duffing equation of the hard spring type.^{6,7} This equation

has been investigated again recently by several authors.⁸⁻¹⁴ These investigations generally solved the equation by the perturbation method or by analog computer. However, there is little experimental work considered on elastic models. The perturbation method⁸⁻¹² is generally restricted to the case of small nonlinearity and small external driving forces. The attempt, in general, is to find the stability of the solution of simple harmonic motion (SHM), in which the predominant component has a period the same as the external force. The analog computer approach^{13,14} shows, in general, a few discrete points which give some information at the unstable regions of the SHM solution. The present investigation shows there exists other equilibrium solutions near the SHM unstable regions in which the SHM component becomes minor and a component with a period other than that of the external force becomes predominant. The responses, other than that of the SHM, will be named either superharmonic motion (SPHM) or subharmonic motion (SBHM). The present paper attempts to point out several features of the SPHM and SBHM which may not have been apparent before. Both analytical and experimental work of the straight beam case are considered in Sections 2, 4, and 6.

The buckled beam case relates to the general problem of the dynamic stability of thin arch and shell structures. This problem has been studied both theoretically and experimentally by a number of authors in the past few years.^{2,10,11, 15-28} Also, the book edited by Herrmann¹⁵ includes a number of investigations on dynamic stability of structures. Humphreys¹⁶ has examined a circular arch under impulse, step, and rectangular pulse loadings by using the analog computer. Lock¹⁷ determined the critical step-pressure loads of an arch by the numerical integration of the equations of motion and by an infinitesimal stability analysis. Some authors^{18,19} have applied the energy method to tackle the buckling problem of an arch, but this is less successful. Van Gulick²⁰ investigated the vibrations of arches and the stability

of the first antisymmetric mode. Mettler¹¹ has applied the method of averaging⁴ (one of the perturbation methods) to investigate the problem of the stability and the vibration of a sine arch under harmonic excitation. In his investigation, he restricted the amplitude of the external force to be small and found the jump phenomena of the SHM, SPHM, and SBHM resonances. His observation, that the jump phenomena is the kinetic snap-through in analogy to the static snap-through, seems inaccurate since this jump to a higher branch solution may not necessarily cause the arch to snap-through. To obtain the correct information of snap-through, one should include the effect of dynamic overshoot. In general, the method of averaging gives good information about the stability condition of the SHM solution under small forcing terms, but will give little information about the snap-through.

In the present investigation of a buckled beam under harmonic excitation, the governing equation of motion reduces to the same form as for the straight beam case, and similar solution techniques are employed. The investigation includes

- a) the steady-state solutions of SHM and SPHM
- b) snap-through analysis
- c) the effects of the initial static deflection

Both analytical and experimental work of the buckled beam case are considered in Sections 3, 4, 5, and 6.

SECTION 2

NONLINEAR VIBRATION OF A STRAIGHT BEAM

2.1 Formulation and General Solution

The governing differential equation of a straight beam with fixed ends excited by the base motion W_B perpendicular to the longitudinal direction of the beam is, (see Fig. 1),

$$EI \frac{\partial^4 W}{\partial x^4} - \frac{\partial}{\partial x} \left(N_x \frac{\partial W}{\partial x} \right) = -m \left(\frac{\partial^2 W}{\partial t^2} + \frac{\partial^2 W_B}{\partial t^2} \right) - c \frac{\partial W}{\partial t} \quad (2.1)$$

$$N_x = N_0 + \frac{EA}{2l} \int_0^l \left(\frac{\partial W}{\partial x} \right)^2 dx \quad (2.2)$$

and boundary conditions are $W = \frac{\partial W}{\partial x} = 0$ at $x = 0$ and $x = l$,

where E - Young's modulus,

I - moment of inertia,

N_0 - initial tension on the beam,

m - mass/unit length,

W - deflection of beam,

A - beam cross section,

l - beam length,

x - longitudinal axis,

c - damping coefficient,

t - time in seconds.

For a rectangular cross beam, where $A = bh$ and $I = bh^3/12$, with the following dimensionless variables

$$\Phi = \frac{W}{h}, \quad \Phi_B = \frac{W_B}{h} \quad \text{and} \quad \xi = \frac{x}{l} \quad (2.3)$$

Eqs. 2.1 and 2.2 can be combined and rearranged into

$$\frac{\partial^2 \bar{\Phi}}{\partial t^2} + \frac{c}{m} \frac{\partial \bar{\Phi}}{\partial t} + \frac{EI}{ml^4} \frac{\partial^4 \bar{\Phi}}{\partial \xi^4} - \left[\frac{N_0}{ml^2} + \frac{6EI}{ml^4} \int_0^1 \left(\frac{\partial \bar{\Phi}}{\partial \xi} \right)^2 d\xi \right] \frac{\partial^2 \bar{\Phi}}{\partial \xi^2} = - \frac{\partial^2 \bar{\Phi}_B}{\partial t^2} \quad (2.4)$$

Boundary conditions become $\bar{\Phi} = \frac{\partial \bar{\Phi}}{\partial \xi} = 0$, at $\xi = 0$ and 1.

For the present frequency of interest, the solution of Eq. 2.4 can be approximated as

$$\bar{\Phi}(\xi, t) = \tilde{q}_1(t) \phi_1(\xi) \quad (2.5)$$

where $\tilde{q}_1(t)$ is the first generalized coordinate and $\phi_1(\xi)$ is the first free vibration mode of a clamped-clamped beam.¹⁶

$$\phi_1 = \frac{1}{1.588} \left[\cosh m_1 \xi - \cos m_1 \xi + \beta (\sin m_1 \xi - \sinh m_1 \xi) \right] \quad (2.6)$$

$$\cos m_1 \cosh m_1 = 1.0 \quad (2.7)$$

$$\beta = (\sinh m_1 - \sin m_1) / (\cosh m_1 - \cos m_1) \quad (2.8)$$

For the first mode solution, $m_1 = 4.73$, $\beta = .9825$, and $\phi_1(\frac{1}{2}) = 1.0$.
Substituting Eq. 2.5 into Eq. 2.4 gives

$$\begin{aligned} \phi_1 \frac{d^2 \tilde{q}_1}{dt^2} + \frac{c}{m} \phi_1 \frac{d \tilde{q}_1}{dt} + \frac{EI}{m l^4} \frac{d^4 \phi_1}{d\xi^4} \tilde{q}_1 - \left[\frac{N_0}{m l^2} \right. \\ \left. + \frac{6EI}{m l^4} \tilde{q}_1^2 \int_0^1 \left(\frac{d\phi_1}{d\xi} \right)^2 d\xi \right] \frac{d^2 \phi_1}{d\xi^2} \tilde{q}_1 = - \frac{\partial^2 \Phi_B}{\partial t^2} \end{aligned} \quad (2.9)$$

Using Galerkin's method, Eq. 2.9 is now multiplied by ϕ_1 and integrated in ξ from 0 to 1 which leads to an ordinary differential equation in q_1 as

$$\begin{aligned} B_1 \frac{d^2 \tilde{q}_1}{dt^2} + \frac{c}{m} B_1 \frac{d \tilde{q}_1}{dt} + \frac{EI}{m l^4} C_1 \tilde{q}_1 - \left(\frac{N_0}{m l^2} \right. \\ \left. + \frac{6EI}{m l^4} D_1 \tilde{q}_1^2 \right) E_1 \tilde{q}_1 = - F_1 \frac{\partial^2 \Phi_B}{\partial t^2} \end{aligned} \quad (2.10)$$

where

$$\begin{aligned} B_1 &= \int_0^1 \phi_1^2 d\xi = .397 \\ C_1 &= \int_0^1 \phi_1 \frac{d^4 \phi_1}{d\xi^4} d\xi = 198.5 \\ D_1 &= \int_0^1 \left(\frac{d\phi_1}{d\xi} \right)^2 d\xi = 4.88 \\ E_1 &= \int_0^1 \phi_1 \frac{d^2 \phi_1}{d\xi^2} d\xi = -4.88 \\ F_1 &= \int_0^1 \phi_1 d\xi = .523 \end{aligned} \quad (2.11)$$

Assuming harmonic excitation of the base, $W_B = A_{F_0} \sin \omega_F t$, Eq. 2.10 can be transformed to

$$\frac{d^2 \tilde{\theta}_1}{dt^2} + \frac{c}{m} \frac{d \tilde{\theta}_1}{dt} + K_1 \omega_1^2 \tilde{\theta}_1 + K_2 \omega_0^2 \tilde{\theta}_1^3 = K_3 \frac{A_{F_0}}{h} \omega_F^2 \sin \omega_F t \quad (2.12)$$

where

$$K_1 = 1.0$$

$$K_2 = .655$$

$$K_3 = 1.319$$

$$\omega_0^2 = 500.6 \frac{EI}{m l^4}$$

$$\omega_T^2 = 12.306 N_0 / (m l^2) \quad (2.13)$$

$$\omega_1^2 = \omega_0^2 + \omega_T^2$$

Equation 2.12 is the well known Duffing equation with an acceleration-type forcing function. In here, ω_F represents the forcing frequency, and ω_1 the linear natural frequency of the beam. For calculation purposes, it is convenient to introduce the following dimensionless variables such that,

$$n \tau = \omega_F t \quad , \quad n \text{ is any integer} \quad (2.14)$$

$$\theta_1 = \frac{\omega_0}{\omega_1} \tilde{\theta}_1 \quad (2.15)$$

$$A_F = \frac{\omega_0}{\omega_1} \frac{A_{F_0}}{h} \quad (2.16)$$

and then, Eq. 2.12 reduces to the nondimensional form,

$$\frac{d^2 q_1}{d\tau^2} + 2n\zeta\sqrt{\alpha} \frac{dq_1}{d\tau} + n^2 K_1 \alpha q_1 + n^2 K_2 \alpha q_1^3 = n^2 K_3 A_F \sin n\tau \quad (2.17)$$

where

$$\alpha = (\omega_1/\omega_F)^2 = 1/\Omega^2 \quad (2.18)$$

$$\zeta = c/(2m\omega_1) \quad , \quad \text{critical damping ratio.}$$

For the basic equation 2.17, the general steady state periodic solution of SHM, SPHM (order 3, 2, 3/2) and SBHM (order 2/3, 1/2, 1/3) can be written in the form

$$q_1 = y_0 + \sum_{k=1}^3 (x_k \sin k\tau + y_k \cos k\tau) \quad (2.19)$$

Substituting Eq. 2.19 into Eq. 2.17 and equating the coefficients of the terms containing constant, $\sin \tau$, $\cos \tau$, $\sin 2\tau$, $\cos 2\tau$, $\sin 3\tau$ and $\cos 3\tau$ separately to zero yields (this method is named as Harmonic Balance),

$$A_0 y_0 + \frac{3}{4} n^2 K_2 \alpha \left\{ y_2 (y_1^2 - x_1^2) + 2x_1 y_1 x_2 + 2 \left[y_3 (y_1 y_2 - x_1 x_2) + x_3 (y_1 x_2 + x_1 y_2) \right] \right\} = 0 \quad (2.20a)$$

$$A_1 x_1 - 2n\zeta\sqrt{\alpha} y_1 + 3n^2 K_2 \alpha \left\{ y_0 (y_1 x_2 - x_1 y_2 + y_2 x_3 - x_2 y_3) + \frac{1}{4} \left[x_3 (x_2^2 - y_2^2 - x_1^2 + y_1^2) + 2y_3 (x_2 y_2 - x_1 y_1) \right] \right\} = n^2 K_3 A_F \delta_{n_1} \quad (2.20b)$$

$$2n\zeta\sqrt{\alpha} x_1 + A_1 y_1 + 3n^2 K_2 \alpha \left\{ y_0 (x_1 x_2 + y_1 y_2 + x_2 x_3 + y_2 y_3) + \frac{1}{4} \left[y_3 (y_2^2 - x_2^2 - x_1^2 + y_1^2) + 2x_3 (x_1 y_1 + x_2 y_2) \right] \right\} = 0 \quad (2.20c)$$

$$A_2 x_2 - 4 n \mathcal{J} \sqrt{\alpha} y_2 + 3 n^2 K_2 \alpha \left\{ y_0 (x_1 y_1 - x_1 y_3 + x_3 y_1) + \frac{1}{2} [(x_1 x_2 + y_1 y_2) x_3 + y_3 (x_1 y_2 - x_2 y_1)] \right\} = n^2 K_3 A_F \delta_{n2} \quad (2.20d)$$

$$4 n \mathcal{J} \sqrt{\alpha} x_2 + A_2 y_2 + 3 n^2 K_2 \alpha \left\{ y_0 \left[x_1 x_3 + y_1 y_3 + \frac{1}{2} (y_1^2 - x_1^2) \right] + \frac{1}{2} \left[y_3 (x_1 x_2 + y_1 y_2) + x_3 (y_1 x_2 - x_1 y_2) \right] \right\} = 0 \quad (2.20e)$$

$$A_3 x_3 - 6 n \mathcal{J} \sqrt{\alpha} y_3 + 3 n^2 K_2 \alpha \left\{ y_0 (x_1 y_2 + x_2 y_1) + \frac{1}{4} \left[x_1 (x_2^2 - y_2^2) + 2 y_1 x_2 y_2 + x_1 y_1^2 - \frac{x_1^3}{3} \right] \right\} = n^2 K_3 A_F \delta_{n3} \quad (2.20f)$$

$$6 n \mathcal{J} \sqrt{\alpha} x_3 + A_3 y_3 + 3 n^2 K_2 \alpha \left\{ y_0 (y_1 y_2 - x_1 x_2) + \frac{1}{4} \left[y_1 (y_2^2 - x_2^2) + 2 x_1 x_2 y_2 - y_1 x_1^2 + \frac{y_1^3}{3} \right] \right\} = 0 \quad (2.20g)$$

where

δ_{nj} = Kronecker delta

$$A_0 = n^2 \alpha \left\{ K_1 + K_2 \left[y_0^2 + \frac{3}{2} (r_1^2 + r_2^2 + r_3^2) \right] \right\} \quad (2.21a)$$

$$A_1 = n^2 K_1 \alpha - 1 + \frac{3}{4} n^2 K_2 \alpha (4 y_0^2 + r_1^2 + 2 r_2^2 + 2 r_3^2) \quad (2.21b)$$

$$A_2 = n^2 K_1 \alpha - 4 + \frac{3}{4} n^2 K_2 \alpha (4 y_0^2 + 2 r_1^2 + r_2^2 + 2 r_3^2) \quad (2.21c)$$

$$A_3 = n^2 K_1 \alpha - 9 + \frac{3}{4} n^2 K_2 \alpha (4 y_0^2 + 2 r_1^2 + 2 r_2^2 + r_3^2) \quad (2.21d)$$

$$r_i^2 = x_i^2 + y_i^2 \quad , \quad i = 1, 2, 3 \quad . \quad (2.22)$$

For $\zeta = 0$, all y components are zero, $r_1 = x_1$, and only Eqs. 2.20b, d, and f apply.

Equations 2.20 are the general steady-state periodic solution. It will now be applied to some specific cases.

2.2 Specific Cases

2.2.1 SHM and SPHM Order 3

From Eqs. 2.17 and 2.20 with $n = 1$, it is readily seen that $y_0 = x_2 = y_2 = 0$ satisfies Eqs. 2.20 a, d, and e, leaving only Eqs. 2.20 b, c, f, and g to be solved. Eliminating x and y components in the above remaining equations gives

$$\left[\left(A_1 - \frac{3A_3 r_3^2}{r_1^2} \right)^2 + 4\zeta^2 \alpha \left(1 + \frac{r_3^2}{r_1^2} \right)^2 \right] r_1^2 = K_3^2 A_F^2 \quad (2.23a)$$

$$A_3^2 r_3^2 + 36\zeta^2 \alpha r_3^2 = \frac{K_2^2 \alpha^2}{16} r_1^6 \quad (2.23b)$$

There exists two equilibrium solutions in Eqs. 2.23, one of them is $|r_1| \gg |r_3|$, the other is $|r_1| \ll |r_3|$.

For the solution of $|r_1| \gg |r_3|$, further simplification is obtained by neglecting x_3 and y_3 components and discarding the associated Eq. 2.23b which reduces to the standard solution of SHM as

$$\left[\left(K_1 \alpha - 1 + \frac{3}{4} K_2 \alpha r_1^2 \right)^2 + 4\zeta^2 \alpha \right] r_1^2 = K_3^2 A_F^2 \quad (2.24)$$

This gives the conventional cubic equation in r_1^2 . The numerical results of Eq. 2.24 for r_1 show that the solution of low damping ratio, say $\zeta < .01$, is indistinguishable from that of no damping

case for amplitudes of interest here. Since very low damping ratio, $\zeta < .001$, is considered here, only the no damping solution is shown in Fig. 2 plotted with absolute value of r_1 versus Ω . The dash-lines in the figure mean unstable solutions which are never physically realized. The nonlinear natural frequency solution can also be obtained from Eq. 2.24 with $A_F = 0$, $\zeta = 0$ and $r_1 \neq 0$, which leads to the so-called 'backbone curve' solution

$$r_1^2 = \frac{4(1 - K_1\alpha)}{3K_2\alpha} = \frac{4(\Omega^2 - K_1)}{3K_2} \quad (2.25)$$

Here, Ω becomes ω/ω_1 , ω is the nonlinear frequency and ω_1 is the linear natural frequency. The backbone curve (see Fig. 2) divides SHM Solution into two regions; on the left side of the backbone curve the displacement of SHM is out-of-phase with the base displacement, and the other side is in-phase. Similar form to Eq. 2.25 will also appear in the SPHM, SBHM cases to be studied.

For more accurate solutions involving small but nonzero r_3 , solution of Eqs. 2.23 can be obtained by iterating from $r_3 = 0$ solution given by Eq. 2.24. The numerical results for r_1 and r_3 are shown in Fig. 3. The r_1 results are indistinguishable from those given previously by Eq. 2.24 alone.

For the $|r_3| \gg |r_1|$ case, the solution is somewhat difficult to realize directly from Eqs. 2.23, however, it can easily be seen in the case of $\zeta = 0$ which gives

$$\left(A_1 - \frac{3A_3 r_3^2}{r_1^2} \right) r_1 = K_3 A_F \quad (2.26a)$$

$$A_3 r_3 = \frac{K_2 \alpha}{4} r_1^3 \quad (2.26b)$$

Equation 2.26b can be rewritten as

$$(K_1\alpha - 9 + \frac{3}{4}K_2\alpha r_3^2) r_3 = \frac{K_2\alpha}{4} (r_1 - 6r_3) r_1^2 \quad (2.27)$$

By the assumption $|r_3| \gg |r_1|$, Eq. 2.27 can be approximated as

$$r_3^2 \approx \frac{4(9 - K_1\alpha)}{3K_2\alpha} - 2r_1^2 \quad (2.28a)$$

or

$$r_3^2 \approx \frac{4(9\Omega^2 - K_1)}{3K_2} - 2r_1^2 \quad (2.28b)$$

$$A_3 \approx 0 \quad (2.28c)$$

Equation 2.26a then reduces simply to

$$(17 - K_1\alpha - \frac{9}{4}K_2\alpha r_1^2) r_1 = K_3 A_F \quad (2.28d)$$

Equations 2.28 give almost identical result for r_1 and r_3 as from Eqs. 2.26, yet Eqs. 2.28 now gives very clear physical significance which means that the equilibrium solution of $|r_3| \gg |r_1|$ only exists at $k_1 \alpha < 9$ or ($\Omega > 1/3$). Similar forms to Eqs. 2.28 will also appear in SPHM and SBHM of other orders.

The numerical results for r_1 and r_3 corresponding to SPHM order 3 are shown in Figs. 3 and 4. They appear to bifurcate from the main SHM solution near where the "shifted backbone curve order 3,"

$$r_3^2 = \frac{4(9 - K_1 \alpha)}{3K_2 \alpha} = \frac{4(9\Omega^2 - K_1)}{3K_2} \quad (2.29)$$

intersects the SHM solution.* From Figs. 3 and 4, one notices that with fixed A_F , amplitude $|r_1|$ corresponding to the external forcing frequency decreases as Ω increases. For small forcing amplitudes A_F , this bifurcation point would be near $\Omega = 1/3$ and the bifurcation point moves toward the increasing Ω as A_F increases. The above results seem to be in agreement with those of Caughey⁸ for small forcing amplitudes A_F and those of Atkinson¹³ for large A_F . For very large A_F , see Szemplinska-Stupnicka¹⁴.

The details of the actual transition between these two solutions, $|r_1| > |r_3|$ and $|r_3| > |r_1|$, can be found by solving Eqs. 2.23 numerically using a Newton iteration method (see Appendix A). This transition is shown in Fig. 5 for $\zeta = 0$ and is seen to be continuous. On the left-hand side (which is plotted in solid line), the displacement of the r_3 component is out-of-phase with the base displacement; the other side is in-phase, but the displacement of the r_1 component is always out-of-phase. There also exists an unstable branch which is never physically realized. This type of detailed behavior will also appear for all the other SPHM and SBHM solutions to be studied.

For small damping $\zeta < .001$, the solutions are very close to the $\zeta = 0$ case. It is of interest, though, to note from Eq. 2.23b that there exists a limiting maximum ratio of r_3/r_1 , depending on the damping. Since all three terms of Eq. 2.23b are always positive,

* The shifted backbone curve order k is defined by replacing Ω of Eq. 2.25 with $k\Omega$ where $k \neq 1$.

$$36\beta^2\alpha r_3^2 \leq \frac{K_2^2\alpha^2}{16} r_1^6 \quad (2.30)$$

This can be rearranged to give

$$\left| \frac{r_3}{r_1} \right| \leq \frac{K_2\sqrt{\alpha}}{24\beta} r_1^2 \quad (2.31)$$

Hence, the smaller ζ is, the more prominent will be the third superharmonic component. Also, for small forcing amplitudes A_F which would result in small r_1 , very low damping is necessary to bring out a dominant third superharmonic.*

2.2.2 SPHM Order 2

To obtain the solution of this SPHM, the complete equations of Eq. 2.20 with $n=1$ must be taken into consideration. For simplicity, first consider the $\zeta = 0$ case in which Eq. 2.20d reduces to

$$A_2 r_2 + \frac{3K_2\alpha}{2} r_1 r_2 r_3 = 0 \quad (2.32)$$

Since $r_2 \neq 0$, the equation leads to

$$r_2^2 = \frac{4(4 - K_1\alpha)}{3K_2\alpha} - 2(r_1^2 + r_1 r_3 + r_3^2) \quad (2.33)$$

Because $(r_1^2 + r_1 r_3 + r_3^2) > 0$, SPHM order 2 exists only at $\alpha < 4$, or at $\Omega > 1/2$. Equation 2.33 together with Eqs. 2.20b and f form the complete solution for the $\zeta = 0$ case. Neglecting the small component of r_3 and discarding the associated equation 2.20f will give the simple form of

*The criterion given in Eq. 2.31 may be modified somewhat if the 5th order harmonics are included in the solution, Eq. 2.19.

$$(7 - K_1\alpha - \frac{9}{4}K_2\alpha r_1^2) r_1 = K_3 A_F \quad (2.34a)$$

$$r_2^2 = \frac{4(4 - K_1\alpha)}{3K_2\alpha} - 2r_1^2 \quad (2.34b)$$

The numerical results of Eqs. 2.34 for r_1 and r_2 are shown in Figs. 2 and 6. The bifurcation from the SHM solution near $\Omega = 1/2$ is noted. It is also found that only the solution of positive r_1 together with negative r_2 is stable; i.e., the displacement of the r_2 component is in-phase with the base displacement and the r_1 component is out-of-phase. For the small A_F case, say $A_F < .5$, the SPHM order 2 solution is very close to the shifted backbone order 2. The complete solution of Eqs. 2.20 gives a very small r_3 component, while not affecting r_1 and r_2 of Eq. 2.34 significantly. Similarly, Eqs. 2.34 gives a good approximation for small damping $\zeta < .001$ present.

2.2.3 SPHM order 3/2

Similar to the previous case, with $n = 2$, and $\zeta = 0$ in Eqs. 2.20, Eq. 2.20f reduces to

$$\begin{aligned} (K_1\alpha - \frac{9}{4} + \frac{3}{4}K_2\alpha r_3^2) r_3 + \frac{3}{4}K_2\alpha \left[(2r_3 + r_1) r_2^2 \right. \\ \left. + (2r_3 - \frac{r_1}{3}) r_1^2 \right] = 0 \end{aligned} \quad (2.35)$$

Since $|r_3| \gg |r_2| \gg |r_1|$, Eq. 2.35 becomes, approximately

$$r_3^2 \approx \frac{4}{3K_2\alpha} \left(\frac{9}{4} - K_1\alpha \right) - 2(r_1^2 + r_2^2) \quad (2.36a)$$

Again Eq. 2.36a shows the SPHM of 3/2 exists only at $k_1 \alpha < 9/4$ or at $\Omega > 2/3$. The complete solution for r_1 , r_2 , and r_3 can be obtained by solving Eqs. 2.20b, d, and f in the $\zeta = 0$ case.

Further approximation can be obtained by neglecting the r_1 component and discarding Eq. 2.20b. This gives

$$(14 - 4K_1\alpha - 9K_2\alpha r_2^2) r_2 = 4K_3 A_F \quad (2.37a)$$

$$r_3^2 = \frac{4}{3K_2\alpha} \left(\frac{9}{4} - K_1\alpha \right) - 2r_2^2 \quad (2.37b)$$

The numerical results of Eqs. 2.37 for r_3 and r_2 are shown in Fig. 3. The bifurcation from the SHM solution near $\Omega = 2/3$ is noted. Also, it is to be noted here that the r_2 component corresponds to the forcing frequency ω_F . The stable solution of Eqs. 2.37 is that the r_3 and r_2 components are in- and out-of-phase with the base displacement, respectively.

The complete solution of Eqs. 2.20 gives a very small r_1 component while not affecting the r_2 and r_3 components of Eqs. 2.37 significantly. Similarly, Eqs. 2.37 give a very good approximation for the small damping $\zeta < .001$ present.

2.2.4 SBHM Order 1/3

The solution can be obtained from Eqs. 2.20 with $n = 3$ in which $y_0 = x_2 = y_2 = 0$ satisfies Eqs. 2.20a, b, and e. Similar to the case of SPHM order 3, there are 2 equilibrium solutions in the present case; one is $r_1 = 0$, the other is $|r_1| \gg |r_3|$. The $r_1 = 0$ solution is essentially the SHM solution discussed previously, since $n = 3$ here.

For the $|r_1| \gg |r_3|$ case, first consider $\zeta = 0$, in which Eqs. 2.20 reduce to

$$9K_1\alpha - 1 + \frac{27}{4}K_2\alpha (r_1^2 - r_1 r_3 + 2r_3^2) = 0 \quad (2.38a)$$

$$A_3 r_3 - \frac{9}{4}K_2\alpha r_1^3 = 9K_3 A_F \quad (2.38b)$$

Equation 2.38a shows SBHM order 1/3 exists only for $\alpha < 1/9$ or for $\Omega > 3$. The numerical results obtained by solving Eqs. 2.38 simultaneously for r_1 and r_3 are shown in Fig. 7. The bifurcation from the SHM solution near $\Omega = 3$ is noted. The stable solution of Eqs. 2.38 is that the r_1 and r_3 components are in-phase with base displacements. For small damping $\zeta < .01$, the solutions are close to those from Eqs. 2.38. Sizable forcing components r_3 are present here since the "effective" forcing amplitude A_{eff} is relatively larger than for the superharmonic case. This "effective" forcing amplitude for Duffing's equation, Eq. 2.12 would be

$$A_{eff} \propto \Omega^2 A_F \quad (2.39)$$

2.2.5 SBHM Order 1/2

In this case, the solution can be obtained from Eqs. 2.20 with $n = 2$. Again considering the $\zeta = 0$ case first; Eq. 2.20b reduces to

$$\left[K_1 \alpha - \frac{1}{4} + \frac{3}{4} K_2 \alpha (r_1^2 + 2r_2^2 + 2r_3^2) \right] r_1 + \frac{3K_2 \alpha}{4} (r_2^2 - r_1^2) r_3 = 0 \quad (2.40)$$

Since $|r_1|, |r_2| \gg |r_3|$, Eq. 2.40 can be approximated as

$$r_1^2 \approx \frac{4(\frac{1}{4} - K_1 \alpha)}{3K_2 \alpha} - 2r_2^2 \quad (2.41a)$$

Equation 2.41a shows this SBHM occurs only for $\alpha < 1/4$ or for $\Omega > 2$. Complete solution can be obtained by solving Eqs. 2.20b, d, and f in the case $\zeta = 0$.

Similar to the previous cases, neglecting the r_3 effects will give a simple solution by solving Eq. 2.41a together with the following equation, Eq. 2.41b.

$$(K_1\alpha + \frac{1}{2} + \frac{9}{4}K_2\alpha r_2^2)r_2 = -K_3 A_F \quad (2.41b)$$

The numerical results of Eqs. 2.41 give a good approximation to the complete solution of Eqs. 2.20 (with $\zeta = 0$ and small damping, $\zeta < .001$), and are shown in Fig. 7. The bifurcation from the SHM solution near $\Omega = 2$ is noted. Similar to the case SBHM order 3, the solution with the r_1 and r_2 components having the same phase as base displacement is stable. Again, A_{eff} is relatively large, thus leading to substantial forcing components r_2 .

2.2.6 SBHM Order 2/3

The solution can be obtained from Eqs. 2.20 with $n = 3$. Considering the $\zeta = 0$ case first, Eq. 2.20d reduces to (for $r_2 \neq 0$)

$$r_2^2 = \frac{4}{3K_2\alpha} \left(\frac{4}{9} - K_1\alpha \right) - 2(r_1^2 + r_1r_3 + r_3^2) \quad (2.42)$$

Equation 2.42 shows that SBHM order 2/3 occurs only at $\alpha < 4/9$ or at $\Omega > 3/2$. Equation 2.42 together with Eqs. 2.20b and f will give the solution for $\zeta = 0$.

Similar to the previous cases, neglecting r_1 effects will lead to a simple form as

$$r_2^2 = \frac{4}{3K_2\alpha} \left(\frac{4}{9} - K_1\alpha \right) - 2r_3^2 \quad (2.43a)$$

$$\left(\frac{1}{9} + K_1\alpha + \frac{9}{4}K_2\alpha r_3^2 \right) r_3 = -K_3 A_F \quad (2.43b)$$

The numerical results of Eqs. 2.43 give a good approximation to the complete solution of Eqs. 2.20 (with $\zeta = 0$ and $\Omega < .001$), and are shown in Fig. 7. The solution having the r_2 and r_3 components in phase with the base displacement is the only stable solution.

The bifurcation from the SHM solution near $\Omega = 3/2$ is noted. Again, substantial r_3 components are present due to relatively large A_{eff} .

2.3 Exact Solution of Free Vibration

The free vibration equation can be easily obtained from Eq. 2.17 with $\zeta = 0$, $A_F = 0$, and $n^2\alpha = \omega_1^2$, which gives

$$\frac{d^2 q_1}{dt^2} + K_1 \omega_1^2 q_1 + K_2 \omega_1^2 q_1^3 = 0 \quad (2.44)$$

Equation 2.44 is now multiplied by dq_1/dt , then integrated once with respect to time, t , which results in

$$\frac{1}{2} \left(\frac{dq_1}{dt} \right)^2 + \frac{1}{2} K_1 \omega_1^2 q_1^2 + \frac{1}{4} K_2 \omega_1^2 q_1^4 = e \quad (2.45)$$

where "e" is an integral constant and can be determined from the initial condition. It is noticed that Eq. 2.45 represents the law of conservation of energy. The left-hand side of Eq. 2.45 represents the total kinetic and potential energy which is equal to the sum of the initial kinetic and potential energy. For simplicity, the initial condition is taken as $q_1 = q_u$, $dq_1/dt = 0$ at $t = 0$ which leads Eq. 2.45 to

$$\frac{dq_1}{dt} = \omega_1 \left\{ (q_u^2 - q_1^2) [K_1 + .5 K_2 (q_u^2 + q_1^2)] \right\}^{1/2} \quad (2.46)$$

The period, T , of a complete cycle is easily obtained from Eq. 2.46 as

$$T = 2 \int_{q_l}^{q_u} \frac{dq_1}{\omega_1 \left\{ (q_u^2 - q_1^2) [K_1 + .5 K_2 (q_u^2 + q_1^2)] \right\}^{1/2}} \quad (2.47)$$

The lower bound q_l of the integral is determined at the position at which the value of the square root in Eq. 2.47 becomes zero; that is, the position where the velocity dq_1/dt becomes zero.

Obviously, $q_l = -q_u$. Since the integrand of Eq. 2.47 is symmetric, one can rewrite Eq. 2.47 as

$$T = \int_0^{q_u} \frac{4 d q_1}{\omega_1 \left\{ (q_u^2 - q_1^2) [K_1 + .5 K_2 (q_u^2 + q_1^2)] \right\}^{1/2}} \quad (2.48)$$

Equation 2.48 (or Eq. 2.47) is the first kind of elliptic integral.²⁹ Its numerical result is shown in Fig. 8, plotted in $\Omega = \omega/\omega_1$ versus r_1 where $r_1 = q_u$ and $\omega = 2\pi/T$. Figure 8 also shows the good approximation of the 'backbone curve', Eq. 2.25.

SECTION 3

NONLINEAR VIBRATION OF A BUCKLED BEAM

3.1 Formulation and General Solution

The governing differential equation of a buckled beam (the beam originally flat, which has been compressed past the critical buckling load, P_{cr} , to a static deflection position W_0) with fixed ends excited by the base motion W_B is (see Fig. 1)

$$EI \frac{\partial^4}{\partial x^4}(W+W_0) - \frac{\partial}{\partial x} \left[N_x \frac{\partial}{\partial x}(W+W_0) \right] = -m \left(\frac{\partial^2 W}{\partial t^2} + \frac{\partial^2 W_0}{\partial t^2} \right) - c \frac{\partial W}{\partial t} \quad (3.1)$$

$$N_x = -P_0 + \frac{EA}{2l} \int_0^l \left[\frac{\partial}{\partial x}(W+W_0) \right]^2 dx \quad (3.2)$$

Boundary conditions are $W = \frac{\partial W}{\partial x} = 0$, at $x = 0$ and l , where E , I , W , x , m , t , c , A and l are the same as in Section 2.1; P_0 is a fictitious compressive force on the beam defined by

$$P_0 = P_{cr} + \frac{EA}{2l} \int_0^l \left(\frac{dW_0}{dx} \right)^2 dx \quad (3.3)$$

For example P_0 may be considered to result from thermal expansion in which case

$$P_0 = AE\alpha_T \Delta T \quad (3.4)$$

and $P_0 > P_{cr}$ or $\Delta T > P_{cr}/(AE\alpha_T)$, where α_T is the thermal expansion coefficient and ΔT is the increment of temperature.

The initial static deflection W_0 satisfies

$$EI \frac{d^4 W_0}{dx^4} + P_{cr} \frac{d^2 W_0}{dx^2} = 0 \quad (3.5)$$

and $W_0 = \frac{dW_0}{dx} = 0$ at $x = 0$ and l , where P_{cr} is the fundamental buckling load of a clamped-clamped beam, i.e.,

$$P_{cr} = \frac{4\pi^2 EI}{l^2} \quad (3.6)$$

The solution of Eq. 3.5 is

$$W_0 = \frac{ah}{2} \left(1 - \cos \frac{2\pi x}{l} \right) \quad (3.7)$$

where h is the thickness of beam and 'a' is the ratio of W_c/h , with $W_c = W_0(\frac{l}{2})$. Equation 3.7 is the first buckling mode of a clamped-clamped beam. Substituting Eqs. 3.6 and 3.7 into Eq. 3.3, and using $Ah^2 = 12I$ gives

$$P_0 = \frac{4\pi^2 EI}{l^2} (1 + .75a^2) \quad (3.8)$$

From Eqs. 3.4 and 3.8 one can obtain the relation between initial static deflection 'a' and temperature increment ΔT as

$$a = \left(\frac{4}{\pi^2} \frac{l^2}{h^2} \alpha_T \Delta T - \frac{4}{3} \right)^{1/2} \quad (3.9)$$

Similar expression as Eq. 3.9 also appears in the problem on the vibrations of thermally buckled bars and plates.³⁰

Placing Eq. 3.2 into Eq. 3.1 and using the relations of Eqs. 3.3 and 3.5, one can obtain

$$EI \frac{\partial^4 W}{\partial x^4} + P_{cr} \frac{\partial^2 W}{\partial x^2} - \left\{ \frac{AE}{2l} \int_0^l \left[\left(\frac{\partial W}{\partial x} \right)^2 + 2 \frac{\partial W}{\partial x} \frac{\partial W_0}{\partial x} \right] dx \right\} \left(\frac{\partial^2 W}{\partial x^2} + \frac{\partial^2 W_0}{\partial x^2} \right) + m \frac{\partial^2 W}{\partial t^2} + c \frac{\partial W}{\partial t} = -m \frac{\partial^2 W_B}{\partial t^2} \quad (3.10)$$

Using the following nondimensional variables,

$$\Phi = \frac{W}{ah}, \quad \Phi_o = \frac{W}{ah}, \quad \Phi_B = \frac{W_B}{ah} \quad \text{and} \quad \xi = \frac{x}{l}, \quad (3.11)$$

Equation 3.10 is transformed to

$$\begin{aligned} \frac{\partial^2 \Phi}{\partial t^2} + \frac{c}{m} \frac{\partial \Phi}{\partial t} + \frac{P_{cr}}{ml} \frac{\partial^2 \Phi}{\partial \xi^2} - \left\{ \frac{AEa^2 h^2}{2l^2} \int_0^1 \left[\left(\frac{\partial \Phi}{\partial \xi} \right)^2 \right. \right. \\ \left. \left. + 2 \frac{\partial \Phi}{\partial \xi} \frac{\partial \Phi_o}{\partial \xi} \right] d\xi \right\} \left(\frac{\partial^2 \Phi}{\partial \xi^2} + \frac{\partial^2 \Phi_o}{\partial \xi^2} \right) + \frac{EI}{ml^4} \frac{\partial^4 \Phi}{\partial \xi^4} = - \frac{\partial^2 \Phi_B}{\partial t^2} \end{aligned} \quad (3.12)$$

Let the solution of Eq. 3.12 be the form of

$$\Phi = \sum_{n=1}^2 \tilde{q}_n(t) \phi_n(\xi) \quad (3.13)$$

where \tilde{q}_1 and \tilde{q}_2 are first and second generalized coordinates, respectively. ϕ_1 and ϕ_2 are the first and second buckling modes of the beam, respectively,

$$\phi_1 = \frac{1}{2} (1 - \cos 2\pi \xi) \quad (3.14)$$

$$\phi_2 = \left[\beta (\sin k\xi - k\xi) + \cos k\xi - 1 \right] \quad (3.15)$$

where

$$\tan \frac{k}{2} = \frac{k}{2} \quad (3.16)$$

$$\beta = \frac{1 - \cos k}{\sin k - k} = \frac{-2}{k} \quad (3.17)$$

$$k = 8.986 \quad (3.18)$$

The purpose of the choice Eqs. 3.14 and 3.15 will be readily seen later.

Substituting Eq. 3.13 into Eq. 3.12 and applying Galerkin's method gives

$$\frac{d^2 \tilde{q}_n}{dt^2} + \frac{c}{m} \frac{d \tilde{q}_n}{dt} + \frac{E_n P_{cr}}{B_n m l^2} \tilde{q}_n - \frac{AE a^2 h^2}{2 B_n m l^4} \left[\sum_{k=1}^2 (D_k \tilde{q}_k^2 + 2 G_k \tilde{q}_k) \right] (E_n \tilde{q}_n + H_n) + \frac{E I C_n}{m l^4 B_n} \tilde{q}_n = - \frac{F_n}{B_n} \frac{d^2 \Phi_B}{dt^2} \quad (3.19)$$

where $n = 1$ and 2 ,

$$B_n = \int_0^1 \phi_n^2 d\xi$$

$$C_n = \int_0^1 \phi_n \frac{d^4 \phi_n}{d\xi^4} d\xi$$

$$D_n = \int_0^1 \left(\frac{d\phi_n}{d\xi} \right)^2 d\xi$$

$$E_n = \int_0^1 \phi_n \frac{d^2 \phi_n}{d\xi^2} d\xi$$

$$F_n = \int_0^1 \phi_n d\xi$$

$$G_n = \int_0^1 \frac{d\phi_n}{d\xi} \frac{d\phi_n}{d\xi} d\xi$$

$$H_n = \int_0^1 \phi_n \frac{d^2 \phi_n}{d\xi^2} d\xi \quad (3.20)$$

The coefficients in Eq. 3.20 can be obtained by substituting Eqs. 3.7, 3.14 and 3.15 into Eq. 3.20, and are shown in the following table

	B _n	C _n	D _n	E _n	F _n	G _n	H _n
n = 1	.375	195.	4.935	-4.935	.500	4.935	-4.935
n = 2	.6045	3260	22.34	-22.34	0	0	0

(Note: Above coefficients, with n = 1, are close to those of Eq. 2.11). Substituting coefficients above and Eq. 3.6 into Eq. 3.19 and using $A_E h^2 = 12EI$ yields two non-linear coupled equations in q_1 and q_2 , under the harmonic excitation of the base, $W_B = A_{F0} \sin \omega_F t$, as

$$\frac{d^2 \tilde{q}_1}{dt^2} + \frac{c}{m} \frac{d \tilde{q}_1}{dt} + \omega_1^2 \tilde{q}_1 + \frac{3}{2} \omega_1^2 \tilde{q}_1^2 + \frac{1}{2} \omega_1^2 \tilde{q}_1^3 + 2.263 \omega_1^2 (\tilde{q}_1 + 1) \tilde{q}_2^2 = \frac{4}{3} A_F \omega_F^2 \sin \omega_F t \quad (3.21)$$

$$\frac{d^2 \tilde{q}_2}{dt^2} + \frac{c}{m} \frac{d \tilde{q}_2}{dt} + \frac{5.05}{a^2} \omega_1^2 \tilde{q}_2 + 6.356 \omega_1^2 \tilde{q}_2^3 + 1.404 \omega_1^2 (\tilde{q}_1^2 + 2 \tilde{q}_1) \tilde{q}_2 = 0 \quad (3.22)$$

where $A_F = A_{F0}/ah$ and ω_1 is the natural frequency of the first mode in infinitesimal amplitude and has the value,

$$\omega_1^2 = \frac{8\pi^4 EI}{m l^4} a^2 \quad (3.23a)$$

It is noticed from Eq. 3.23a that ω_1 is linearly proportional to 'a' and equal to zero when $a = 0$, which corresponds to classical buckling theory. This was the purpose of choosing the first and second buckling modes, Eqs. 3.14 and 3.15, rather than beam vibration modes, Eq. 2.6 for this buckled case. The numerical result of Eq. 3.23 is shown in Fig. 9. The natural frequency of the second mode in infinitesimal amplitude is found from Eq. 3.22 to be

$$\omega_2^2 = 3940. \frac{EI}{m l^4} \quad (3.23b)$$

This result is also plotted in Fig. 9. It is interesting to note that when $a = 2.25$, the first and second mode frequencies become equal.

Let $\omega_F t = n\tau$ and $\tilde{q}_1 = q_1 - 1$, $\tilde{q}_2 = q_2$, Eqs. 3.21 and 3.22 become

$$\begin{aligned} \frac{d^2 \tilde{q}_1}{d\tau^2} + 2n\delta\sqrt{\alpha} \frac{d\tilde{q}_1}{d\tau} + n^2 K_1 \alpha \tilde{q}_1 + n^2 K_2 \alpha \tilde{q}_1^3 + n^2 K_4 \alpha \tilde{q}_1 \tilde{q}_2^2 \\ = n^2 K_3 A_F \sin n\tau \end{aligned} \quad (3.24)$$

$$\begin{aligned} \frac{d^2 \tilde{q}_2}{d\tau^2} + 2n\delta\sqrt{\alpha} \frac{d\tilde{q}_2}{d\tau} + \frac{n^2 K_5}{a^2} \alpha \tilde{q}_2 + n^2 K_6 \alpha \tilde{q}_2^3 \\ + n^2 K_7 \alpha (\tilde{q}_1^2 - 1) \tilde{q}_2 = 0 \end{aligned} \quad (3.25)$$

where n is any integer,

$$K_1 = -.5 \quad , \quad K_2 = .5$$

$$K_3 = 1.333 \quad , \quad K_4 = 2.263$$

$$K_5 = 5.05 \quad , \quad K_6 = 6.356$$

$$K_7 = 1.404 \quad ,$$

$$\alpha = (\omega_1/\omega_F)^2 = 1/\Omega^2$$

$$\xi = c/(2m\omega_1) \quad (3.26)$$

It is readily seen that $q_2 = 0$ satisfies the solution of Eqs. 3.24 and 3.25. The governing differential equation for q_1 when $q_2 = 0$, becomes

$$\frac{d^2 q_1}{d\tau^2} + 2n\xi\sqrt{\alpha} \frac{dq_1}{d\tau} + n^2 K_1 \alpha q_1 + n^2 K_2 \alpha q_1^3 = n^2 K_3 A_F \sin n\tau \quad (3.27)$$

Equation 3.27 is the same form as Eq. 2.15, except with different coefficients in K_1 's. The general solution of Eq. 3.27 before snapping through is the same as in Eqs. 2.19 and 2.20, and will be discussed in the following subsections.

Of course, Eq. 3.27 is valid only when $q_2 = 0$. This means that q_2 does not become parametrically excited by the first mode oscillations q_1 , i.e., any infinitesimal disturbance in q_2 will eventually die out. The study of the unstable regions for q_2 will be discussed in Section 4.2. For the present Section 3, the specific cases to be studied will deal with the $q_2 = 0$ solution, i.e., Eq. 3.27.*

*The effects of SPHM order 3/2 is less important than those of SPHM order 2 and 3 and will not be discussed here.

3.2 Specific Cases

3.2.1 SHM and SPHM Order 3

The solutions of these cases can be obtained from Eqs. 2.20 with $n = 1$. For simplicity, first consider the $\zeta = 0$ case in which y_1, x_2 and y_3 are equal to zero and $r_1 = x_1, r_2 = y_2, r_3 = x_3$, then Eqs. 2.20 becomes

$$A_0 y_0 + \frac{3}{4} K_2 \alpha (2 r_1 r_2 r_3 - r_1^2 r_2) = 0 \quad (3.28a)$$

$$A_1 r_1 + \frac{3}{4} K_2 \alpha \left[4 y_0 (r_2 r_3 - r_1 r_2) - r_3 (r_1^2 + r_2^2) \right] = K_3 A_F \quad (3.28b)$$

$$A_2 r_2 + \frac{3}{2} K_2 \alpha \left[y_0 (2 r_1 r_3 - r_1^2) - r_1 r_2 r_3 \right] = 0 \quad (3.28c)$$

$$A_3 r_3 + \frac{3}{4} K_2 \alpha \left[4 y_0 r_1 r_2 - r_1 r_2^2 - \frac{r_1^3}{3} \right] = 0 \quad (3.28d)$$

The existence of y_0 and r_2 components in Eqs. 3.28 is due to the contribution of the quadratic term in Eq. 3.21 or equivalently, the fact that the coefficient k_1 in Eq. 3.27 is negative. For the solution of $|r_1| \gg |r_2|$ and $|r_3|$, further simplification can be made by neglecting r_2 and r_3 components in the equations above and discarding the associated equations 3.28c and d, which leads to

$$A_0 y_0 = 0 \quad (3.29a)$$

$$A_1 r_1 = K_3 A_F \quad (3.29b)$$

Since $y_0 \neq 0$, Eqs. 3.29 becomes

$$A_0 = \alpha \left[K_1 + K_2 \left(y_0^2 + \frac{3}{2} r_1^2 \right) \right] = 0 \quad (3.30)$$

or

$$y_0^2 = -\frac{K_1}{K_2} - \frac{3}{2} r_1^2 \quad (3.31a)$$

and

$$\left(-2K_1\alpha - 1 - \frac{15}{4} K_2\alpha r_1^2 \right) r_1 = K_3 A_F \quad (3.31b)$$

The nonlinear natural frequency relation can be obtained from Eq. 3.31 by setting $A_F = 0$, $r_1 \neq 0$, which gives the 'backbone curve' as

$$r_1^2 = -\frac{4(2K_1\alpha + 1)}{15K_2\alpha} = -\frac{4(2K_1 + \Omega^2)}{15K_2} \quad (3.32)$$

where $\Omega = \omega/\omega_1$, ω is the nonlinear natural frequency and ω_1 is the linear natural frequency.

The numerical results of Eqs. 3.31b and 3.32 are shown in Fig. 10. From the figure, one can see that Eq. 3.31b is a soft-spring type solution and there exists jump points which are the basic information to investigate dynamic snap-through criterion to be discussed in Section 5.2. Similar to the hard-spring case, the backbone curve divides the solution of Eq. 3.31b into two regions. On the left-hand side of the curve, the displacement of SHM is out-of-phase with the base displacement, and the other side is in-phase. In general, Eqs. 3.31 gives very good approximation to the complete solution with small forcing term, $A_F < .2$, and Ω not close to 1/2 or 1/3. For the $A_F > .2$ case, even Ω not close to 1/2 or 1/3, the r_2 component becomes significant although $|r_2|$ is still less than $|r_1|$. Also Eq. 3.27 is a good approximation for the small damping ratio, ζ , case, say $\zeta < .01$.

For the $|r_3| > |r_1| \gg |r_2|$ case, neglecting the r_2 component and discarding the associated Eq. 3.28c gives an approximate solution as

$$A_0 y_0 = 0 \quad (3.33a)$$

$$A_1 r_1 - \frac{3}{4} K_2 \alpha r_3 r_1^2 = K_3 A_F \quad (3.33b)$$

$$A_3 r_3 - \frac{K_2 \alpha}{4} r_1^3 = 0 \quad (3.33c)$$

Since $y_0 \neq 0$, Eq. 3.33a becomes $A_0 = 0$
or

$$y_0^2 = -\frac{K_1}{K_2} - \frac{3}{2} (r_1^2 + r_3^2) \quad (3.34)$$

Similar argument to the SPHM order 3 case of Section 2.1, one can easily show that for the $|r_3| \gg |r_1|$ solution

$$A_3 \approx 0 \quad (3.35)$$

or

$$K_1 \alpha - 9 + \frac{3}{4} K_2 \alpha (4y_0^2 + 2r_1^2 + r_3^2) = 0 \quad (3.36)$$

Placing Eq. 3.34 into Eq. 3.36 gives

$$r_3^2 = -\frac{4(2K_1 \alpha + 9)}{15 K_2 \alpha} - \frac{4}{5} r_1^2 \quad (3.37)$$

Equation 3.37 shows that the $|r_3| > |r_1|$ solution exists only at $-2k_1 - 9\Omega^2 > 0$ or $\Omega < 1/3$ (Note: $k_1 = -.5$, $k_2 = +.5$, $\Omega^2 = 1/\alpha$).
By the assumption $|r_3| \gg |r_1|$, Eq. 3.37 can be approximated as

$$r_3^2 \approx -\frac{4(2K_1\alpha + 9)}{15K_2\alpha} \quad (3.38)$$

(Note: + sign for r_3 will give the stable solution). Eliminating y_0 and r_3 components in Eqs. 3.33b by using Eqs. 3.34 and 3.38 gives

$$\left\{ 6.2 - .4 K_1\alpha - K_2\alpha \left[3.75 r_1^2 + \sqrt{\frac{-24(2K_1\alpha + 9)}{K_2\alpha}} r_1 \right] \right\} r_1 = K_3 A_F \quad (3.39)$$

For the small A_F case, say $A_F < .2$. Equations 3.34, 3.38 and 3.39 give almost identical result for y_0 , r_1 and r_3 as from Eqs. 3.33. The numerical results of Eqs. 3.34, 3.38 and 3.39 for r_1 and r_3 corresponding to SPHM order 3 are shown in Fig. 11. They appear to bifurcate from the main SHM solution near where the "shifted backbone curve order 3." i.e., Eq. 3.38, intersects the SHM solution.

The details of the actual transition between these two solutions, $|r_1| > |r_3|$ and $|r_3| > |r_1|$, can be found by solving the complete Eqs. 3.28 and is shown in Fig. 12. (Note: Eqs. 3.28 give a very small r_2 component while not affecting y_0 , r_1 and r_3 of Eqs. 3.33. This negligible r_2 component is not shown in the figure.) The r_1 and r_3 components of the upper branch solution are out-of-phase with the base displacement; for the lower branch solution, r_1 is out-of-phase and r_3 is in-phase. Incidentally, it is interesting to know that for the complete Eqs. 3.28 there exists a certain solution in which $r_2 = 0$. From Eq. 3.28c, it is readily seen that the $r_2 = 0$ solution occurs at $r_1 = 2r_3$. The numerical results of Eqs. 3.28 show that the $r_2 = 0$ solution occurs before the jump point of the third harmonic component with the predominant r_1 component.

For the $\zeta \neq 0$ case, the complete Eqs. 2.20 has to be solved. In order to obtain the solution of SPHM order 3, the critical damping ration, ζ , must be very small. An approximate damping criterion for the existence of SPHM order 3 can be obtained by neglecting the r_2 component, which leads to Eq. 2.31. Similarly, Eqs. 3.34, 3.38 and 3.39 give a good approximation for the $\zeta < .001$ case.

3.2.2 SPHM Order 2

For the $\zeta = 0$ case, Eqs. 3.28 still are applicable to the solution of SPHM order 2. By the assumption $|r_2| > |r_1| \gg |r_3|$, the r_3 component can be neglected. Discarding the associated Equation 3.28d, the approximate solution becomes

$$A_0 y_0 - \frac{3}{4} K_2 \alpha r_2 r_1^2 = 0 \quad (3.40a)$$

$$A_1 r_1 - 3 K_2 \alpha y_0 r_1 r_2 = K_3 A_F \quad (3.40b)$$

$$A_2 r_2 - \frac{3}{2} K_2 \alpha y_0 r_1^2 = 0 \quad (3.40c)$$

Equations 3.40a and c can be rearranged as

$$K_1 \alpha y_0 + K_2 \alpha \left(y_0^3 + \frac{3}{2} r_2^2 y_0 + \frac{3}{2} r_1^2 y_0 - \frac{3}{4} r_1^2 r_2 \right) = 0 \quad (3.41)$$

$$(K_1 \alpha - 4) r_2 + \frac{3}{4} K_2 \alpha \left(4 y_0^2 r_2 + r_2^3 + 2 r_1^2 r_2 - 2 y_0 r_1^2 \right) = 0 \quad (3.42)$$

For the $|y_0| > |r_2| \gg |r_1|$ case, the underline terms in Eqs. 3.41 and 3.42 will drop out leaving the following two simple equations as

$$y_0^2 = - \frac{K_1}{K_2} - \frac{3}{2} r_2^2 \quad (3.43)$$

$$K_1 \alpha - 4 + \frac{3}{4} K_2 \alpha (4 y_0^2 + r_2^2) = 0 \quad (3.44)$$

Solving Eqs. 3.43 and 3.44 will give

$$y_0^2 = -\frac{K_1}{K_2} - \frac{2(2K_1 \alpha + 4)}{5K_2 \alpha} \quad (3.45a)$$

$$r_2^2 = -\frac{4(2K_1 \alpha + 4)}{15K_2 \alpha} \quad (3.45b)$$

Equation 3.45b is the "shifted backbone curve order 2," which shows that the SPHM order 2 solution exists only for $\Omega < .5$. Substituting Eqs. 3.45 into Eq. 3.40b will give a simple equation in r_1 as (Note: for stable solution r_2 is negative)

$$\left\{ 2.2 - .4 K_1 \alpha + 4 K_2 \alpha \left[-\frac{K_1}{K_2} + \frac{2(2K_1 \alpha + 4)}{5K_2 \alpha} \right]^{1/2} \left[\frac{-4(2K_1 \alpha + 4)}{15K_2 \alpha} \right]^{1/2} + \frac{3}{4} K_2 \alpha r_1^2 \right\} r_1 = K_3 A_F \quad (3.45c)$$

For the small A_F case, say $A_F < .2$, Eqs. 3.45 give a close result as from Eqs. 3.40.

The numerical results of Eq. 3.45 are shown in Fig. 13. They appear to bifurcate from the main SHM solution near where the "shifted backbone curve order 2" intersects the SHM solution.

The complete solution can be obtained by solving Eqs. 3.28 which give a very small r_3 component while not affecting y_0 , r_1 and r_2 of Eqs. 3.40. The numerical results of Eqs. 3.28 are shown in Fig. 14 (Note: the small r_3 component is not shown in the figure). The upper branch solution r_1 is positive and r_2 is negative; for the lower branch solution, r_1 and r_2 are positive.

Eqs. 3.45 or Eqs. 3.28 also give a good approximation for the small $\zeta < .001$ case.

3.3 Exact Solution of Free Vibration

Since the free vibration form of Eq. 3.27 is the same as Eq. 2.44, (except now $k_1 = -.5$, $k_2 = +.5$), Equation 2.47 also is the solution for free vibrations. For the case of the smaller vibrations without snap-through, the lower bound, q_l , is taken to be the root of the equation,

$$K_1 + .5 K_2 (q_u^2 + q_l^2) = 0 \quad (3.46)$$

or

$$q_l = \pm \left(-\frac{2K_1}{K_2} - q_u^2 \right)^{1/2} \quad (3.47)$$

Note: q_l is taken to have the same sign as q_u . Since the quantity in the square root has to be positive, it leads to a conclusion that free vibrations without snap-through exist if and only if

$$|q_u| < \sqrt{\frac{-2K_1}{K_2}} = \sqrt{2} \quad (3.48)$$

Or, it is equivalent to say that the total energy, e , in Eq. 2.45 has to be less than zero.

For $|q_u| > \sqrt{2}$ case, free vibrations with snap-through will take place, and the lower bound q_l in Eq. 2.47 becomes $q_l = -q_u$ which is a root of $q_u^2 - q_l^2 = 0$ in Eq. 2.47. Due to the symmetrical property of the integrand of Eq. 2.47, the snap-through free vibration solution can be obtained from Eq. 2.48 with $|q_u| > \sqrt{2}$.

The numerical results of the exact free vibration solutions are shown in Fig. 15 plotted with $r_1 = .5(q_u - q_l)$ versus $\Omega = \omega/\omega_1$. (Note the gap between the two solutions at $\Omega = 0$ reflects the transition from one-sided vibrations to symmetric, equal-sided

vibrations once snap-through has been achieved.) Figure 15 also shows the approximate solution for the vibrations without snap-through as obtained from the 'backbone curve' of Eq. 3.32. The agreement is seen to be good here. The approximate solution of free vibrations with snap-through can be obtained from Eqs. 3.28 by setting $A_F = y_0 = r_2 = 0$ and neglecting r_3 component and its associated Equation 3.28d, which gives

$$r_1^2 = \frac{4}{3K_2} (\Omega^2 - K_1) \quad (3.49)$$

where $\Omega = \omega/\omega_1$ and ω is the nonlinear frequency of snap-through case. These results are also shown in Fig. 15. It is seen that the approximation is good for $r_1 > 1.8$.*

3.4 Numerical Analysis of Steady State Solutions

Here, the Runge-Kutta numerical integration method is employed to investigate the steady state periodic solutions of Eq. 3.27. The initial conditions for solving Eq. 3.27 are taken from the steady state solutions obtained in Section 3.2, and a time increment $\Delta\tau = .05$ radians was used. Some typical steady state responses obtained numerically are shown in Fig. 16-19. From these figures it is seen that two solutions (upper and lower branches) exist at a certain frequency Ω , depending on the initial conditions. The steady state response of the upper branch solution can be obtained by using the numerical results presented in Section 3.2 as the initial conditions for all values of amplitude $|r_1|$ up to about 0.4. When the initial conditions corresponding to a value of amplitude $|r_1|$ greater than 0.4 are used, however, the response solution to the upper branch becomes unobtainable, and the resulting solution goes to the lower branch solution at the same Ω . This implies that the steady state solution obtained in Section 3.2 is a good approximation for those cases where the maximum amplitude is less than 0.4.

*For lower values of r_1 , the r_3 component should be included in the free vibration solution.

SECTION 4

STABILITY CONDITION OF THE PERIODIC SOLUTIONS

4.1 Stability Condition of the Periodic Solutions

The periodic steady state solutions determined by the method in Sections 2 and 3 are not always existent, but are actually able to exist only so long as they are stable. To investigate the stability of the equilibrium states, one may employ the variational method.⁷

One assumes,

$$q_i = q_{1s} + \eta \quad (4.1)$$

where q_{1s} is the steady state solution Eq. 2.19 which satisfies Eq. 2.17, and η is the infinitesimal variation from equilibrium state. Substituting Eq. 4.1 into Eq. 2.17 and only keeping the first order terms in η gives

$$\frac{d^2\eta}{d\tau^2} + 2n\beta\sqrt{\alpha} \frac{d\eta}{d\tau} + (K_1 n^2 \alpha + 3K_2 n^2 q_{1s}) \eta = 0 \quad (4.2)$$

Now, placing the steady state solution q_{1s} which is Eq. 2.19 into Eq. 4.2 and using new variable $\bar{\tau} = \tau/2$, will result in the extended form of the Mathieu-Hill equation,

$$\frac{d^2\eta}{d\bar{\tau}^2} + 4n\beta\sqrt{\alpha} \frac{d\eta}{d\bar{\tau}} + \left[\theta_0 + 2 \sum_{\nu=1}^6 (\theta_{S\nu} \sin 2\nu\bar{\tau} + \theta_{C\nu} \cos 2\nu\bar{\tau}) \right] \eta = 0 \quad (4.3)$$

where

$$\theta_0 = 4n^2\alpha \left[K_1 + 1.5 K_2 (2y_0^2 + x_1^2 + y_1^2 + x_2^2 + y_2^2 + x_3^2 + y_3^2) \right]$$

$$\theta_{s1} = 6n^2K_2\alpha (2y_0x_1 - x_1y_2 + y_1x_2 - x_2y_3 + y_2x_3)$$

$$\theta_{s2} = 6n^2K_2\alpha (2y_0x_2 + x_1y_1 + y_1x_3 - x_1y_3)$$

$$\theta_{s3} = 6n^2K_2\alpha (2y_0x_3 + x_1y_2 + y_1x_2)$$

$$\theta_{s4} = 6n^2K_2\alpha (x_1y_3 + y_1x_3 + x_2y_2)$$

$$\theta_{s5} = 6n^2K_2\alpha (x_2y_3 + y_2x_3)$$

$$\theta_{s6} = 6n^2K_2\alpha x_3y_3$$

(4.4)

$$\theta_{c1} = 6n^2K_2\alpha (2y_0y_1 + x_1x_2 + y_1y_2 + x_2x_3 + y_2y_3)$$

$$\theta_{c2} = 6n^2K_2\alpha (.5y_1^2 - .5x_1^2 + 2y_0y_2 + x_1x_3 + y_1y_3)$$

$$\theta_{c3} = 6n^2K_2\alpha (2y_0y_3 - x_1x_2 + y_1y_2)$$

$$\theta_{c4} = 6n^2K_2\alpha (.5y_2^2 - .5x_2^2 + y_1y_3 - x_1x_3)$$

$$\theta_{c5} = 6n^2K_2\alpha (-x_2x_3 + y_2y_3)$$

$$\theta_{c6} = 3n^2K_2\alpha (y_3^2 - x_3^2)$$

Following the same procedures as in Hayashi⁷, except here more terms are involved for the general purpose and better accuracy, the unstable solutions of Eq. 4.3 of the form

$$\eta = e^{\mu \bar{t}} \left\{ \sum_{k=1}^3 \left[b_{2k-1} \sin(2k-1)\bar{t} + C_{2k-1} \cos(2k-1)\bar{t} \right] \right\} \quad (4.5)$$

will result if

$$\Delta_{\text{odd}} =$$

$$\begin{vmatrix} \theta_0 - 1 - \theta_{c1} & \theta_{s1} - 4n\beta\sqrt{\alpha} & \theta_{c1} - \theta_{c2} & \theta_{s2} - \theta_{s1} & \theta_{c2} - \theta_{c3} & \theta_{s3} - \theta_{s2} \\ \theta_{s1} + 4n\beta\sqrt{\alpha} & \theta_0 - 1 + \theta_{c1} & \theta_{s1} + \theta_{s2} & \theta_{c1} + \theta_{c2} & \theta_{s2} + \theta_{s3} & \theta_{c2} + \theta_{c3} \\ \theta_{c1} - \theta_{c2} & \theta_{s1} + \theta_{s2} & \theta_0 - 9 - \theta_{c3} & \theta_{s3} - 12n\beta\sqrt{\alpha} & \theta_{c1} - \theta_{c4} & \theta_{s4} - \theta_{s1} \\ \theta_{s2} - \theta_{s1} & \theta_{c1} + \theta_{c2} & \theta_{s3} + 12n\beta\sqrt{\alpha} & \theta_0 - 9 + \theta_{c3} & \theta_{s1} + \theta_{s4} & \theta_{c1} + \theta_{c4} \\ \theta_{c2} - \theta_{c3} & \theta_{s2} + \theta_{s3} & \theta_{c1} - \theta_{c4} & \theta_{s1} + \theta_{s4} & \theta_0 - 25 - \theta_{c5} & \theta_{s5} - 20n\beta\sqrt{\alpha} \\ \theta_{s3} - \theta_{s2} & \theta_{c2} + \theta_{c3} & \theta_{s4} - \theta_{s1} & \theta_{c1} + \theta_{c4} & \theta_{s5} + 20n\beta\sqrt{\alpha} & \theta_0 - 25 + \theta_{c5} \end{vmatrix} < 0. \quad (4.6)$$

Similarly, unstable solutions of the form

$$\eta = e^{\mu \bar{t}} \left\{ \sum_{k=0}^3 \left[b_{2k} \sin 2k\bar{t} + C_{2k} \cos 2k\bar{t} \right] \right\} \quad (4.7)$$

will result if

$$\Delta_{\text{even}} =$$

θ_0	θ_{s1}	θ_{c1}	θ_{s2}	θ_{c2}	θ_{s3}	θ_{c3}
$2\theta_{s1}$	$\theta_0 - 4 - \theta_{c2}$	$\theta_{s2} - 8n\beta\sqrt{\alpha}$	$\theta_{c1} - \theta_{c3}$	$\theta_{s3} - \theta_{s1}$	$\theta_{c2} - \theta_{c4}$	$\theta_{s4} - \theta_{s2}$
$2\theta_{c1}$	$\theta_{s2} + 8n\beta\sqrt{\alpha}$	$\theta_0 - 4 + \theta_{c2}$	$\theta_{s1} + \theta_{s3}$	$\theta_{c1} + \theta_{c3}$	$\theta_{s2} + \theta_{s4}$	$\theta_{c2} + \theta_{c4}$
$2\theta_{s2}$	$\theta_{c1} - \theta_{c3}$	$\theta_{s1} + \theta_{s3}$	$\theta_0 - 16 - \theta_{c4}$	$\theta_{s4} - 16n\beta\sqrt{\alpha}$	$\theta_{c1} - \theta_{c5}$	$\theta_{s5} - \theta_{s1}$
$2\theta_{c2}$	$\theta_{s3} - \theta_{s1}$	$\theta_{c1} + \theta_{c3}$	$\theta_{s4} + 16n\beta\sqrt{\alpha}$	$\theta_0 - 16 + \theta_{c4}$	$\theta_{s1} + \theta_{s5}$	$\theta_{c1} + \theta_{c5}$
$2\theta_{s3}$	$\theta_{c2} - \theta_{c4}$	$\theta_{s2} + \theta_{s4}$	$\theta_{c1} - \theta_{c5}$	$\theta_{s1} + \theta_{s5}$	$\theta_0 - 36 - \theta_{c6}$	$\theta_{s6} - 24n\beta\sqrt{\alpha}$
$2\theta_{c3}$	$\theta_{s4} - \theta_{s2}$	$\theta_{c2} + \theta_{c4}$	$\theta_{s5} - \theta_{s1}$	$\theta_{c1} + \theta_{c5}$	$\theta_{s6} + 24n\beta\sqrt{\alpha}$	$\theta_0 - 36 + \theta_{c6}$

< 0

(4.8)

Utilizing the above results, it is seen that small disturbances to the steady-state solutions $\eta(\bar{\tau})$ will grow if either Δ_{odd} or Δ_{even} is negative. This defines an unstable steady-state solution. All of the steady-state solutions studied in Sections 2 and 3 have been examined by this stability analysis. The unstable steady-state solutions are shown by dash-lines in the previously mentioned figures.

4.2 Stability Analysis of the Second Mode Solution

As mentioned in Section 3.1, to insure the only existence of the first mode solution q_1 , the second mode solution q_2 in Eq. 3.25 must not be parametrically excited by the first mode oscillations. To investigate the stability of q_2 in Eq. 3.25, one may employ the method used by Lock,¹⁷ Van Gulick,²⁰ etc., in which q_2 is taken as an infinitesimal variational variable. Substituting

the steady-state solution q_1 which satisfies Eq. 3.27 into Eq. 3.25 and neglecting its higher order term, q_2^3 , one can obtain the same equation as Eq. 4.3 with the same time variable $\bar{\tau}$, except here one has now,

$$\begin{aligned} K_1 &= \frac{5.05}{a^2} - 1.404 \\ K_2 &= .468 \end{aligned} \tag{4.9}$$

Then the stability criterion for q_2 can be easily obtained by substituting the new variables of Eq. 4.9 into Eqs. 4.4, 4.6, and 4.8.

Numerical evaluations of these stability determinants, Eqs. 4.6 and 4.8, were carried out for the SHM, SPHM order 3, and SPHM order 2 solutions. These were evaluated for the range $\Omega < 1.2$, $|r_i| < 0.4$, and the initial static deflection variable 'a' = 0.5 to 5.0. These numerical results showed that unstable solutions of q_2 appeared only when 'a' > 2.0. For all experimental and theoretical cases considered here, 'a' was less than 2.0 and hence, the second mode did not play any role here.

In order to better understand this effect of the initial static deflection 'a' on the stability of the second mode q_2 , the following simplified stability investigation for the no damping, $\zeta = 0$, case was made. Assuming the SHM motion for the first mode,

$$q_{1s} = y_0 + x_1 \sin \tau \tag{4.10}$$

the stability equation for the second mode will be Eq. 4.3 where θ_0 , θ_{s1} , and θ_{c2} are given by Eqs. 4.4 and all other θ 's are zero. From Eq. 3.31a, one has

$$y_0^2 = 1 - \frac{3}{2} x_1^2 \tag{4.11}$$

and this together with K_1 and K_2 from Eq. 4.9 yields

$$\theta_0 = \frac{20.2}{a^2 \Omega^2} - \frac{5.616}{\Omega^2} x_1^2 \quad (4.12a)$$

$$\theta_{s1} = \frac{5.616}{\Omega^2} x_1 \sqrt{1 - 1.5 x_1^2} \quad (4.12b)$$

$$\theta_{c2} = - \frac{1.404}{\Omega^2} x_1^2 \quad (4.12c)$$

Using the simplified, uncoupled forms for the stability determinants of Eqs. 4.6 and 4.8, the stability boundaries for $\zeta = 0$ can be expressed roughly as,⁷

$$\theta_0 = n^2 \pm \theta_n \quad \text{for } n = 1, 2, 3, \dots \quad (4.13)$$

where

$$\theta_n \equiv \left[\theta_{cn}^2 + \theta_{sn}^2 \right]^{1/2}$$

These give the conventional V-shaped instability regions in the θ_n, θ_0 plane. One may replot these θ_n, θ_0 stability boundaries onto the x_1, Ω plane of the q_1 solution by solving Eqs. 4.12 together with Eqs. 4.13. For $n = 1$, this gives the boundaries

$$\Omega^2 = \frac{20.2}{a^2} - 5.616 \left(x_1^2 \pm x_1 \sqrt{1 - 1.5 x_1^2} \right) \quad (4.14)$$

while for $n = 2$, it gives

$$\Omega^2 = \frac{5.05}{a^2} - 1.404 x_1^2 (1 \pm .25) \quad (4.15)$$

Typical results of this approximate analysis are shown in Fig. 20 for 'a' = 2. For higher values of 'a', it can readily be seen from Eqs. 4.14 and 4.15 that both of these unstable regions will move further to the left and cause instability of the q_2 mode at lower frequencies Ω .

A similar stability analysis can be made assuming SPHM motion for the first mode to be either

$$q_{1S} \approx y_0 + x_3 \sin 3\tau \quad (4.16)$$

or

$$q_{1S} \approx y_0 + y_2 \cos 2\tau \quad (4.17)$$

For both of these cases, the results for the stability boundaries reduce to the exact same form as Eqs. 4.14 and 4.15, but with Ω^2 replaced by $(k\Omega)^2$ where $k = 2$ for SPHM order 2 and $k = 3$ for SPHM order 3. Since the amplitude-frequency curves for these SPHM responses are essentially "shifted backbone" curves themselves, these criteria will again show that the SPHM responses cannot cause instability of the q_2 mode for $a < 2.25$.

The preceding approximate analyses indicate clearly the trends to be expected from the more complete numerical analysis using the complete stability determinants, Eqs. 4.6 and 4.8. It is of interest to recall that at $a = 2.25$, the natural frequency of the first mode ω_1 equals that of the second mode ω_2 . See Figure 9.

SECTION 5

SNAP-THROUGH ANALYSIS

5.1 Numerical Analysis of Snapping Phenomena

According to the previous stability analysis, one can always find two stable steady-state solutions for the buckled beam at frequencies just below $\Omega = 1/k$, where $k = 1, 2, 3, \dots$ etc. In reality, the upper-branch solution may not be obtained due to the dynamic overshoot which causes the beam to snap through during its attempt to achieve this upper-branch solution. This snapping phenomenon generally occurs near jump points. To study this phenomenon, one has to solve Eq. 3.27 directly by numerical methods. Here, the Runge-Kutta numerical integration method is employed using a time increment $\Delta\tau = 0.05$ radians. The calculations were performed at the vicinity of jump points. In the majority of the cases treated, the damping coefficient $\zeta = 0.001$ was considered, and the following initial condition (I.C.) was employed:

$$q_1 = 1.0 \quad , \quad \frac{dq_1}{d\tau} = 0 \quad ; \quad \text{at } \tau = 0 \quad . \quad (5.1)$$

The snap-through region is shown in Fig. 21 plotted with the nondimensional forcing amplitude A_F versus Ω . The boundary of the snap-through region is defined as follows. If one increases Ω from zero to the first occurrence of snap-through while keeping A_F constant, then the first frequency Ω for which snap-through occurs is taken as a point on the boundary for that A_F . The locus of these points is the boundary of snap-through.

Some typical snapping behavior is given in Figs. 22 through 24. In Fig. 22, the predominant SHM component before the taking place of snap-through is noted. This kind of response is called SHM snap-through. The values of A_F for this SHM snap-through case are $0.02 < A_F < 0.25$, which correspond to the Ω 's lying in the

range $0.91 > \Omega > 0.63$. For the $A_F < 0.02$ case, there is no SHM snap-through and the upper branch solution can always be obtained. Similarly from Figs. 23 and 24, one can see the SPHM order 3 and 2 snap-through responses in which the components of SPHM order 3 and 2, respectively, become significant before the occurrence of snap-through. These SPHM snap-through boundaries together with SHM snap-through can be clearly seen in Fig. 21.

The inclusion of the small damping coefficient $\zeta = 0.001$, will not affect the critical snap-through values of A_F for the cases of SHM and SPHM order 2 as compared with the nondamping case, but it will greatly affect the critical values of A_F for the SPHM order 3 case. The damping effect on the SPHM order 3 case can be seen by the comparison of Figs. 23 and 25. In order to obtain the SPHM order 3 snap-through, the damping coefficient ζ must be less than 0.001. For the case $\zeta < 0.001$ considered here, the critical values of A_F are the same as those of the non-damping case.

It is interesting to compare the static snap-through load (see Appendix B) to the dynamic ones found here. The static force-deflection relation, as obtained in Appendix B, is shown in Fig. 26. For the dynamic case, the amplitude of external load, F_d , (lb/in), is

$$F_d = m \omega_F^2 a h A_F \quad (5.2)$$

and the critical static load, $F_{S_{crl}}$, (lb/in), which is uniformly distributed on the beam, is (see Eq. B.10)

$$F_{S_{crl}} = f_{S_{crl}} m \omega_1^2 a h \quad (5.3)$$

From Eqs. 5.2 and 5.3 one can obtain

$$\frac{F_d}{F_{scr1}} = \frac{\Omega^2 A_F}{f_{scr1}} = \frac{\Omega^2 A_F}{.144} \equiv R \quad (5.4)$$

The dynamic to static force ratio, R , can be obtained by substituting the critical value A_F with the corresponding Ω on the snap-through boundary and is shown in Fig. 27. It is to be noted that ratios of R much less than unity can cause SHM snap-through.

Employing the Runge-Kutta numerical integration method, the free vibration solution of Eq. 3.27 can also be obtained by setting $\Omega = 1.0$ (or $\alpha = 1$) and $A_F = 0$. One typical numerical solution is shown in Fig. 28 with $\zeta = 0.001$ and initial condition:

$$\delta_1 = 1.5 \quad , \quad \frac{d\delta_1}{d\tau} = .0 \quad ; \quad \text{at} \quad \tau = 0 \quad .$$

From Fig. 28, it is easily seen that the response of very large amplitude vibrations with snap-through has the hard-spring-type behavior in which the frequency increases with increasing amplitude. Contrarily, the response of smaller amplitude vibrations without snap-through has the soft-spring-type behavior in which frequency decreases with increasing amplitude. This agrees with the frequency behavior shown in Fig. 15.

The state-plane diagram of the free vibration solution also can be obtained directly by the Runge-Kutta numerical integration method. The diagram is shown in Fig. 29 in which one can see the almost periodic harmonic oscillation at amplitude less than 0.4. This fact leads to the conclusion that the steady-state solutions obtained in Section 3 are sufficiently accurate only when the amplitudes $|r_1|$ are less than 0.4 approximately.

The vibrational behavior of the straight and the buckled beam are summarized in Fig. 30. These show the vibration motion

superimposed on the nonlinear static force-deflection curves for each beam case. For the buckled beam, the transition from the soft spring case at low amplitudes to the hard spring case at large amplitudes is clearly apparent.

5.2 Continuous SHM Snap-Through

The discussion of the preceding Section 5.1 related to the first onset of snap-through, and the response was characterized by an intermittent snap-through behavior. See Figs. 22 to 24. This intermittent snap-through behavior also persists generally at higher forcing amplitudes A_F and higher frequencies ω_F . However under certain conditions, a well-defined, continuous snap-through behavior may exist. This will be discussed briefly here for the case of SHM motion.

An approximate solution for continuous SHM snap-through can be obtained from Eqs. 3.28 by setting $y_0 = r_2 = 0$ and neglecting r_3 component and its associated Eq. 3.28d. This gives simply,

$$(K_1 \alpha - 1 + \frac{3}{4} K_2 \alpha r_1^2) r_1 = K_3 A_F \quad (5.5)$$

Numerical results for this continuous SHM snap-through solution Eq. 5.5 are shown in Fig. 31, together with the previous without snap-through SHM solution Eq. 3.31b. Only the stable branches of each solution are shown. It is to be noted that the condition $|r_1| = |y_0|$ acts as a cut-off to the without snap-through solution, since above this $|r_1|$, the one-sided vibrations spill over to the other side and cause snap-through.

A typical continuous SHM snap-through response is shown in Fig. 32. This was obtained as before by using the Runge-Kutta numerical integration method to solve Eq. 3.27 directly. The development of a continuous SHM snap-through is readily apparent. Another response at the same forcing frequency Ω but with a higher A_F took a much longer time to get to the continuous SHM snap-through solution.

SECTION 6

EXPERIMENTAL INVESTIGATION

6.1 Test Setup

The overall test setup for the nonlinear vibrations of the straight and buckled beams is shown in Fig. 33. The schematic sketch for the overall setup is given in Fig. 34. A spring steel beam (see Fig. 33) with 18-in. length and 0.021-in. x 0.5-in. cross section was rigidly mounted on a shake table. This was the only specimen used for the experimental work. In order to reduce the gravitational effect, the beam was placed such that the axis of the maximum bending rigidity was perpendicular to the gravitational direction. The shake table was oscillated horizontally, and generated a harmonic excitation over a frequency range from 2 to 50 cps. The amplitude and frequency of the shake table was measured by using strain gages mounted on a thin auxiliary beam which was bolted on one end to the shake table and the other end to a big steel channel bar. The response of the test beam specimen was measured by using a capacitor probe at the midpoint of the beam. A two channel Sanborn recorder was used to record the responses of the table and of the beam specimen.

6.2 Test Procedures

6.2.1 Straight Beam Vibration

The clamped-clamped beam, which had a basic frequency $\omega_0 = 13.4$ cps, was subject to some small initial tension to give a natural frequency ω_1 of about 20 cps. It was found that some small tension in the beam was practically unavoidable and the presence of initial tension would reduce the change in natural frequency ω_1 during the test. To obtain the minimum change in natural frequency ω_1 , the test period was taken as short as possible in order to have reliable data. The output of strain gages

was calibrated by using a dial gage to measure the actual amplitude of the table under very low frequency oscillation. By this method, the output of the strain gages appeared to be linearly proportional to the amplitude of the table (see Fig. 35). The static output of the capacitor probe was also calibrated by using a dial gage to measure the distance between the probe and the beam -- with only the probe position being varied. After completing the calibration, the probe was fixed at an appropriate position which had a correspondingly calibrated position on the recorder paper. This correspondingly calibrated position on the recorder paper was called the center position. The center position generally would drift down initially about 1 unit of recording paper out of a total of 10 units in abscissa, but then remained approximately at this final position. Checking the center position drift, it was found that all the first calibration points had drifted down equal units along the abscissa (see Fig. 36). With this drift phenomenon in mind, one can obtain the correct test data so long as one knows the center position before each test run. From Fig. 36, one also can see the insensitive portion of calibration line at the large probe-beam distance. In order to obtain more accurate data, the experimental results, amplitudes of oscillation, were taken according to the sensitive portion -- from center position up to the higher unit of the recording paper. This method had been proved to be valid by checking the small amplitude oscillation which showed symmetry about the center position. During a test run, the experimental data was collected within a very short period, say 2 to 4 minutes, in order to obtain almost constant natural frequency ω_1 during the test.

The static load-deflection was obtained by applying a load at the midpoint of the beam. This is shown in Fig. 37, and one can see the symmetry about the straight line position. The critical damping ratio ζ was found from a transient decay test to be $\zeta = 0.0006$ approximately, and is shown in Fig. 38. It was observed

that the natural frequency of the beam for the large amplitude agreed well with the nonlinear theory relation,

$$\omega = \omega_1 \sqrt{1 + .491 r_1^2} \quad (6.1)$$

where r_1 is the nondimensional amplitude of the oscillations. The experimental results of nonlinear frequency are shown plotted in Figs. 2 and 8, where now $\Omega = \omega/\omega_1$.

Some typical responses of SHM, SPHM, and SBHM as obtained experimentally are shown in Fig. 39. The top trace shows the beam response, while the lower trace shows the base motion. All frequencies are in cps, and the top scale is nonlinear because of the capacitor probe characteristics. Experimental steady-state amplitudes from these responses are shown plotted versus frequency Ω in Figs. 3 through 7, together with the previous theoretical results. In some cases, different superharmonic motions were found to exist at the same forcing frequency ω_F , depending on the initial kick given the beam. The experimental results of SBHM order 3 were not able to be obtained due to the limit frequency of the shake table.

6.2.2 Buckled Beam

The same beam as in the straight beam case was also used here. The beam was compressed to buckle with the nondimensional initial static deflection 'a' approximately equal to 1.5. Checking the symmetric property about the straight beam position, it was found that the initial static deflection 'a' was equal on either side and so was the natural frequency of either side. The test procedure was taken the same as mentioned previously, except, here an almost linear calibration line of the capacitor probe was used by taking advantage that the amplitude was small before the occurrence of snap-through.

The damping coefficient ζ was found to be approximately 0.0007 from a transient decay test. The natural frequency of the

beam for large amplitude but without snap-through agreed well with the nonlinear theory relation

$$\omega = \omega_1 \sqrt{1 - 1.875 \eta_1^2} \quad (6.2)$$

The experimental results of nonlinear frequency without and with snap-through are shown plotted in Figs. 10 and 15 where now, $\Omega = \omega/\omega_1$. Also, Fig. 40 shows an experimental record of the free vibration response in which one can see the hard and soft spring-type responses with and without snap-through, respectively.

Some typical responses of SHM and SPHM, as obtained experimentally, are shown in Fig. 41. Again, the top trace is the beam response, while the lower trace is the base motion. Experimental steady-state amplitudes from these responses are shown in Figs. 11 to 14, together with the previous theoretical results. Also, some typical snapping-through responses of SHM and SPHM obtained experimentally are shown in Figs. 42 through 45.

SECTION 7

COMPARISON OF THEORY AND EXPERIMENT

7.1 Straight Beam Case

The experimental results of nonlinear frequency relation given in Figs. 2 and 8 show that the backbone curve solution is a good approximation. In Fig. 3, one can see that the SHM steady-state amplitudes obtained experimentally agree well with theory for $|r_1| < 1.0$, and for $|r_1| > 1.0$, the experimental results give a little higher $|r_1|$ than the theory. Also from Fig. 3, the good agreement of experiment with theory for the case of SPHM order 2, 3 and 3/2 is seen. The bifurcation from SHM solution is noticed, and one can see the amplitude of the component corresponding to the forcing frequency decreases as Ω increases. It can also be seen that at the same Ω , multiple solutions can be obtained experimentally. Some experimental results for the case of SPHM order 3 and 2 are shown in Figs. 4 and 6 in which one can see the components of SPHM are very close to the shifted backbone curve with some small correction as given by theory

$$r_k^2 = \frac{4(k^2\Omega^2 - K_1)}{3K_2} - 2r_1^2 \quad (7.1)$$

where $k = 2, 3, 3/2$, etc.

The larger the external forcing amplitude A_F , the less dominant is the amplitude of the SPHM component in comparison to the forcing frequency component. This is not obviously seen from Fig. 4, due to the small r_1 component present, but can be seen easily in Fig. 6. Some experimental results of SHM, SBHM order 2/3 and 1/2 are given in Fig. 7 which shows that the agreement between experiment and theory is reasonable. Some typical experimental responses of SHM, SPHM and SBHM are shown in Fig. 39 where the simple ratio between the response and forcing frequencies can

be counted as 1, 3/1, 2/1, 3/2, 2/1, and 2/3. In the SPHM case, due to the small effective external force, $\Omega^2 A_F$, the SPHM component is dominant. In the SBHM cases, one can see the SBHM component is not so dominant, and is not much greater than the external forcing frequency component because of the large effective external force.

7.2 Buckled Beam Case

The experimental points of linear natural frequency versus initial static deflection 'a' agree well with theory as seen in Fig. 9. No experimental points with $a > 2.0$ was obtained due to the second mode becoming unstable. Figures 10 and 15 show good agreement of the experimental results for nonlinear frequency with the theory. An experimental and a theoretical record of free vibration response are shown in Figs. 40 and 28, respectively. Both figures show the similar behavior, i.e., hard-spring-type responses at large amplitudes with snap-through and soft-spring-type responses at smaller amplitudes without snap-through.

The experimental steady-state amplitudes of SPHM order 3 and 2 are shown in Figs. 11 and 13, respectively. Good agreement with theory is obtained.* Figure 41 shows some typical experimental responses of SHM, SPHM order 3 and 2. The simple ratio between response and forcing frequencies is counted as 1/1, 3/1, and 2/1.

Figure 42 shows an experimental record of the SHM snap-through phenomenon with strong SHM component before the occurrence of snap-through. This SHM snap-through phenomenon can also be obtained theoretically by numerical integration method as shown in

* For the SPHM order 3 case, the complete solution, Eqs. 3.28, shown in Fig. 12 agrees better with the experimental points than the approximate solution, Eqs. 3.34, 3.38, and 3.39 given in Fig. 11. This is because the approximate solution is good for $A_F < 0.2$ while the present results are for $A_F = 0.3$.

Fig. 22. Similarly, Figs. 43 and 44 show the experimental results of SPHM order 3 and 2 snap-through, and the predominant components of SPHM order 3 and 2 before snapping through are obvious. These SPHM snap-through phenomena also appear in theoretical results as given in Figs. 23 and 24. The experimental SHM and SPHM snap-through boundaries are shown in Fig. 21, and they seem to match reasonably the theoretical boundaries obtained by numerical integration. Basically, these boundaries appear to be the jump points of SHM and SPHM steady-state solutions. Fig. 45 shows an experimental record of continuous SHM snap-through. This behavior also appears in the theoretical results shown in Fig. 32. At higher amplitudes A_F and the same forcing frequency ω_F , the snap-through became intermittent.

SECTION 8

CONCLUSIONS

8.1 Straight Beam Case

1. In addition to the conventional SHM response for the Duffing equation, there exist other solutions of SPHM order $k = 3/2, 2, 3, \dots$ and SBHM order $k = 2/3, 1/2, 1/3, \dots$ at $\Omega > 1/k$. These additional solutions give superharmonic and subharmonic component amplitudes near the "shifted backbone curve," i.e., replacing Ω by $k\Omega$ in the basic backbone curve, $r^2 = 4(\Omega^2 - k_1)/(3k_2)$. For small forcing amplitudes A_F and very small damping, all these additional solutions are dominated by the superharmonic and subharmonic components, and tend to have the system oscillate near its own natural frequency ω_1 . For larger A_F , these additional solutions involve substantial forcing frequency components as well as the superharmonic and subharmonic components.
2. In the SPHM cases, theoretical and experimental results show that with fixed A_F the amplitude $|r_1|$ corresponding to the external forcing frequency decreases as Ω increases. This behavior is opposite to the conventional perturbation assumption^{8,9,11,12} which assumes $|r_1| = |A_F \omega_F^2 / (\omega_1^2 - \omega_F^2)|$ with $\omega_F < \omega_1$ and gives monotonically increasing $|r_1|$ as ω_F (or Ω) increases.
3. These solutions of SPHM and SBHM are stable over a significant range of their amplitudes. They seem to bifurcate from the main SHM solutions near where the "shifted backbone curve" intersects the SHM solution. For small forcing amplitudes A_F , this bifurcation point would be near $\Omega = 1/k$. The SHM solution itself is unstable near these bifurcation points.

4. Multiple solutions may exist at a fixed Ω depending on the initial conditions.
5. The present analysis agrees well with experiments which were performed for relatively small forcing amplitudes A_F .

8.2 Buckled Beam Case

1. In the present case, the solution is a soft-spring type at small amplitudes before snapping through, and a hard-spring type at large amplitudes after snapping through.
2. For small amplitudes without snap-through, there exist in addition to the conventional SHM solution for the governing differential equation, other solutions of SPHM order $k = 2, 3, \dots$. For small A_F , these additional solutions give SPHM component amplitudes near the "shifted backbone curve order k ," i.e., replacing Ω by $k\Omega$ in the basic backbone curve, $r_1^2 = -4(\Omega^2 + 2k_1)/(15 k_2)$. For small A_F and very small damping, all these additional solutions are dominated by the SPHM components, and tend to have the system oscillate near its own natural frequency ω_1 . For large A_F , these additional solutions involve substantial forcing frequency components as well as the SPHM components.
3. These solutions of SPHM are stable over a significant range of their amplitudes. They seem to bifurcate from SHM solution near where the "shifted backbone curve" intersects the SHM solution. For small A_F , these bifurcation points would be near $\Omega = 1/k$. The SHM solution itself is unstable near these bifurcation points.

4. Multiple solutions may exist at a fixed Ω depending on the initial conditions.
5. One mode approximation is good for initial static deflection 'a' < 2.0 and Ω < 1. Second mode has to be included in the solution for 'a' > 2.0 case, since it may be parametrically excited by the first mode oscillations at Ω < 1.
6. Linear natural frequency ω_1 is linearly proportional to the initial static deflection 'a', with $\omega_1 = 0$ at a = 0 and $\omega_1 = \omega_2$ at a = 2.25.
7. The steady state solution is valid for the maximum response amplitude to be less than 0.4.
8. Dynamic overshoot in transient period will cause the beam to snap-through. The snapping phenomenon generally occurs at jump points of SHM and SPHM solutions.
9. The snap-through behavior is usually intermittent. Under certain conditions, a well-defined, continuous SHM snap-through may exist.
10. The present analysis agrees well with the experiments.

8.3 General

In the present investigation, it has been attempted to show the importance of superharmonics, subharmonics, and snap-through in understanding the vibration behavior of straight and buckled beams. The techniques and the results obtained here can be extended to plates, curved panels, and shells in order to better understand their vibration behavior.

APPENDIX A

NEWTON ITERATION METHOD

Let X be an n -dimensional column vector with components x_1, x_2, \dots, x_n and $G(X)$ an n -dimensional column vector valued functions with components $g_1(X), g_2(X), \dots$. The system to be solved is

$$X = G(X) \tag{A.1}$$

The solution (or roots) of Eq. A.1 is some vector, Γ , with components $\gamma_1, \gamma_2, \dots, \gamma_n$ which, of course, is some point in the n -dimensional space. Starting with a point $X^0 = [x_1^0, x_2^0, \dots, x_n^0]$, then the iteration scheme is proceed as

$$X^{(i+1)} = G(X^{(i)}), \quad i = 0, 1, 2, 3, \dots \tag{A.2}$$

provided that the solution of A.1 is convergent for a sufficient close guess of X^0 . (For convergent criteria, see Isaacson and Keller³¹).

In general case, the system to be solved is of the form

$$F(X) = 0 \tag{A.3}$$

where $F(X) = [f_1(X), f_2(X), \dots, f_n(X)]$ is an n -dimensional column vector. Such a system can be rewritten in the form of Eq. A.1 with

$$G(X) = X - A(X)F(X) \tag{A.4}$$

where $A(X)$ is an n square matrix. The Eqs. A.1 and A.4 will have the same set of solutions if $A(X)$ is nonsingular [since in the case $A(X)F(X) = 0$ implies $F(X) = 0$].

In Newton's method one chooses

$$A(X) = J^{-1}(X) \quad (\text{A.5})$$

where

$$J(X) = \left(\frac{\partial f_i(X)}{\partial x_k} \right)$$

$$= \begin{pmatrix} \frac{\partial f_1}{\partial x_1} & \frac{\partial f_1}{\partial x_2} & \cdots & \frac{\partial f_1}{\partial x_n} \\ \frac{\partial f_2}{\partial x_1} & \frac{\partial f_2}{\partial x_2} & \cdots & \frac{\partial f_2}{\partial x_n} \\ \vdots & \vdots & \ddots & \vdots \\ \frac{\partial f_n}{\partial x_1} & \frac{\partial f_n}{\partial x_2} & \cdots & \frac{\partial f_n}{\partial x_n} \end{pmatrix} \quad (\text{A.6})$$

whose determinant is the Jacobian of the function $f_j(X)$. Placing Eq. A.5 into Eq. A.4 the iterations for the Newton's method are:

$$X^{(i+1)} = X^{(i)} - J^{-1}(X^{(i)}) F(X^{(i)}), \quad i=0,1,2,\dots \quad (\text{A.7})$$

From Eq. A.7 one can easily obtain the Newton's iteration for a single function $f(x)$, in which Eq. A.7 reduces to

$$x^{(i+1)} = x^{(i)} - f(x^{(i)}) / \left(\frac{\partial f(x^{(i)})}{\partial x} \right) \quad (\text{A.8})$$

APPENDIX B

STATIC SNAP-THROUGH LOAD

The governing differential equation of a static problem, having a load uniformly distributed on the buckled beam, can be directly obtained from Eq. 3.1 discarding all the time derivative terms in the right hand side of the equal sign and replacing $m \frac{d^2 W_B}{dt^2}$ by a static force F_s - lb/in, which leads to

$$EI \frac{d^4}{dx^4} (W+W_0) - \frac{d}{dx} \left[N_x \frac{d}{dx} (W+W_0) \right] = -F_s \quad (B.1)$$

$$N_x = -P_0 + \frac{EA}{2l} \int_0^l \left[\frac{d}{dx} (W+W_0) \right]^2 dx \quad (B.2)$$

Now substituting Eqs. 3.3, 3.5, 3.6 and 3.7 into Eqs. B.1 and B.2 and following the same expressions and procedures as in Section 3.1 one can obtain (as Eqs. 3.21 and 3.22)

$$\omega_1^2 \tilde{q}_1 + \frac{3}{2} \omega_1^2 \tilde{q}_1^2 + \frac{1}{2} \omega_1^2 \tilde{q}_1^3 + 2.263 \omega_1^2 (\tilde{q}_1 + 1) \tilde{q}_2^2 = -\frac{4F_s}{3ma^2k} \quad (B.3)$$

$$\frac{5.05}{a^2} \omega_1^2 \tilde{q}_2 + 6.356 \omega_1^2 \tilde{q}_2^3 + 1.404 \omega_1^2 (\tilde{q}_1^2 + 2\tilde{q}_1) \tilde{q}_2 = 0 \quad (B.4)$$

ω_1^2 - same as Eq. 3.23a

With $\tilde{q}_1 = q_1 - 1$, $\tilde{q}_2 = q_2$, Eqs. B.3 and B.4 becomes

$$\frac{1}{2} q_1 - \frac{1}{2} q_1^3 + 2.263 q_1 q_2^2 = \frac{4}{3} f_s \quad (B.5)$$

$$\frac{5.05}{a^2} q_2 + 6.356 q_2^3 + 1.404 (q_1^2 - 1) q_2 = 0 \quad (B.6)$$

where $f_s = F_s / (ma\hbar\omega_1^2)$

In Eqs. B.5 and B.6, one can easily see that one solution is $q_2 = 0$ which gives

$$q_1 - q_1^3 = \frac{8}{3} f_s \quad (\text{B.7})$$

Equation B.7 is the deflection-loading relation of the first mode solution, and is plotted in Fig. 26. The first mode snap-through occurs at

$$\frac{df_s}{dq_1} = 0 \quad \text{and} \quad \frac{d^2f}{dq_1^2} < 0 \quad (\text{B.8})$$

which gives

$$f_{s_{crit}} = .144 \quad , \quad \text{at} \quad (q_1)_{crit} = .577 \quad (\text{B.9})$$

or

$$F_{s_{crit}} = f_{s_{crit}} ma\hbar\omega_1^2 = 112.2 \frac{EI\hbar a^3}{l^4} \quad (\text{B.10})$$

To obtain the second mode snap-through load, one can solve Eqs. B.5 and B.6 with $q_2 \neq 0$. Equation B.6 becomes,

$$\frac{5.05}{a^2} + 6.356 q_2^2 + 1.404 (q_1^2 - 1) = 0 \quad (\text{B.11})$$

Solving Eqs. B.5 and B.11 gives

$$q_1 = .742 a^2 f_s \quad (\text{B.12a})$$

$$q_2^2 = .221 - \frac{.795}{a^2} - .121 a^4 f_s^2 \quad (\text{B.12b})$$

The numerical results of Eqs. B.12 with varying initial imperfection 'a' are also shown in Fig. 26. The second mode snap-through will take place before the first mode one, if and only if the bifurcation point, $(q_1)_B$ (the intersecting point of Eqs. B.7 and B.12a) is greater than $(q_1)_{cr1}$, that is,

$$(q_1)_B = \sqrt{1 - \frac{3.60}{a^2}} > .577 \quad (\text{B.13})$$

From Eq. B.13, one can easily obtain that the second mode snap-through occurs only at

$$a > 2.32 \quad (\text{B.14})$$

The corresponding $(f_s)_B$ to the $(q_1)_B$ of Eq. B.13 is

$$(f_s)_B = \frac{1.35}{a^2} \sqrt{1 - \frac{3.60}{a^2}} \quad \text{at } a > 2.32 \quad (\text{B.15})$$

In summary, the snap-through load is $f_{s_{cr1}}$ for the $a < 2.32$ case; and becomes $(f_s)_B$ at $a > 2.32$.

REFERENCES

1. McLachlan, N.W. Theory and Application of Mathieu Functions. Dover Publications, New York, N.Y., 1964.
2. Bolotin, V.V. Dynamic Stability of Elastic Systems. Holden-Day Inc., San Francisco, California, 1964.
3. Weidenhammer, F. "Das Stabilitätsverhalten der nichtlinearen Biegeschwingungen des axial pulsierend belasten Stabes," Ingenieur Archiv, Bd. 24, pp. 53-68, 1956.
4. Minorsky, N. Nonlinear Oscillations. D. Van Nostrand Co., Princeton, New Jersey, 1962.
5. Dugundji, J. and Chhatpar, C.K. Dynamic Stability of a Pendulum under Parametric Excitation. Massachusetts Institute of Technology, Aeroelastic and Structures Research Laboratory Report TR 134-4, Air Force Office of Scientific Research AFOSR 69-0019TR, December 1968.
6. Stoker, J.J. Nonlinear Vibrations. Interscience Publishers, 1966.
7. Hayashi, C. Nonlinear Oscillations in Physical Systems. McGraw-Hill Book Co., Inc., New York, N.Y., 1964.
8. Caughey, T.K. "The Existence and Stability of Ultraharmonics and Subharmonics in Forced Nonlinear Oscillations." J. of Applied Mechanics. pp. 520-525, December 1957.
9. Kronauer, R.E. and Musa, S. "Necessary Conditions for Subharmonic and Superharmonic Synchronization in Weakly Nonlinear Systems." Quarterly J. Applied Mathematics, pp. 153-160, Vol. XXIV, No. 2, 1966.
10. Tondl, A. "On the Internal Resonance of a Nonlinear System with Two Degrees of Freedom." Nonlinear Vibration Problems (Second Conference on Nonlinear Vibrations, Warsaw, 1962), Vol. 5, pp. 205, 1964.

11. Mettler, E. "Stability and Vibration Problems of Mechanical Systems under Harmonic Excitation." Dynamic Stability of Structures, Proceedings of an International Conference held at Northwestern University, Evanston, Illinois, October 1965, Pergamon Press, pp. 169-188, 1967.
12. Tamura, H. "Higher Approximation on Nonlinear Steady Oscillation." Proceedings of the Fourteenth Japan National Congress for Applied Mechanics 1964, Tokyo, Japan, Sept. 7-8; Tokyo, Japan, Central Scientific Publishers, pp. 205-213, December 1965.
13. Atkinson, C.P. "Superharmonic Oscillations as Solutions to Duffing's Equation as Solved by an Electronic Differential Analysis." J. of Applied Mechanics. pp. 520-525, December 1957.
14. Szemplinska-Stupnicka, W., "Higher Harmonic Oscillations in Heteronomous Non-Linear Systems with One Degree of Freedom." International J. Non-Linear Mechanics, Vol. 3, pp. 19-30, Pergamon Press, 1968.
15. Herrmann, G. Dynamic Stability of Structures, Proceedings of an International Conference held at Northwestern University, Evanston, Illinois, October 18-20, 1965. Pergamon Press, 1967.
16. Humphreys, J.S. "Dynamic Snap Buckling of Shallow Arches." AIAA Journal, pp. 878-886, May 1966.
17. Lock, M.H. "Snapping of a Shallow Sinusoidal Arch under a Step Pressure Load." AIAA Journal, pp. 1249-1256, July 1966.
18. Humphreys, J.S. "The Adequacy of Energy Criterion for Dynamic Buckling." AIAA Journal, pp. 921-923, May 1966.
19. Gjelsvik, A. and Bodner, S.R. "The Energy Criterion and Snap-Buckling of Arches." J. Eng. Mech. Div., AM. Soc. Civil Engrs. pp. 89-134, October 1962.

20. Van Gulick, L.A., Flexural Arch Vibrations, Princeton University, Department of Aerospace and Mechanical Sciences, Report 833, June 1968.
21. Fitch, J.R. The Buckling and Postbuckling Behavior of Spherical Caps under Concentrated Load." International J. of Solids and Structures 4, No. 4, pp. 421-446, April 1968.
22. Ziegler, H. Principles of Structural Stability, Waltham, Mass. Blaisdell Publishing Co., 1968.
23. Anderson, D.L. and Lindberg, H.E. "Dynamic Pulse Buckling of Cylindrical Shells under Transient Lateral Pressures." AIAA Journal, Vol. 6, No. 4, pp. 589-598, April 1968.
24. Pian, T.H.H. and Bucciarelli, L.L. Jr., "Buckling of Radially Constrained Circular Rings under Distributed Loading." Internal. J. of Solids and Structures, Vol. 3, No. 5, pp. 715-730, Sept. 1969.
25. Navaratna, D.R., Pian, T.H.H., and Witmer, E.A. "Stability Analysis of Shells of Revolution by the Finite-Element Method." AIAA Journal, Vol. 6, No. 2, pp. 355-361, Feb. 1968.
26. Budiansky, B. and Roth, R.S. "Axisymmetric Dynamic Buckling of Clamped Shallow Spherical Shells." Collected Papers on Instability of Shell Structures - 1962, NASA Langley Research Center TND-1510, December 1962.
27. Lindberg, H.E. and Herbert, R.E. "Dynamic Buckling of a Thin Cylindrical Shell under Axial Impact." American Society of Mechanical Engineers Paper 65 - APMW-17, August 1965.
28. Goodier, J.N. and McIvor, I.K. "The Elastic Cylindrical Shell under Nearly Uniform Radial Impulse." J. Appl. Mech., Vol. 31, pp. 259-266, 1964.
29. Abramowitz, M. and Stegryn, I.A. Handbook of Mathematical Functions, AMS 55, National Bureau of Standards, June 1964.

30. Bisplinghoff, R.L. and Pian, T.H.H. On the Vibrations of Thermally Buckled Bars and Plates. Proc. 9th International Congress of Applied Mechanics, Vol. 7, pp. 307-318, Brussels, 1957. Also Massachusetts Institute of Technology, Aeroelastic and Structures Research Laboratory, Technical Report 25-22, Office of Naval Research Contract N 5 ori-07833, ONR Project NR-064-259, Sept. 1956.
31. Isaacson, E. and Keller, H.B. Analysis of Numerical Methods. John Wiley and Sons, Inc., New York 1966.

Note: Gravitation force \perp paper.
 $W_0 = 0$ for the straight beam case.

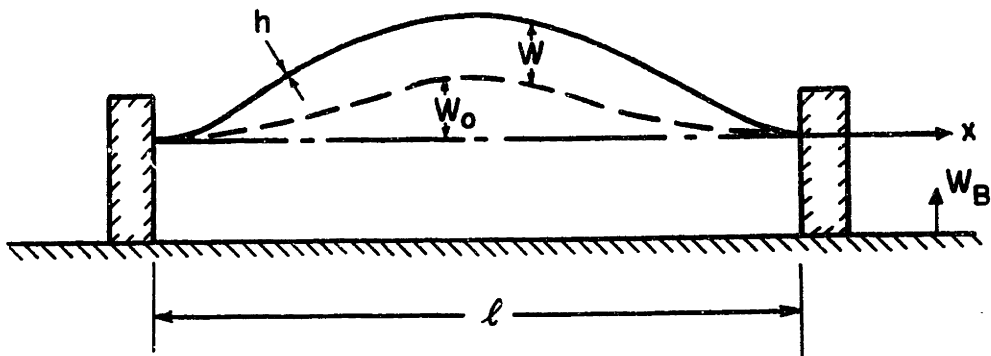


FIG.1 BASIC CONFIGURATION

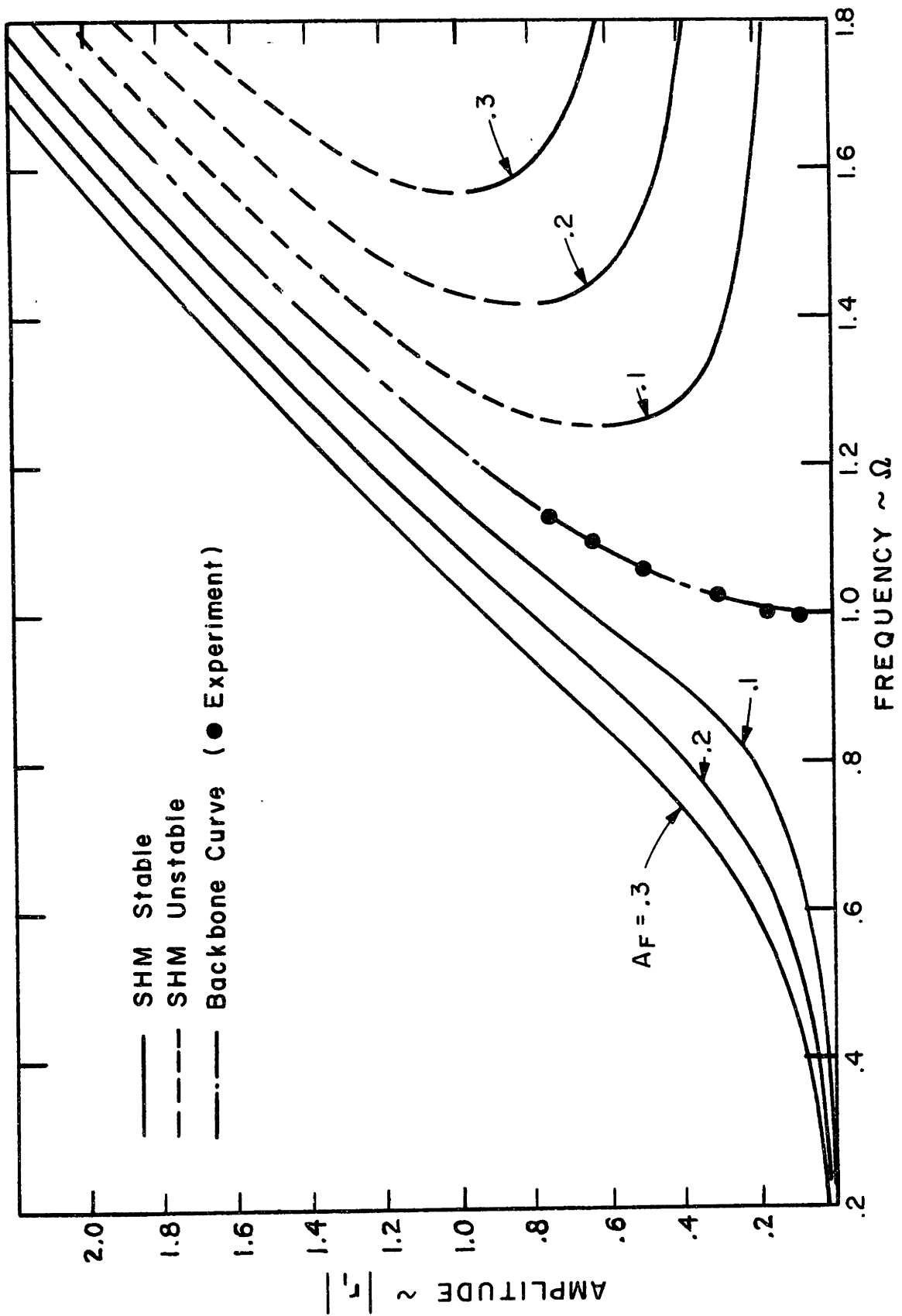


FIG. 2 SHM SOLUTION - STRAIGHT BEAM

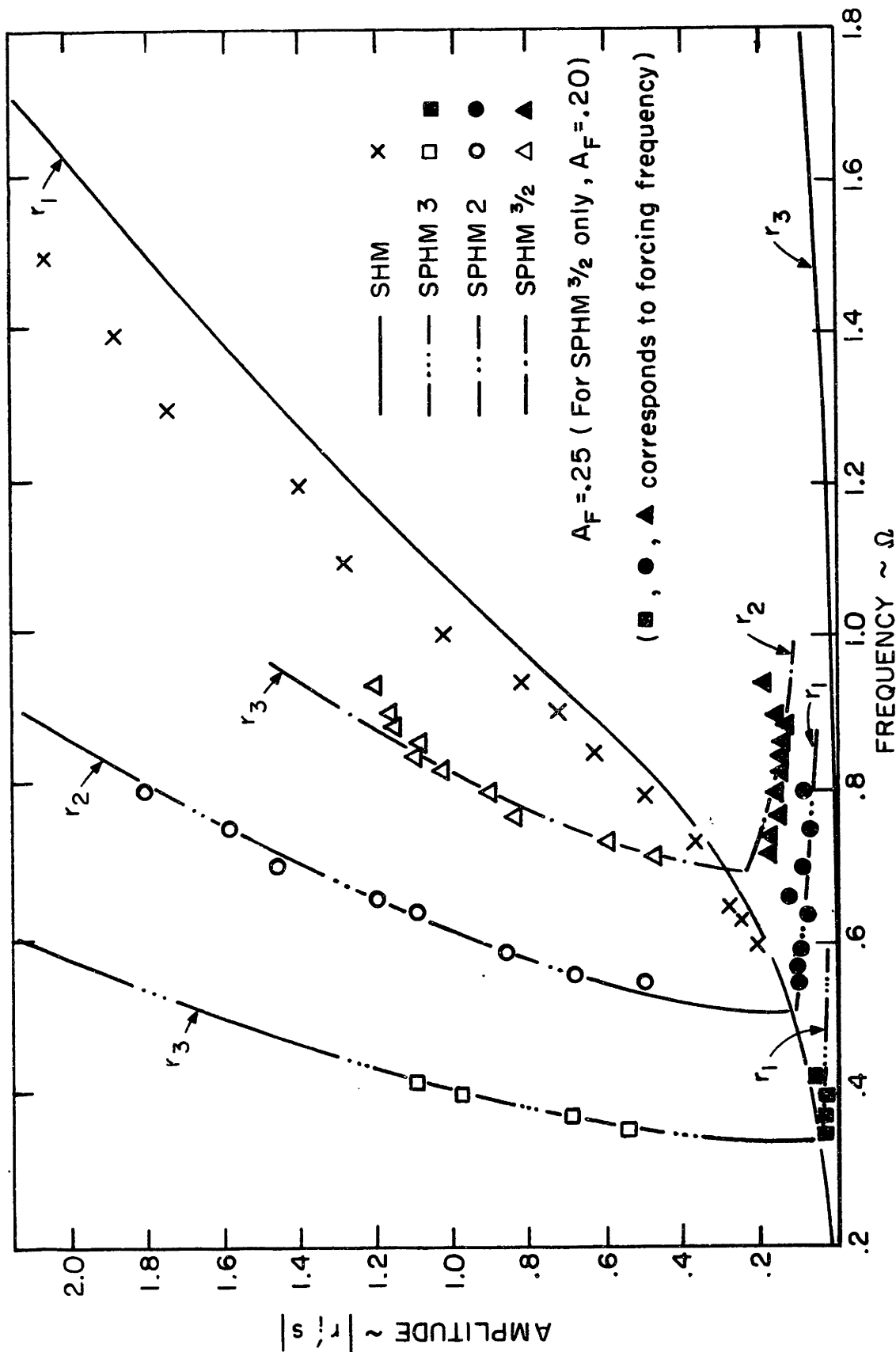


FIG. 3 OVERALL STEADY STATE RESPONSE - SPHM

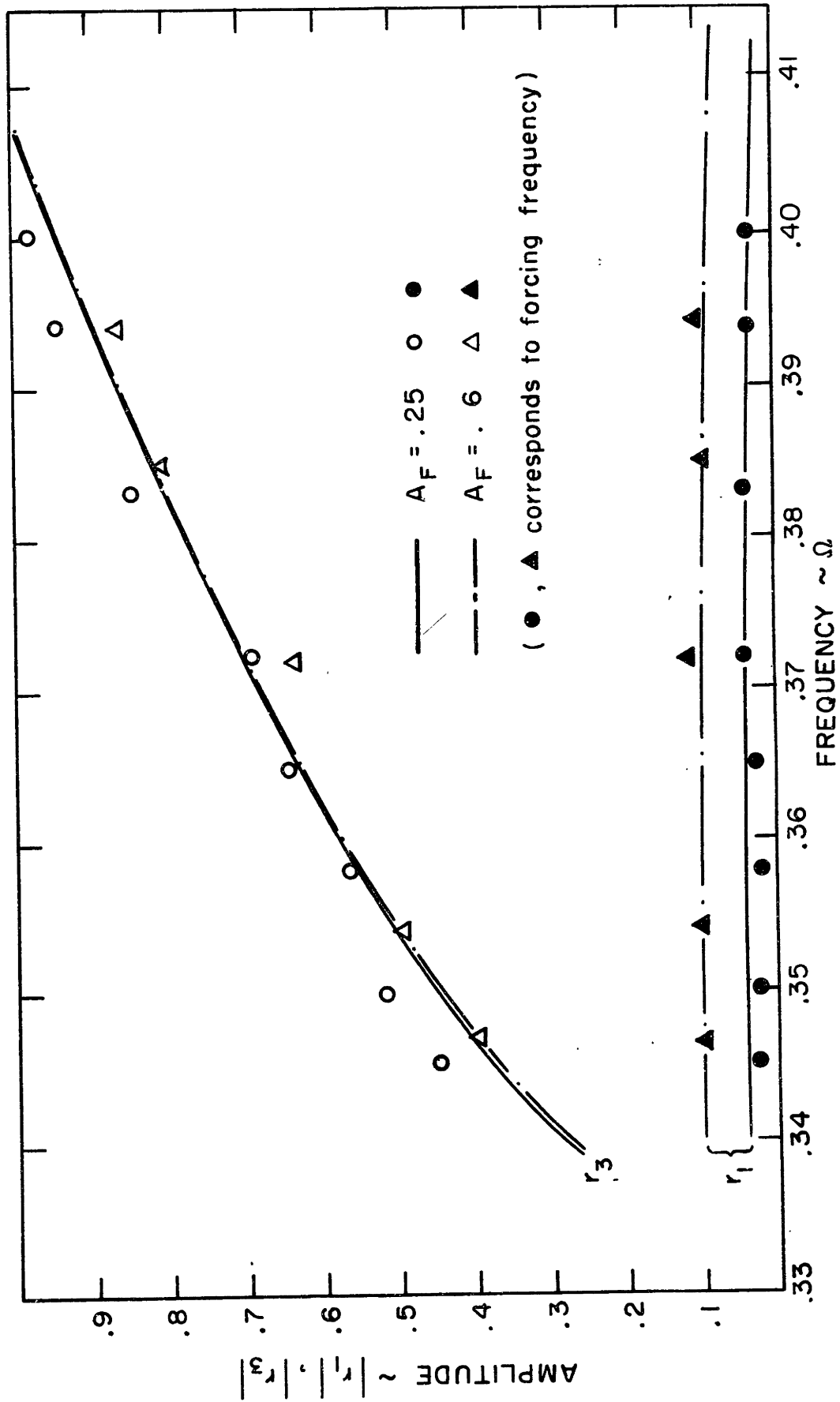


FIG. 4 SPHM ORDER 3 SOLUTION

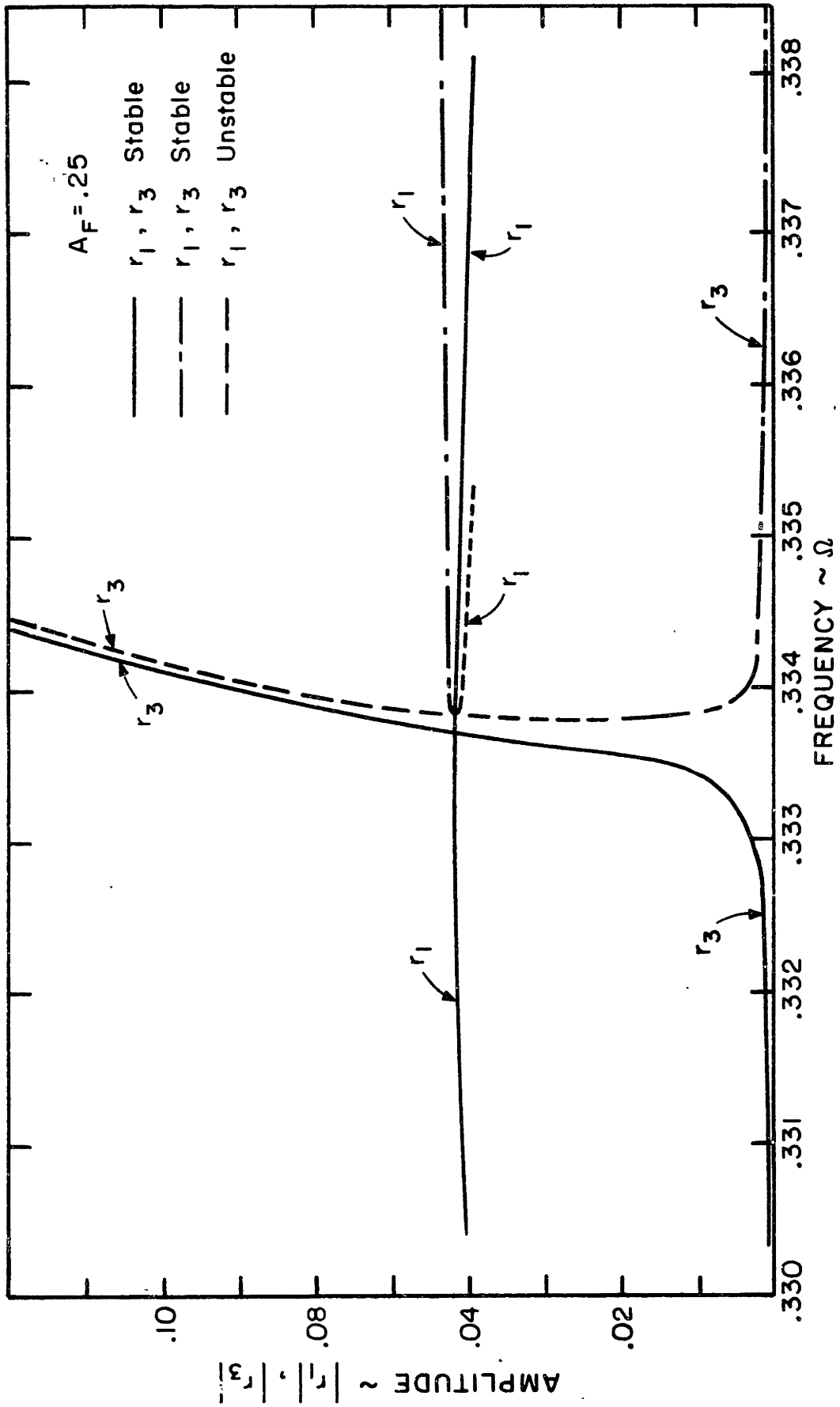


FIG. 5 DETAIL OF TRANSITION OF SPHM ORDER 3

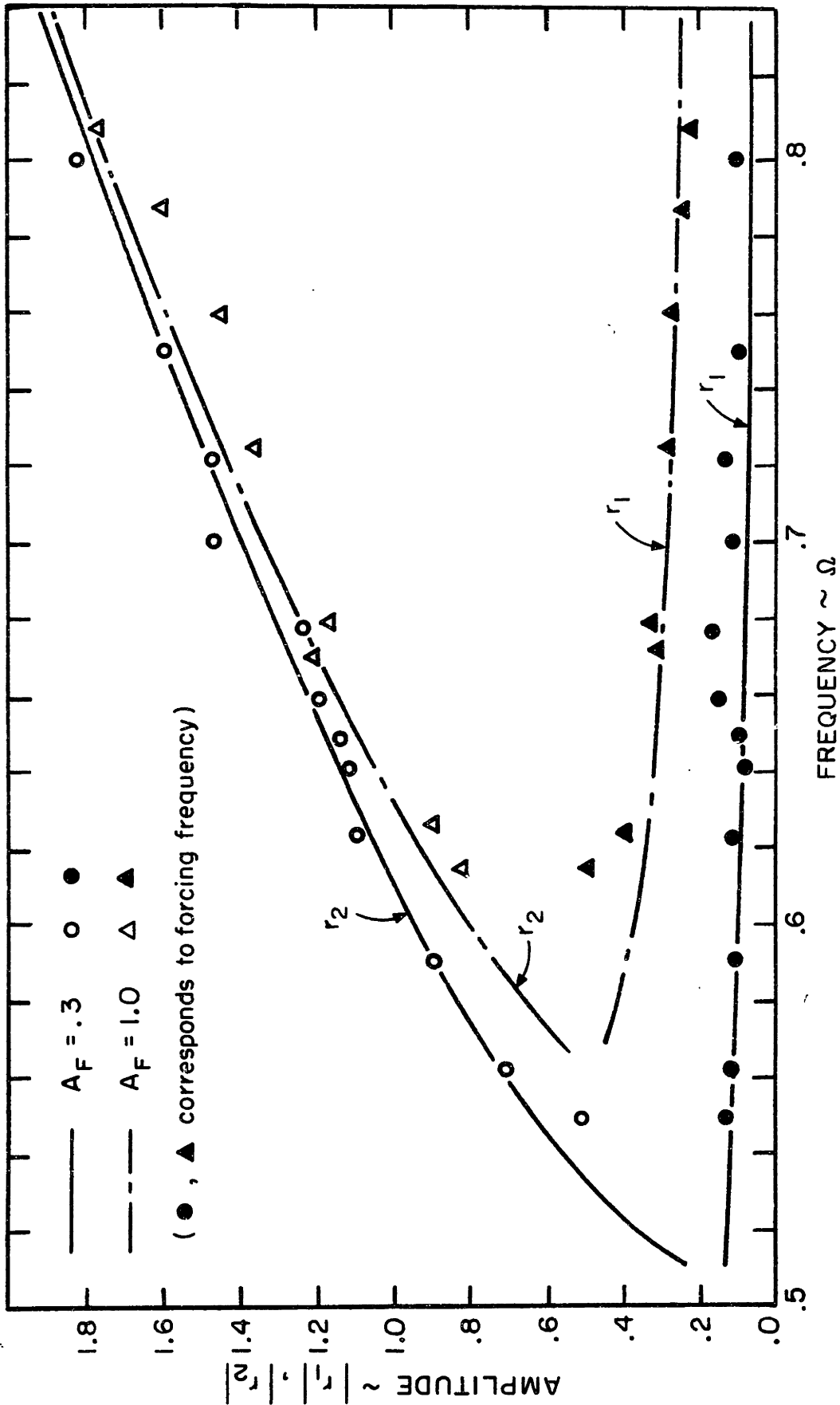


FIG.6 SPHM ORDER 2 SOLUTION

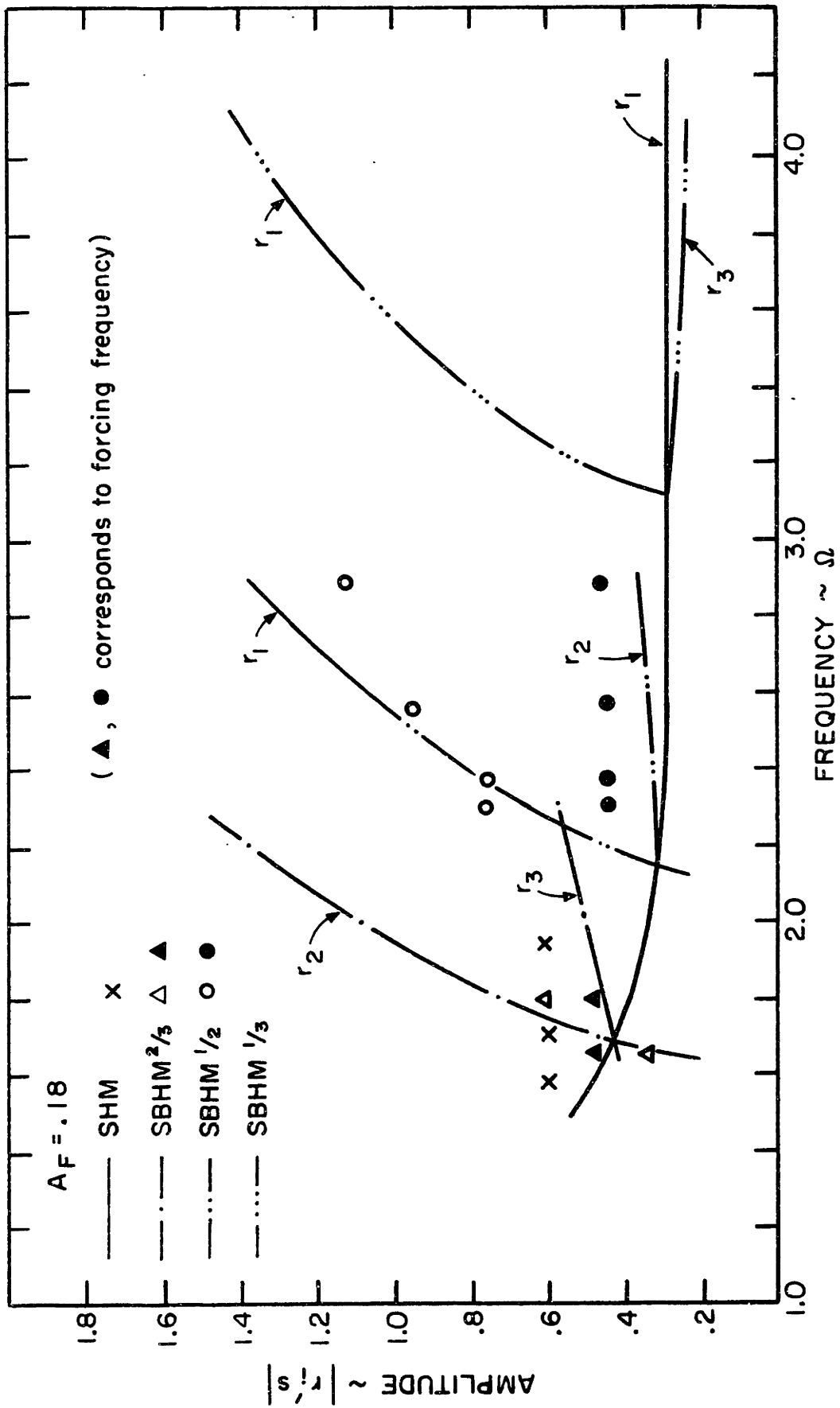


FIG. 7 OVERALL STEADY STATE RESPONSE - SBHM

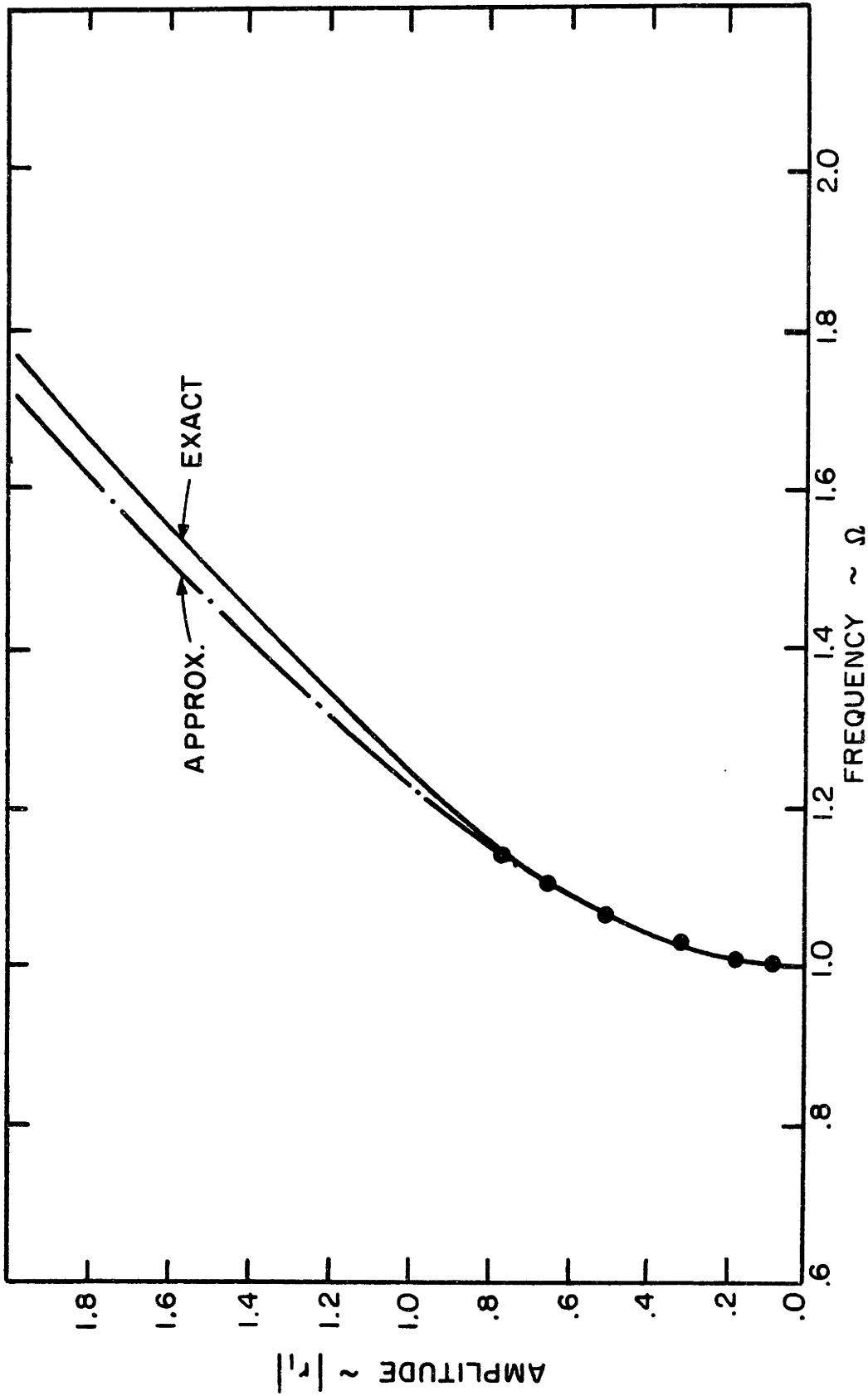


FIG.8 NONLINEAR NATURAL FREQUENCY - STRAIGHT BEAM

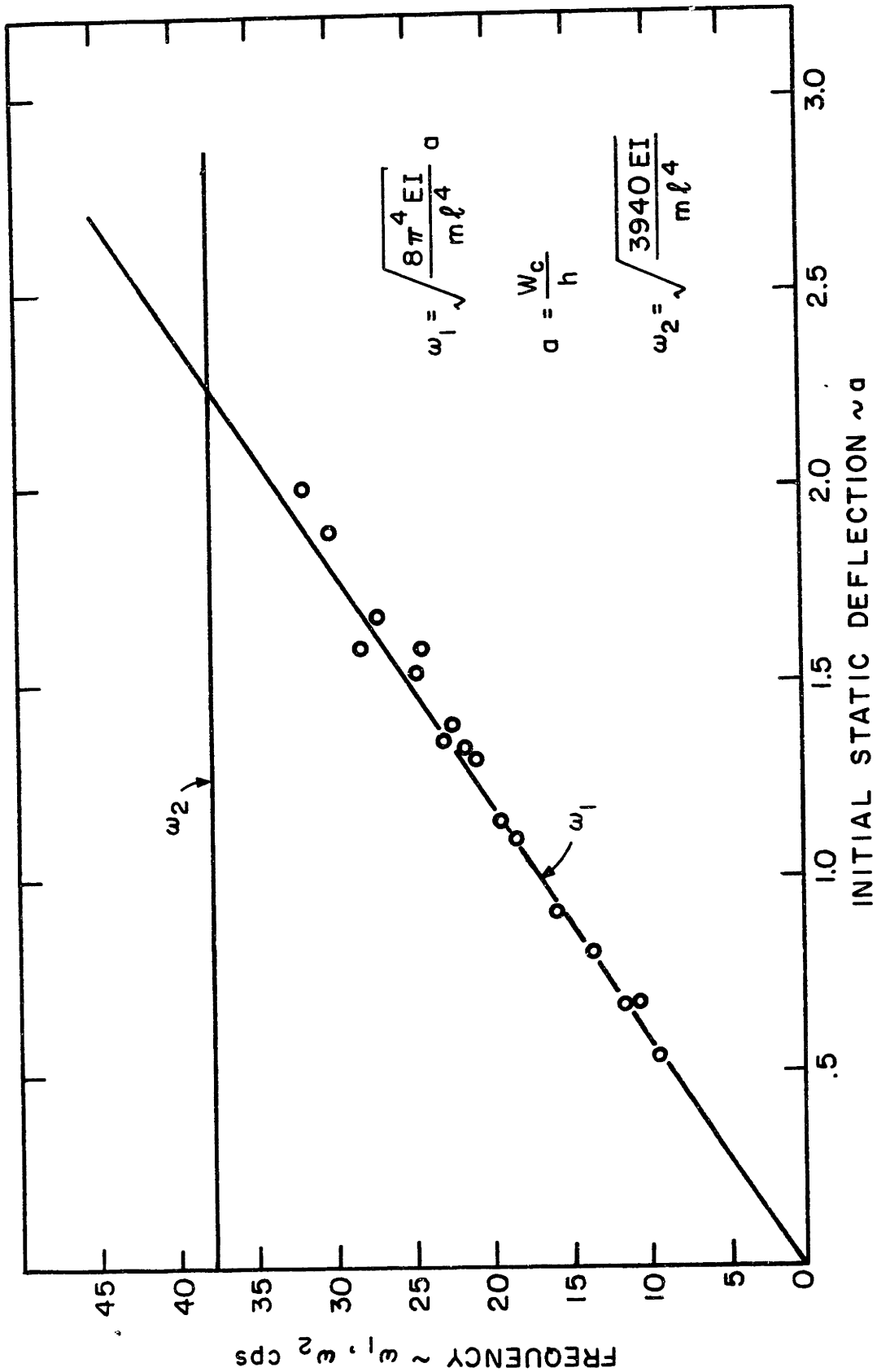


FIG. 9 LINEAR NATURAL FREQUENCY - BUCKLED BEAM

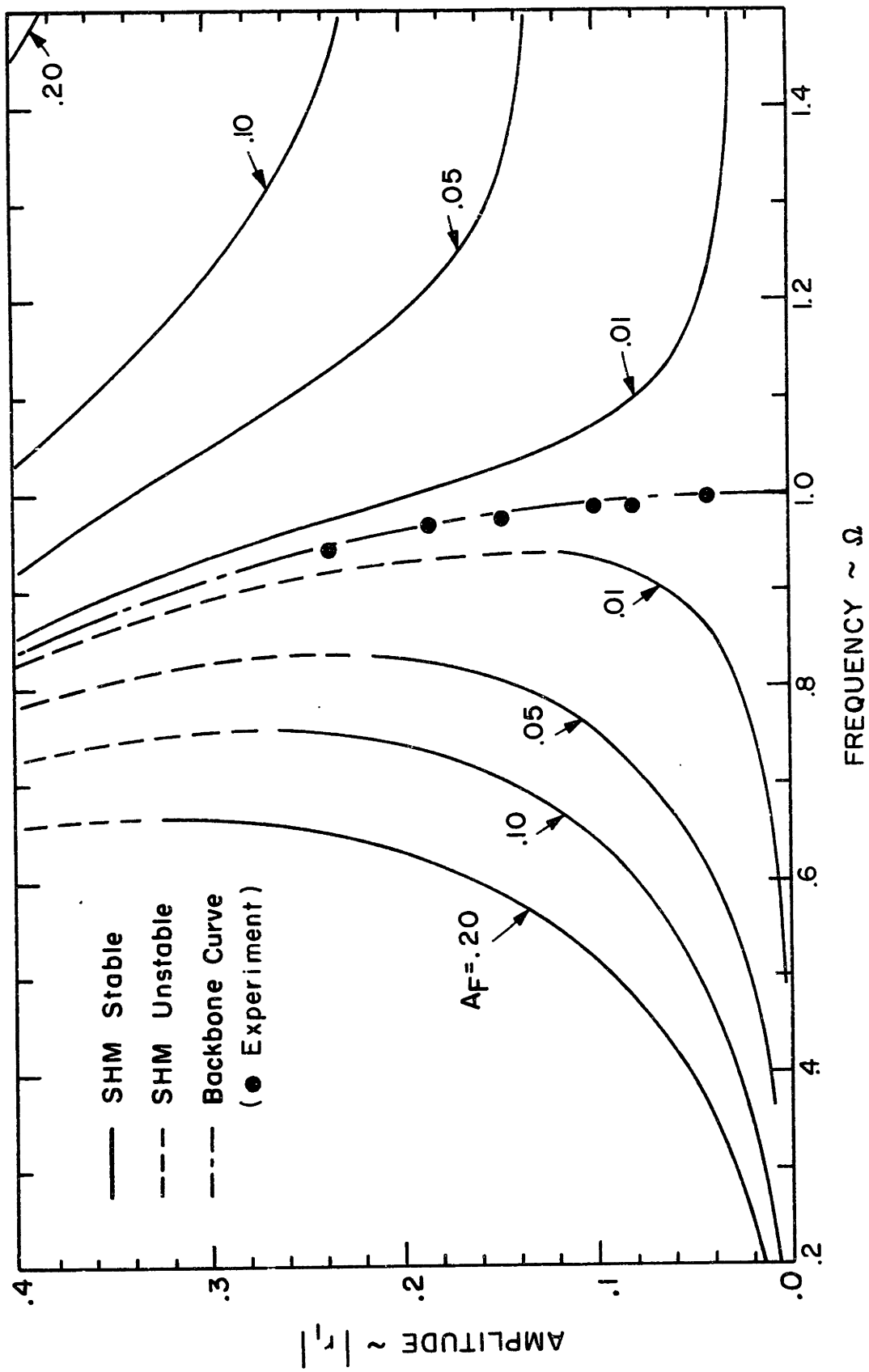


FIG.10 SHM SOLUTION - BUCKLED BEAM

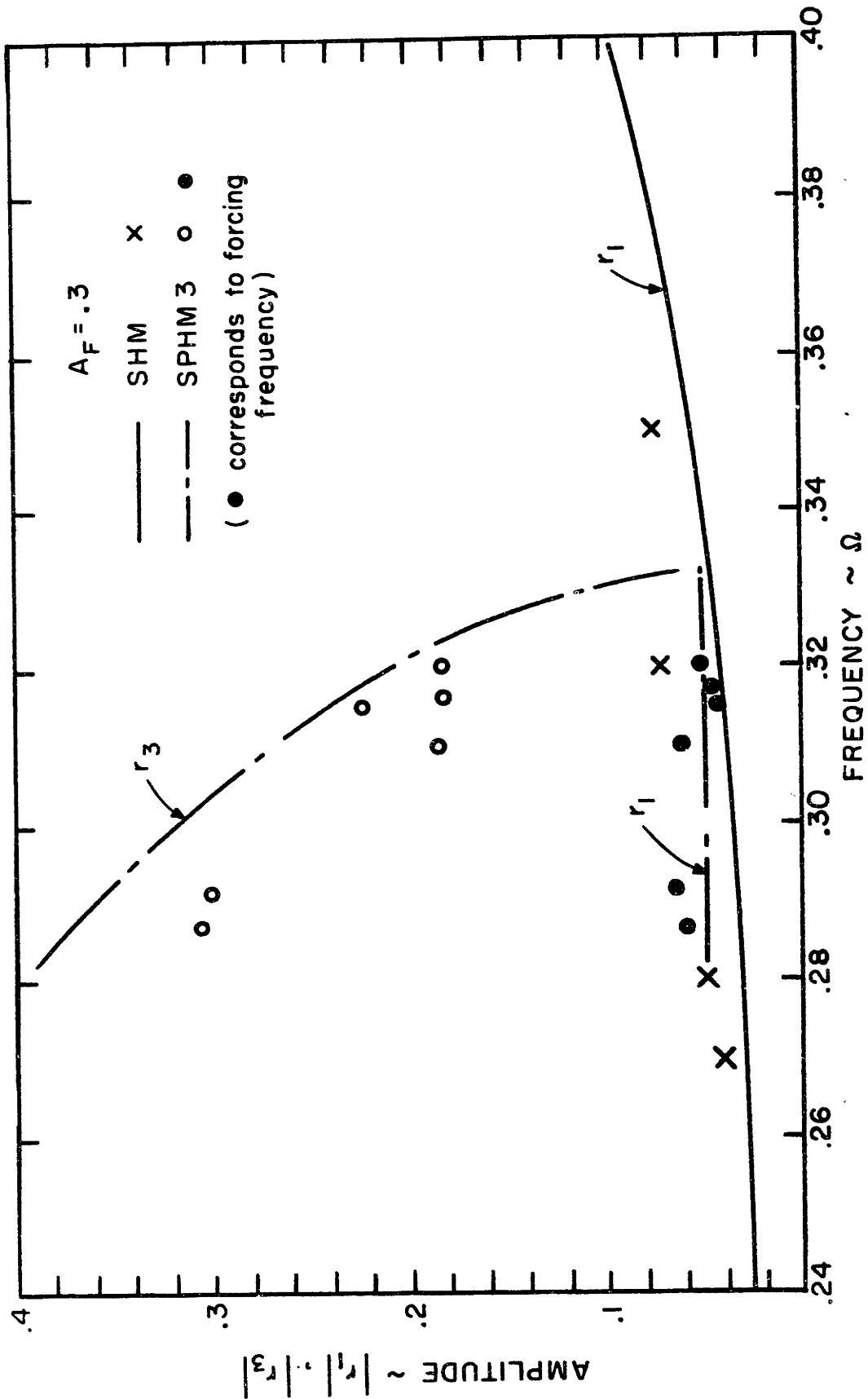


FIG. 11 SPHM ORDER 3 SOLUTION

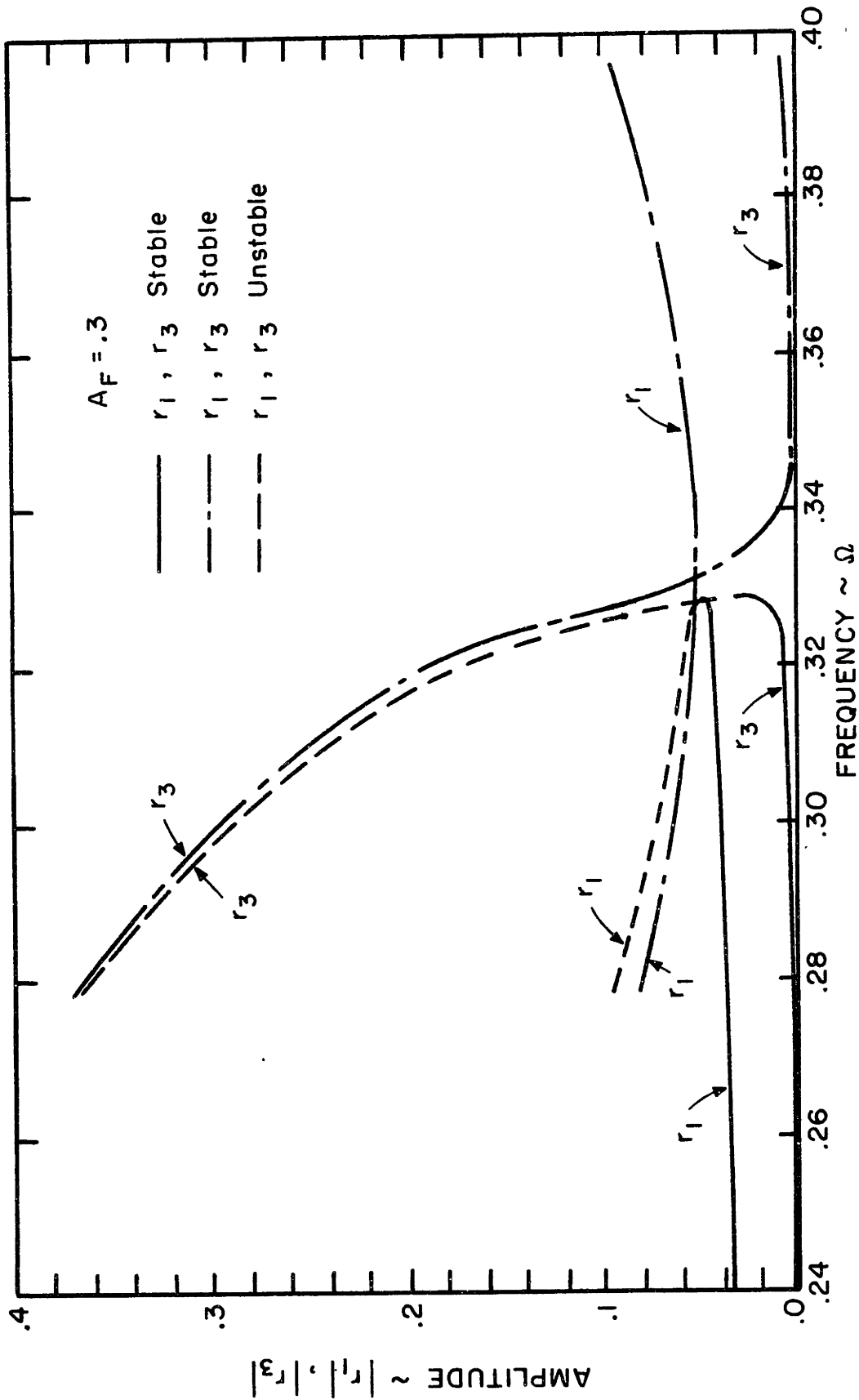


FIG. 12 DETAIL OF TRANSITION OF SPHM ORDER 3

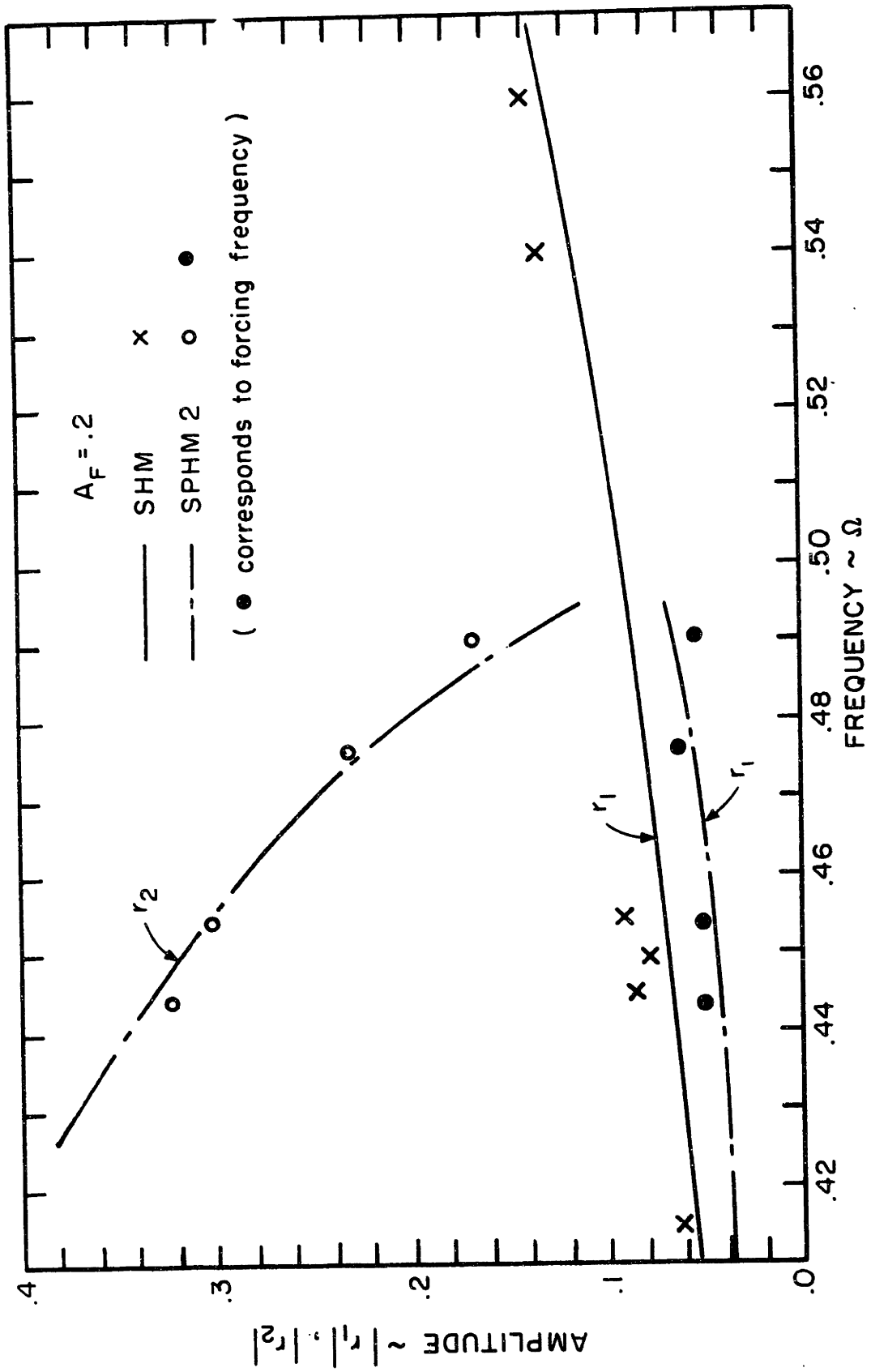


FIG. 13 SPHM ORDER 2 SOLUTION

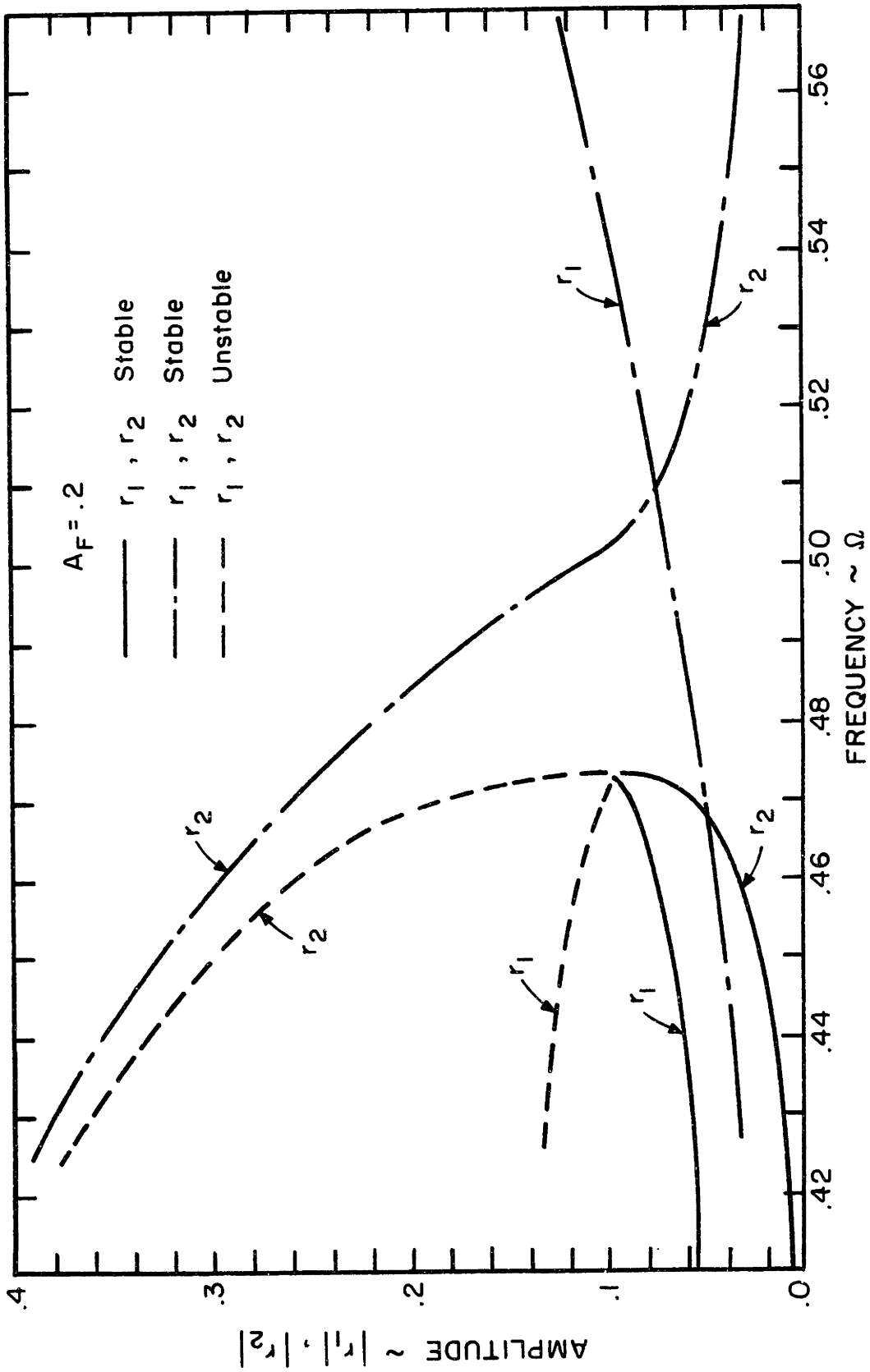


FIG.14 DETAIL OF TRANSITION OF SPHM ORDER 2

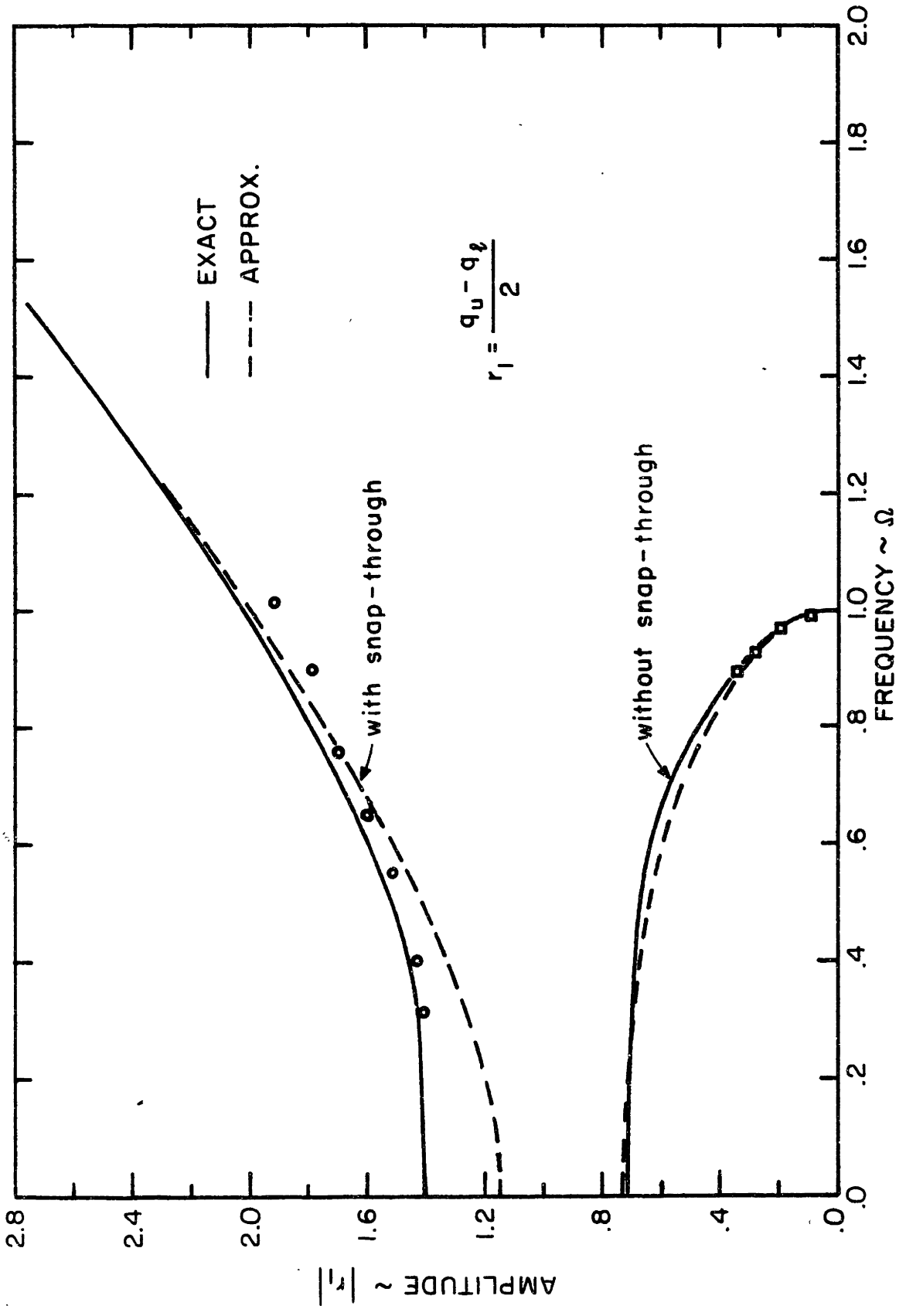


FIG. 15 NONLINEAR NATURAL FREQUENCY - BUCKLED BEAM

$A_F = .4$, $\Omega = .32032$, $\zeta = .0007$

I.C.: $q_1 = 1.00321$, $\dot{q}_1 = .0391$

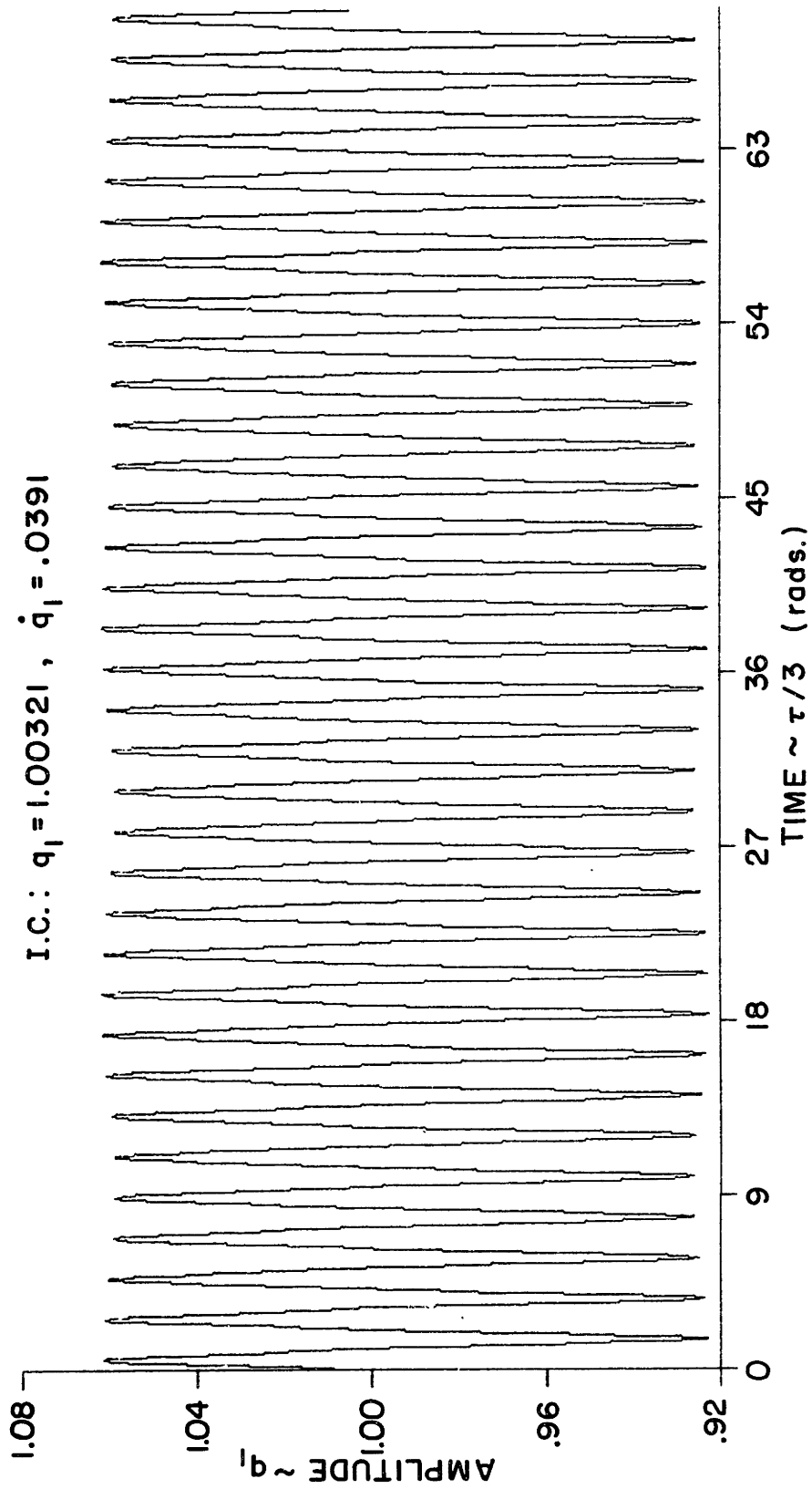


FIG.16 NUMERICAL STEADY STATE RESPONSE ~ SHM

$A_F = .4$, $\Omega = .32032$, $\zeta = .0007$

I.C.: $q_1 = .94893$; $\dot{q}_1 = .57431$

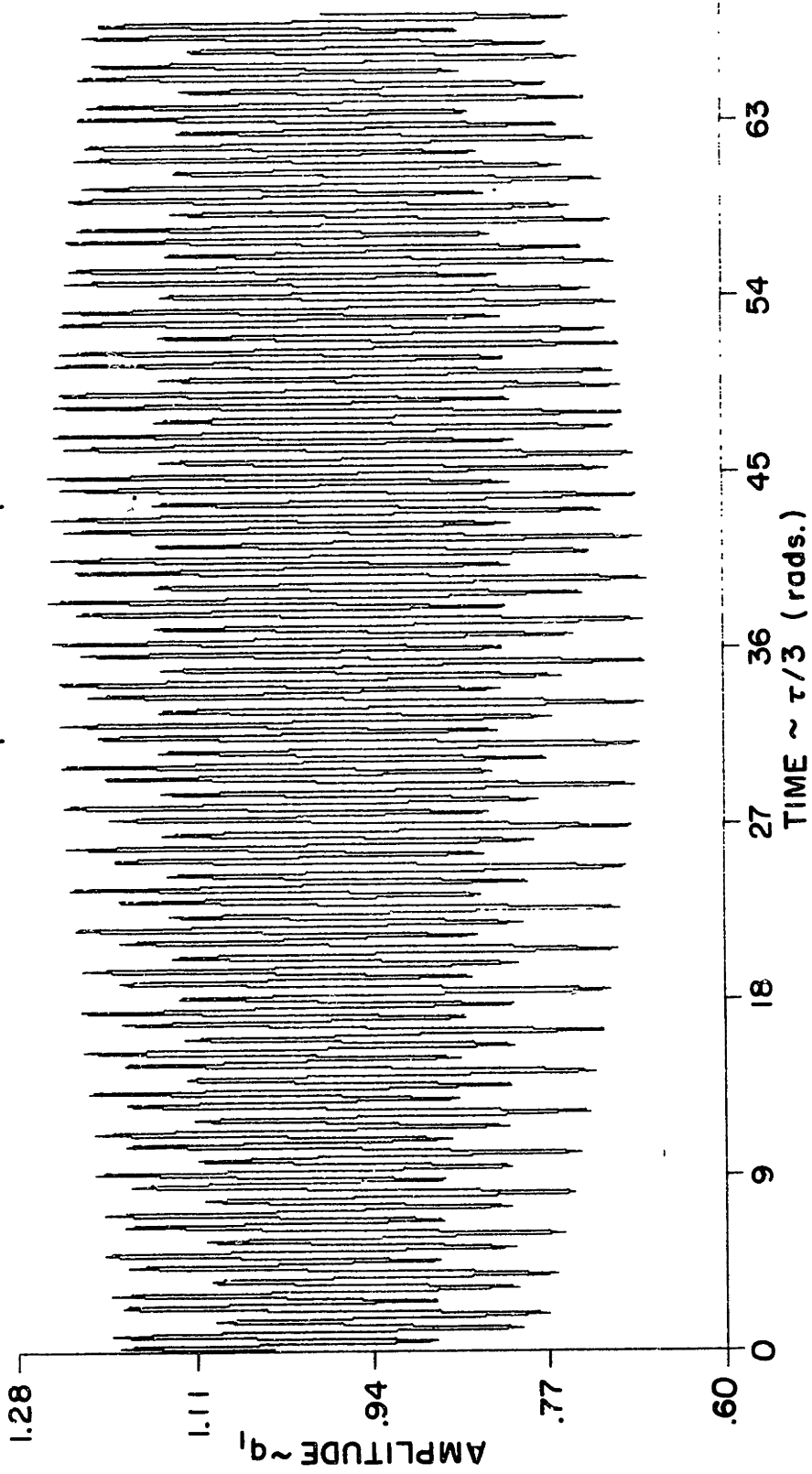


FIG. 17 NUMERICAL STEADY STATE RESPONSE ~ SPHM3

$A_F = .2$, $\Omega = .449$, $\zeta = .001$
I.C.: $q_1 = 1.0122$, $\dot{q}_1 = .05$

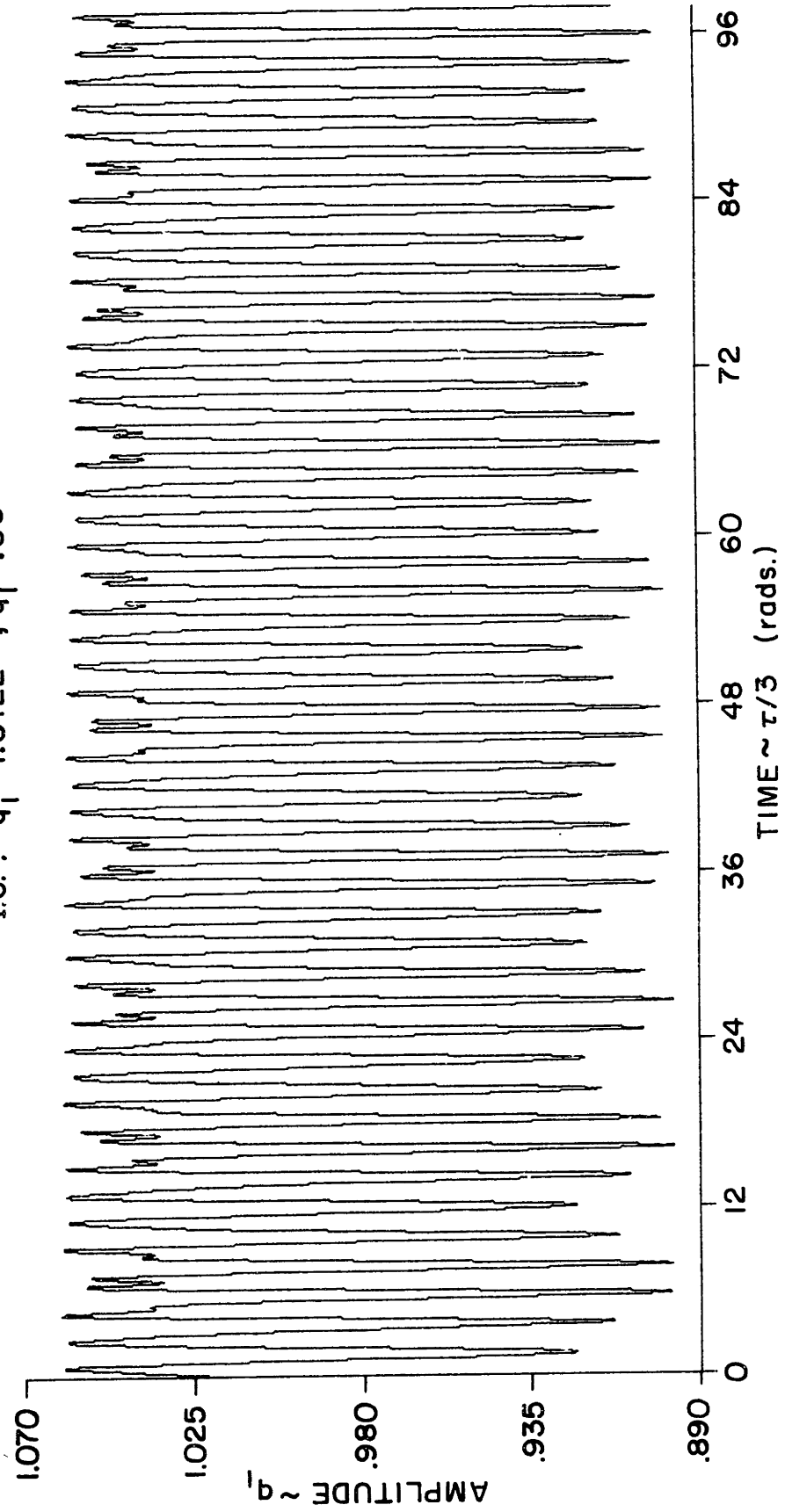


FIG. 18 NUMERICAL STEADY STATE RESPONSE ~ SHM

$A_F = .2$, $\Omega = .449$, $\zeta = .001$

I.C.: $q_1 = .59186$, $\dot{q}_1 = -.01988$

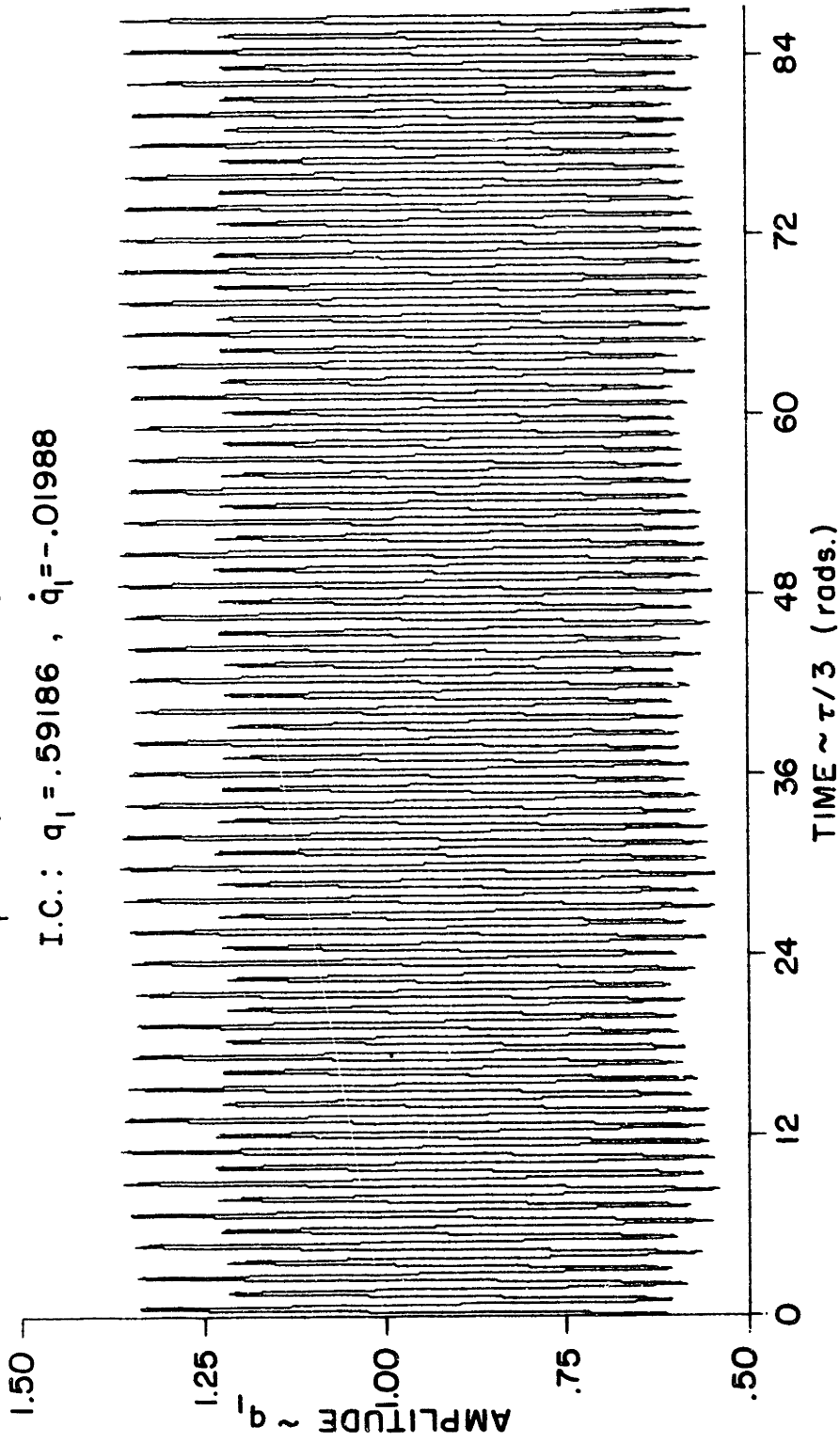


FIG.19 NUMERICAL STEADY STATE RESPONSE \sim SPHM 2

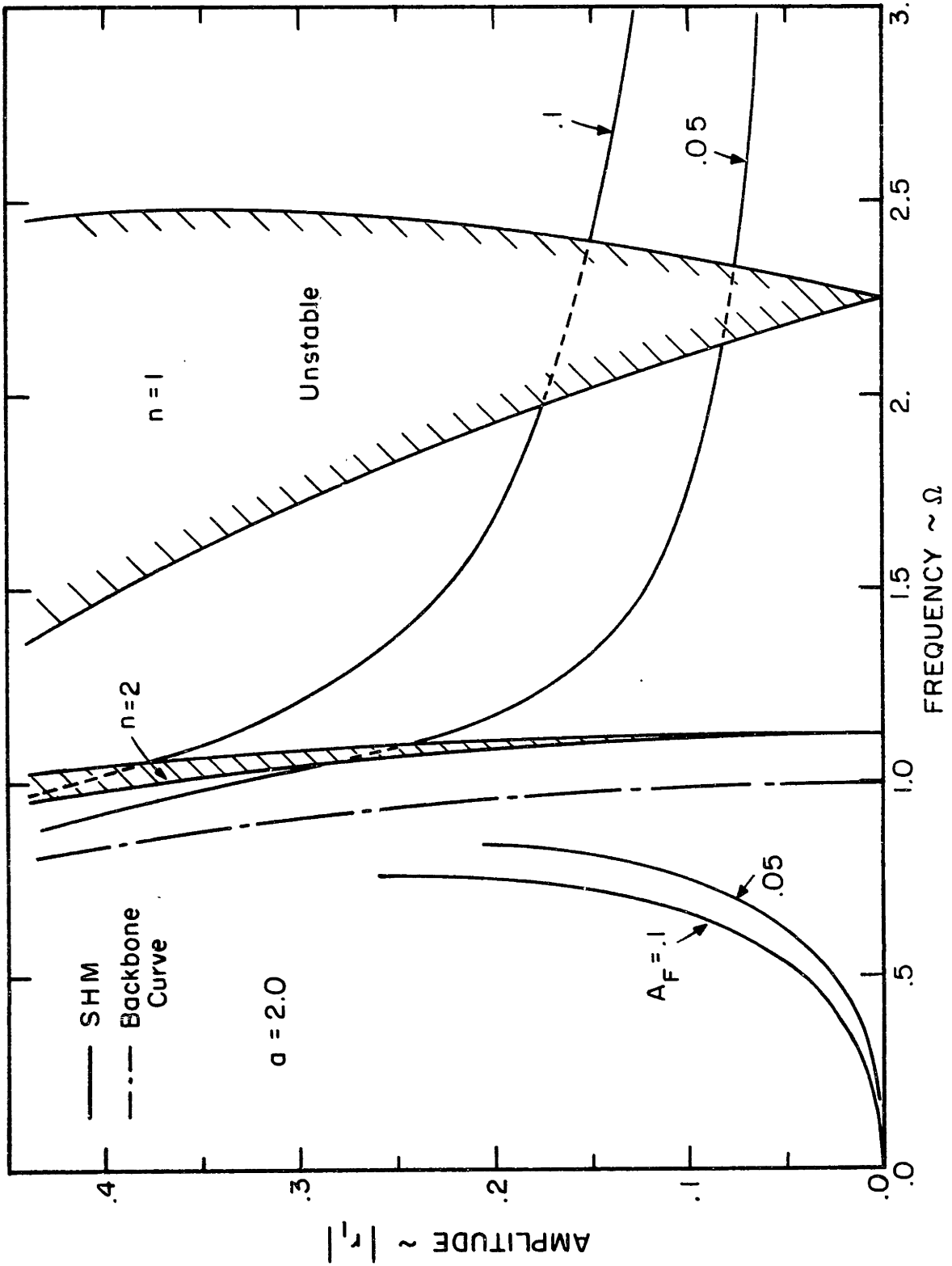


FIG. 20 UNSTABLE REGIONS OF SHM SOLUTION DUE TO EXCITATION OF 2ND MODE

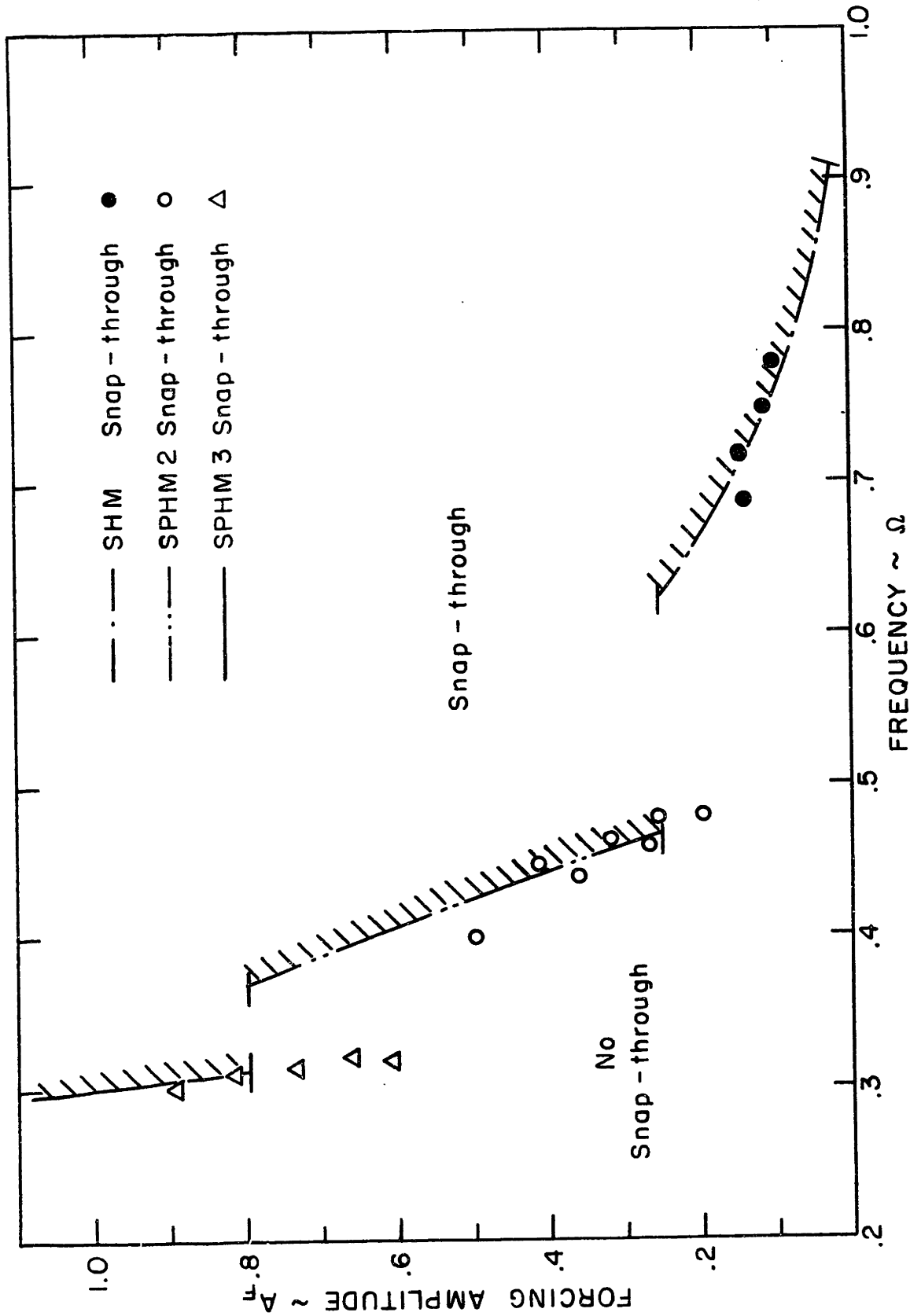


FIG. 21 SNAP-THROUGH REGIONS

$A_F = .025, \Omega = .892, \zeta = .001$

I.C.: $q_1 = 1.0, \dot{q}_1 = 0$

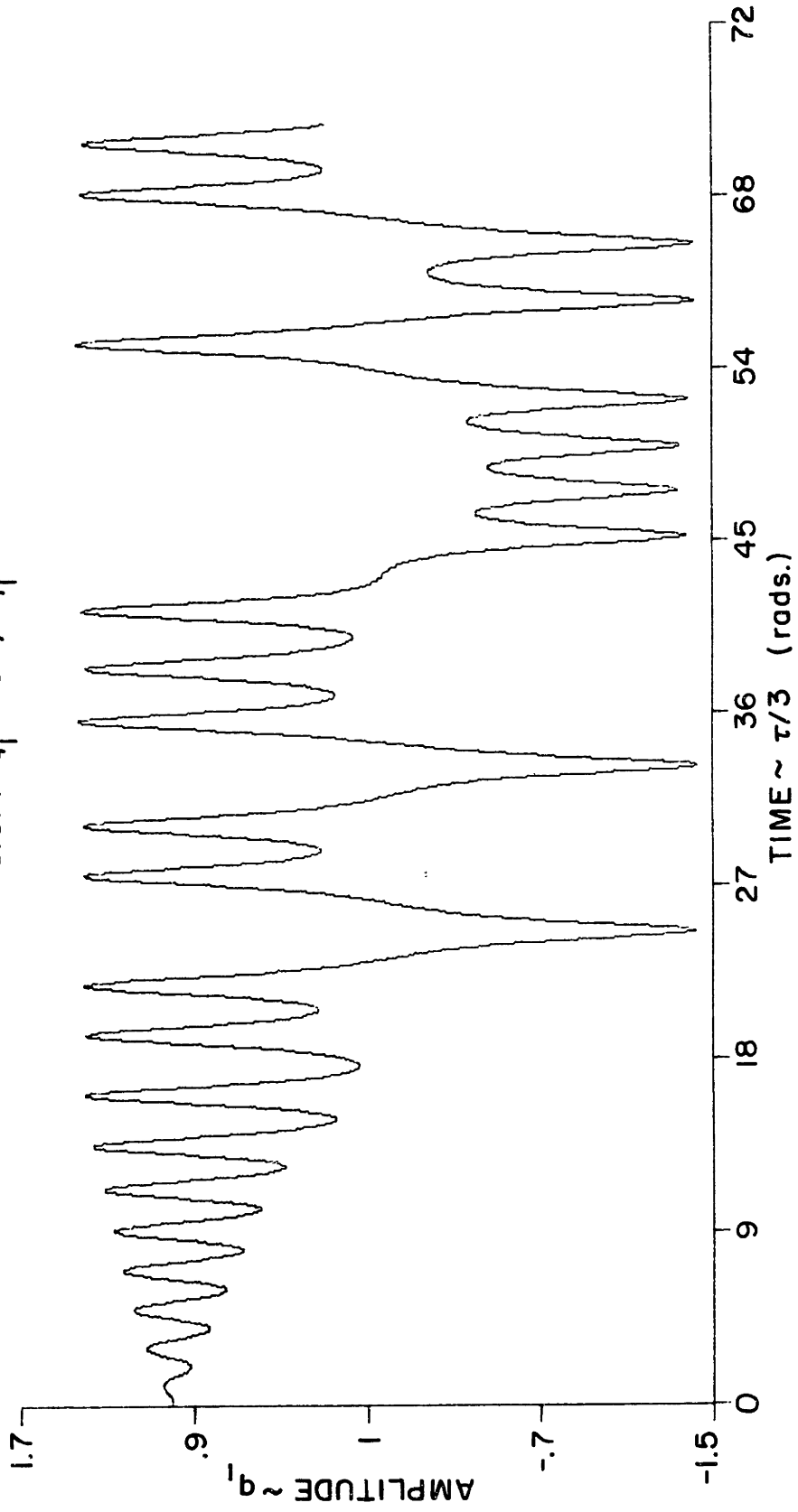


FIG. 22 SHM SNAP - THROUGH RESPONSE

$A_F = 0.9$, $\Omega = 3.15$, $\zeta = 0.0007$

I.C. : $q_1 = 1.0$, $\dot{q}_1 = 0$

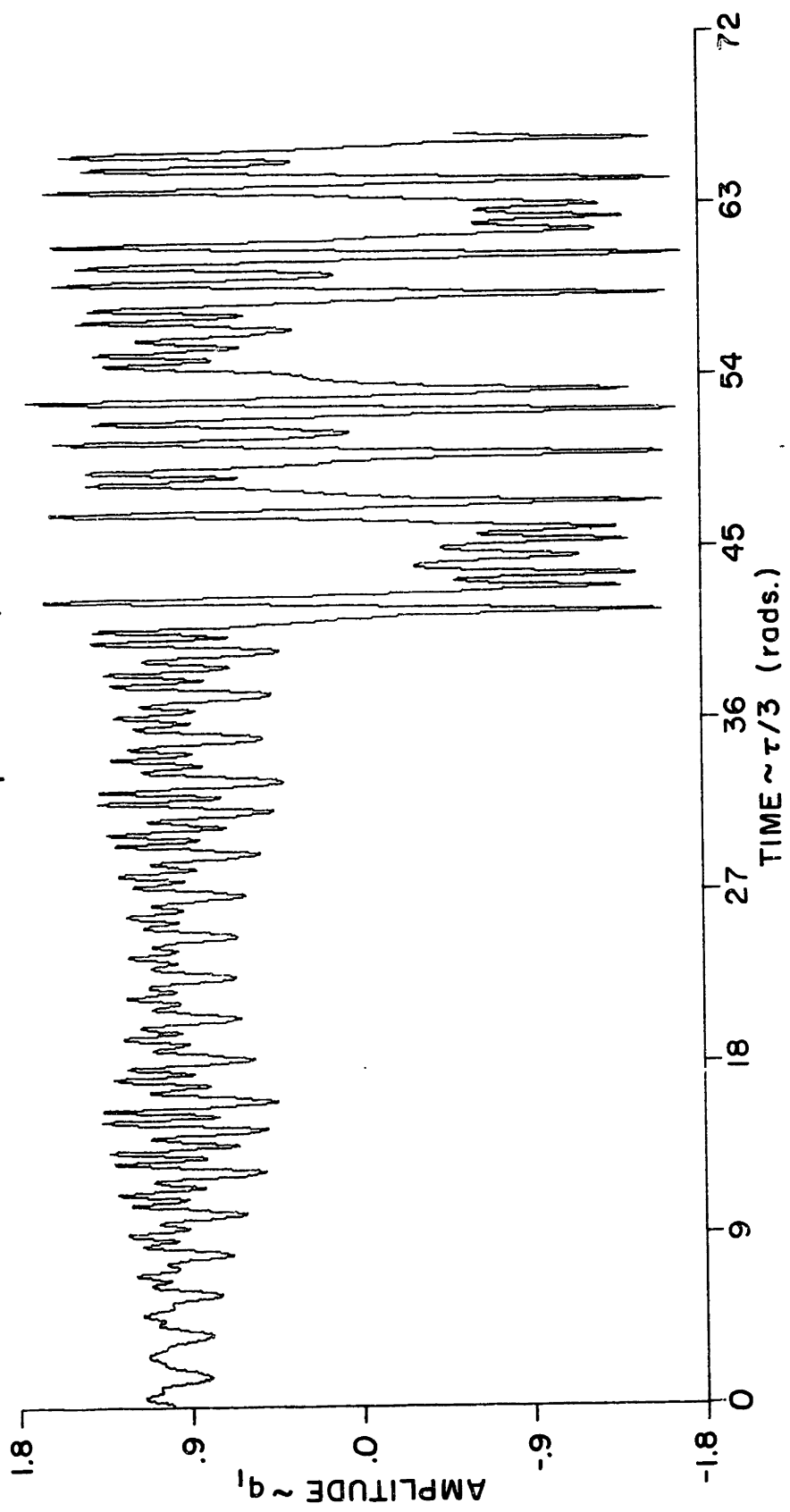


FIG. 23 SPHM ORDER 3 SNAP - THROUGH RESPONSE

$A_F = .3$, $\Omega = .455$, $\zeta = .001$
I.C.: $q_1 = 1.0$, $\dot{q}_1 = 0$

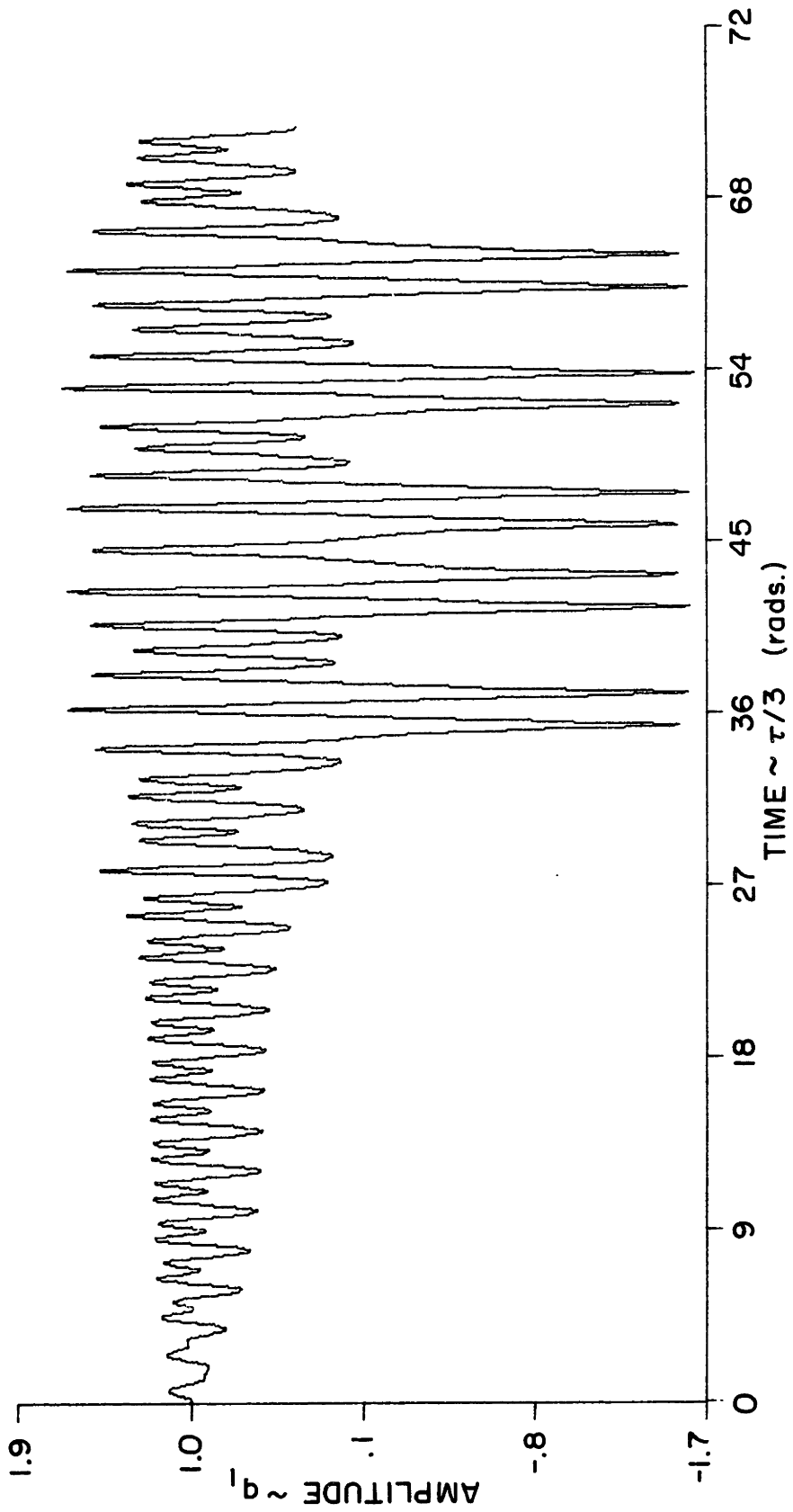


FIG. 24 SPHM ORDER 2 SNAP-THROUGH RESPONSE

$A_F = .9$, $\Omega = .315$, $\zeta = .001$

I.C.: $q_1 = 1.0$ $\dot{q}_1 = 0$

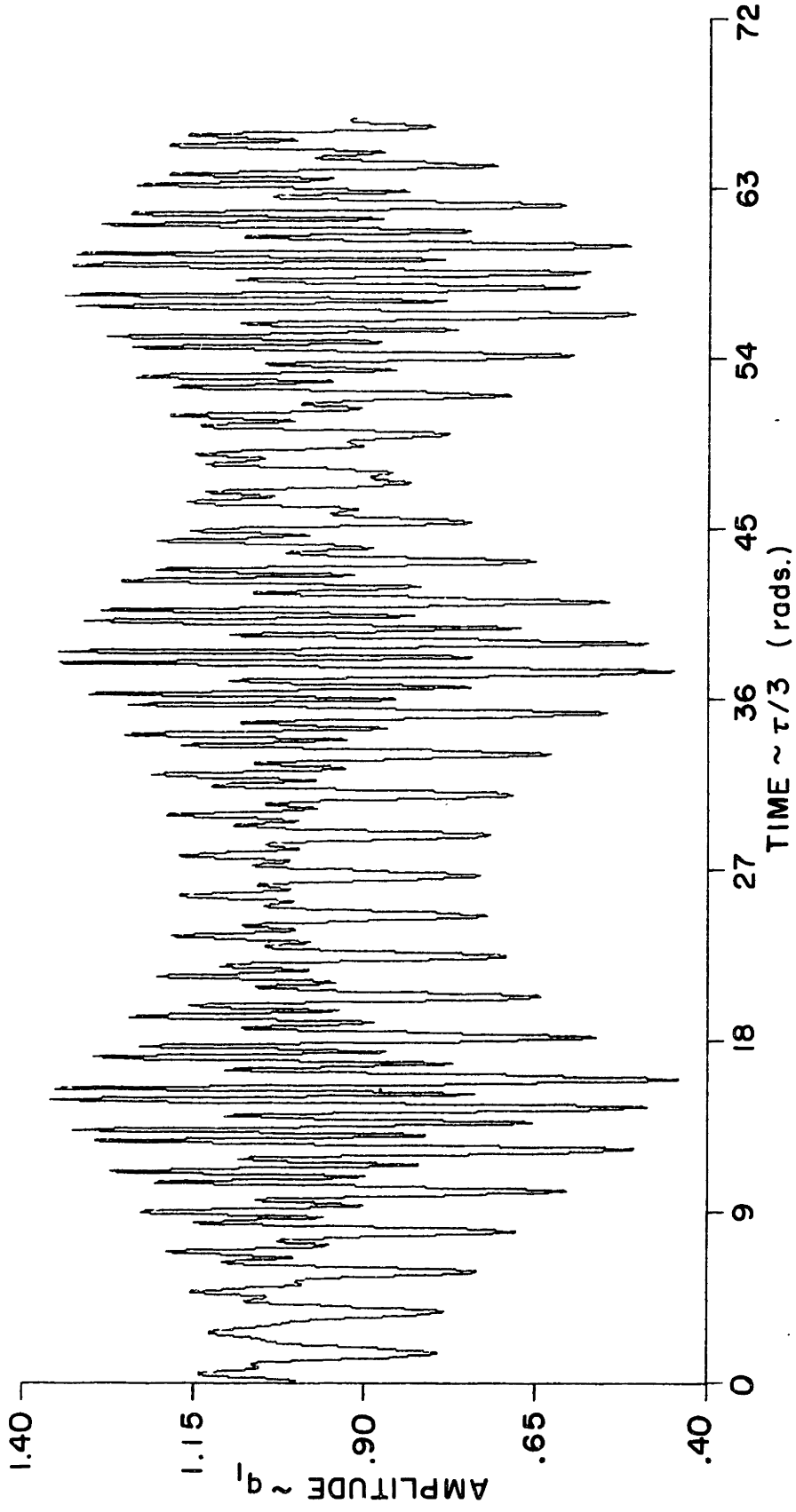


FIG.25 DAMPING EFFECT ON SPHM 3 SNAP THROUGH

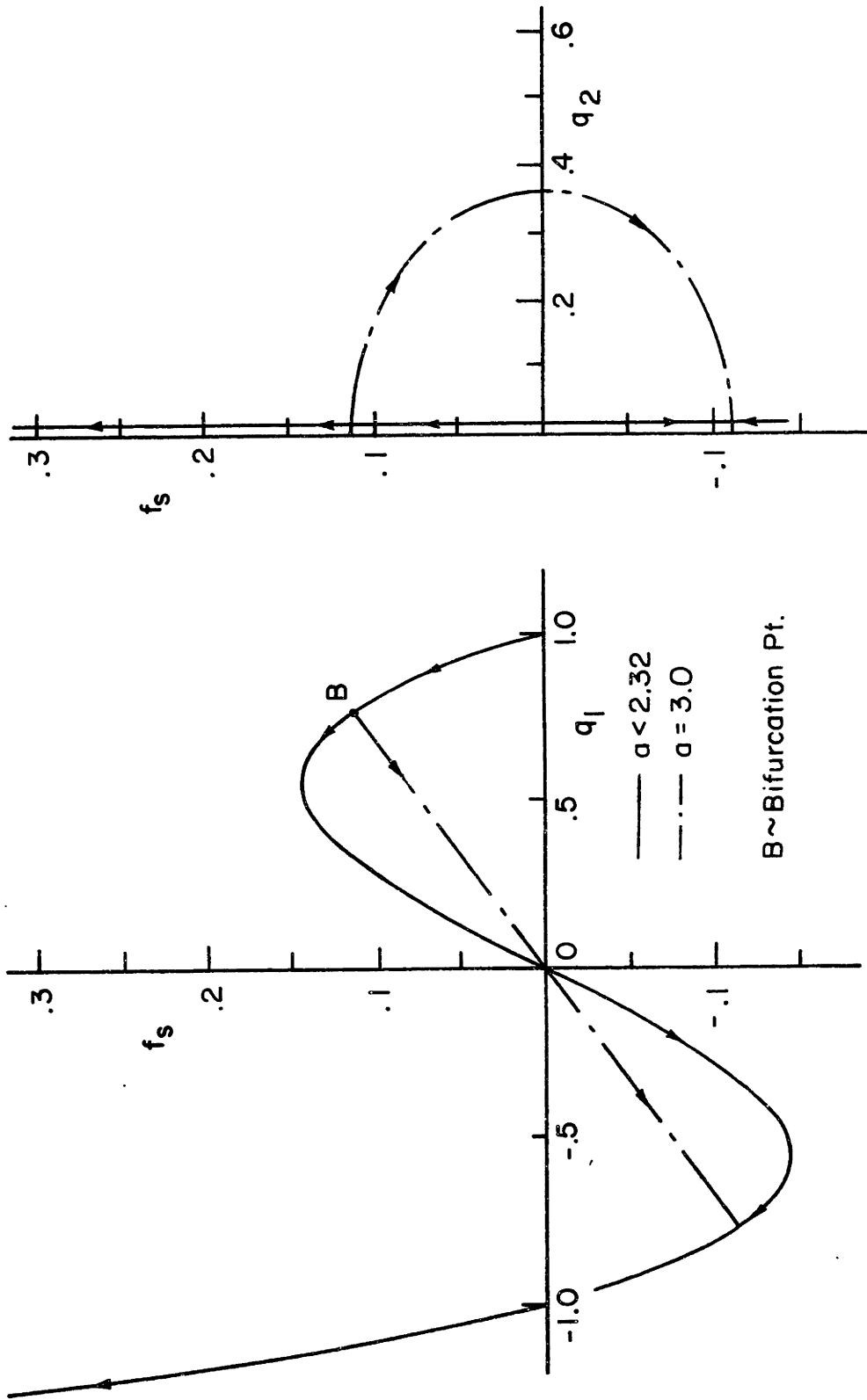


FIG. 26 STATIC FORCE - DEFLECTION RELATION (2 MODES)

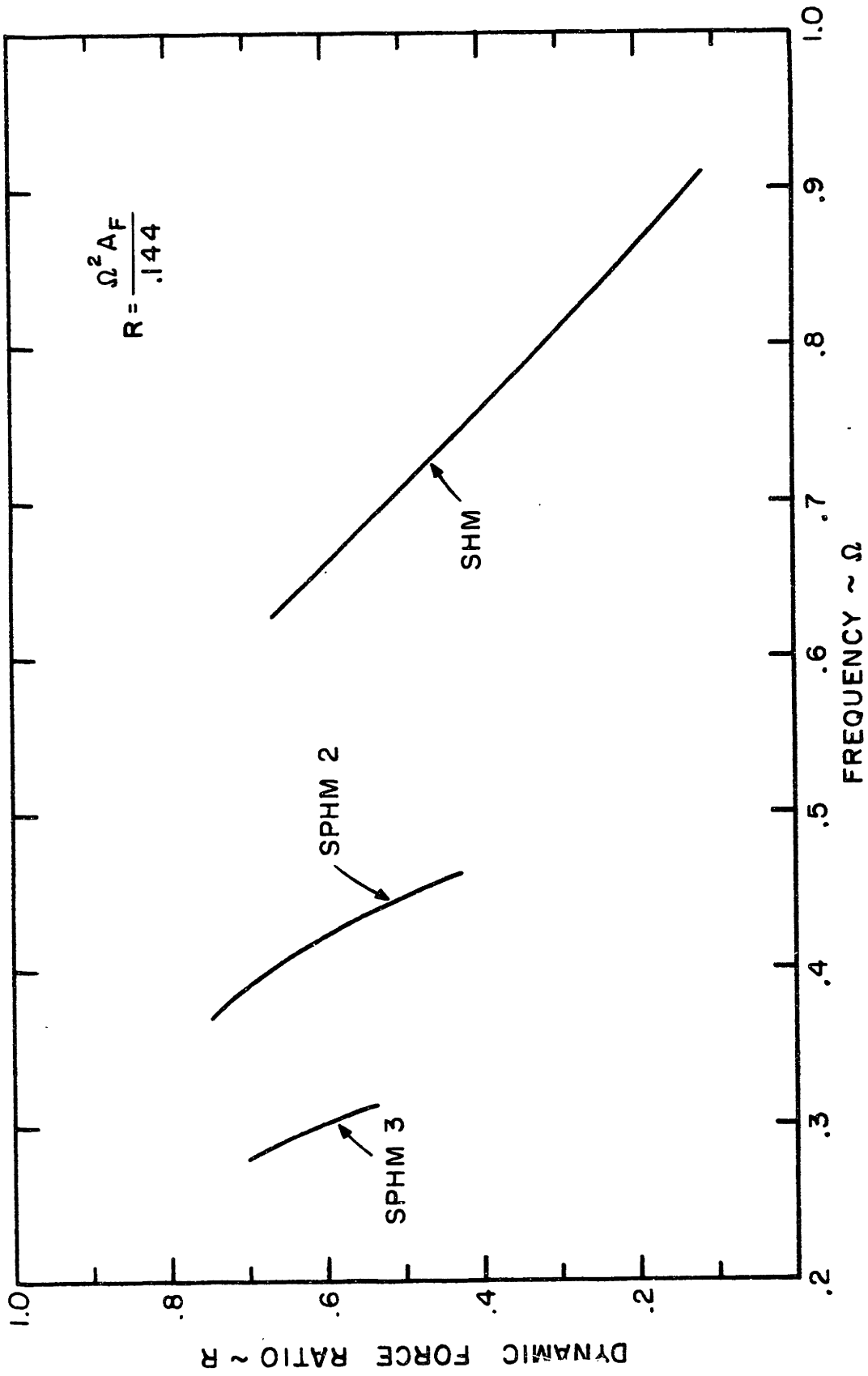


FIG. 27 DYNAMIC TO STATIC FORCE RATIO

$$A_F = 0, \quad \zeta = 0.001$$

$$\text{I.C.: } q_1 = 1.5, \quad \dot{q}_1 = 0$$

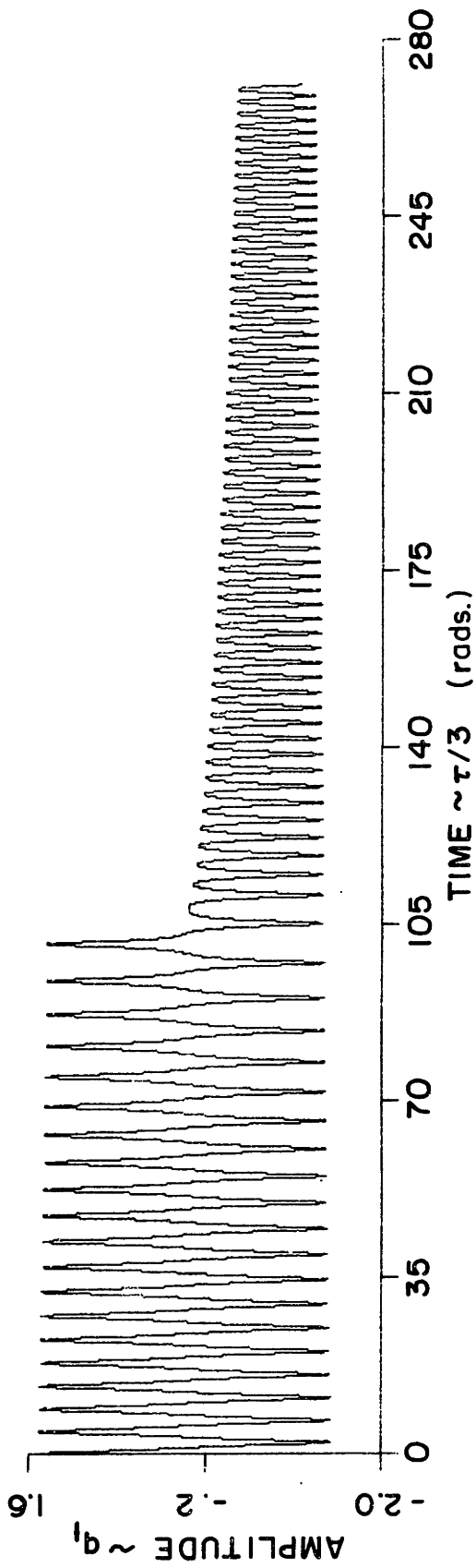


FIG. 28 FREE VIBRATION RESPONSE

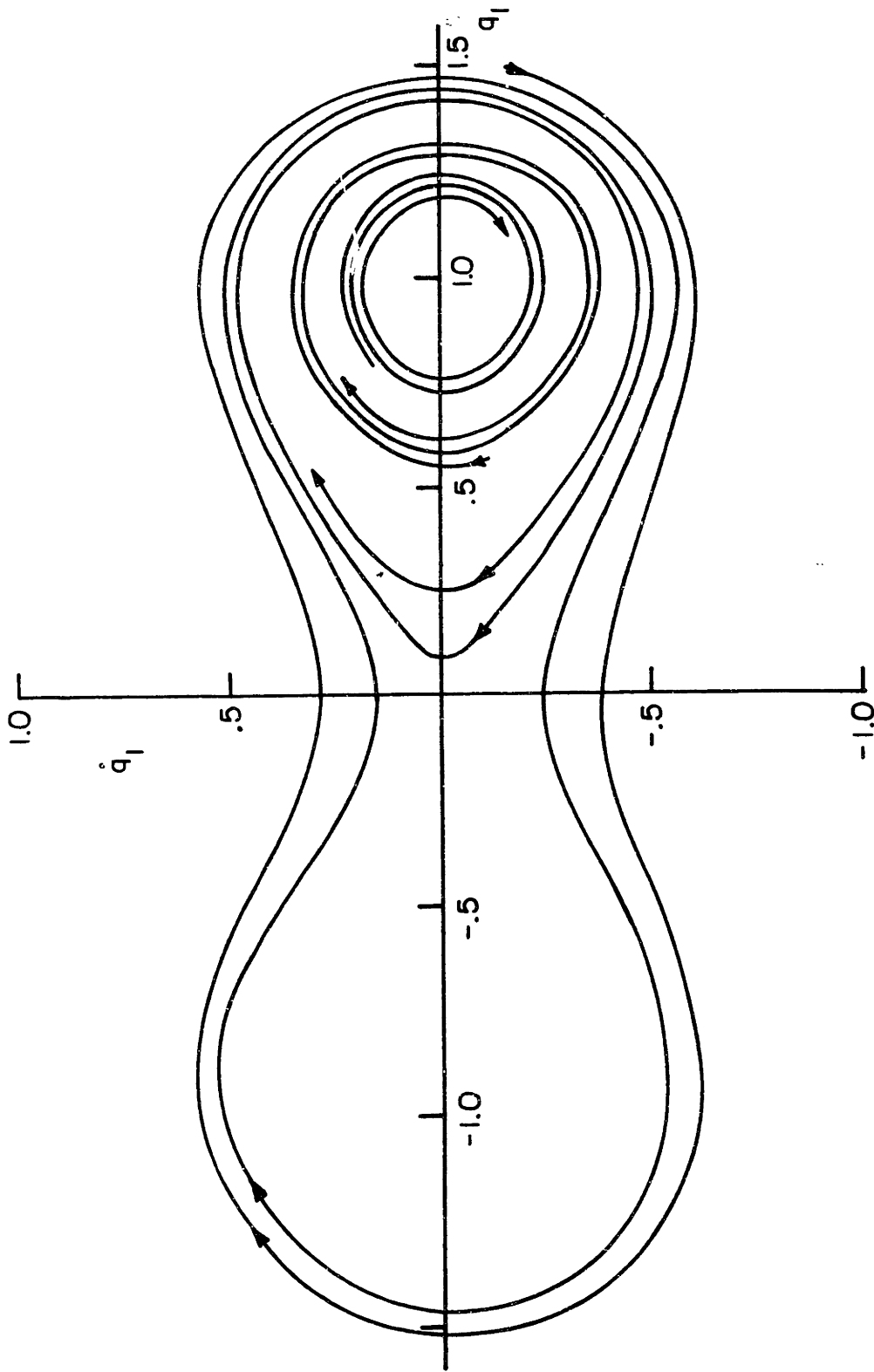
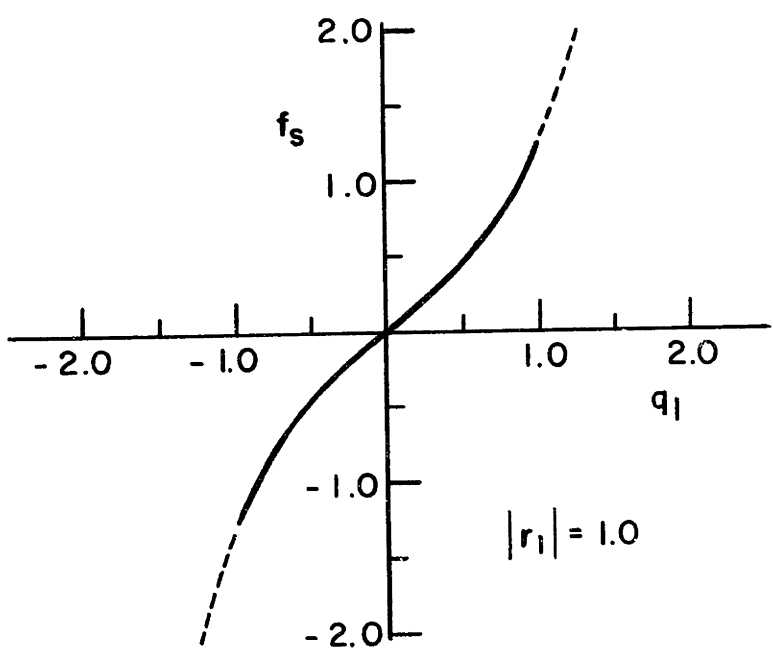


FIG. 29 STATE PLANE DIAGRAM FOR FREE VIBRATIONS

a) Straight Beam



b) Buckled Beam

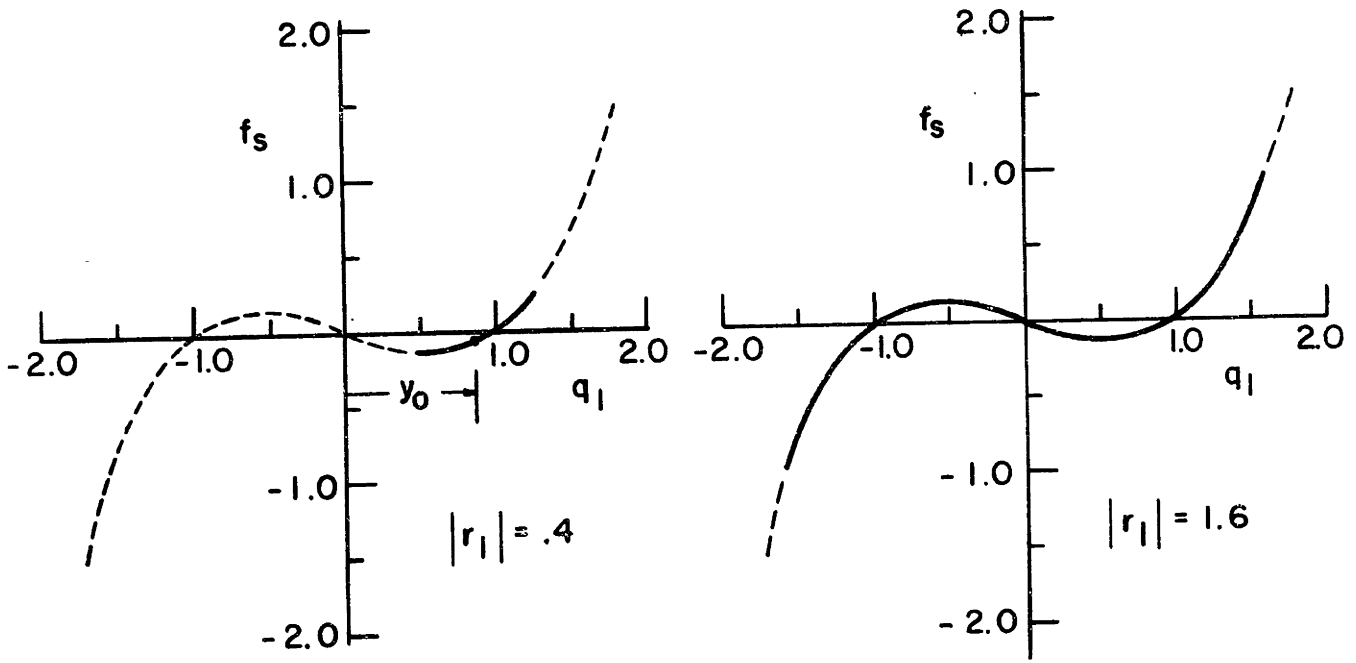


FIG. 30 VIBRATIONAL BEHAVIOR OF STRAIGHT AND BUCKLED BEAMS

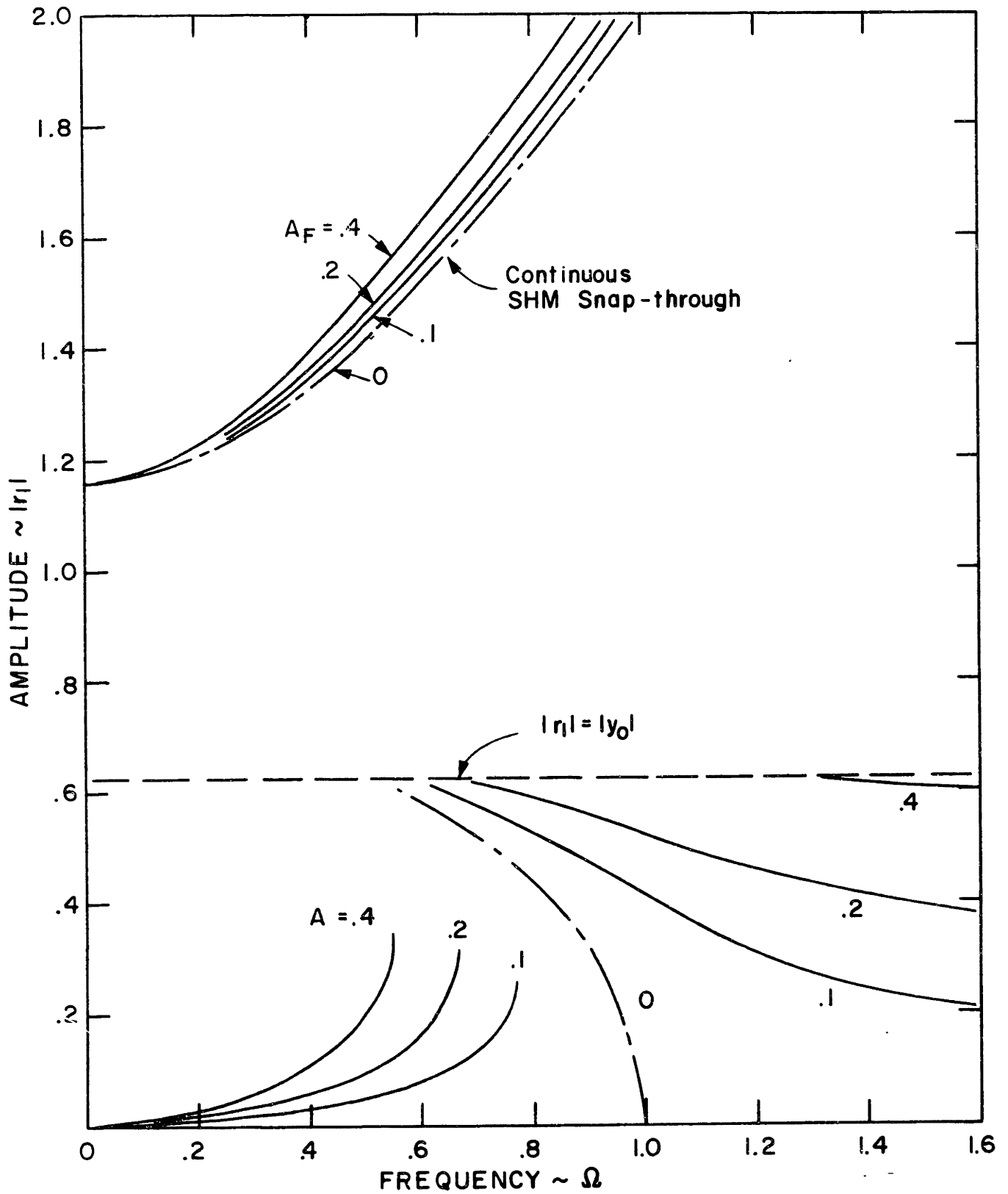


FIG. 31 OVERALL BEHAVIOR OF SHM SOLUTION

$$A_F = 0.1 \quad \Omega = 0.8 \quad , \quad \zeta = 0.001$$

$$\text{I.C. : } q_1 = 1.0 \quad \dot{q}_1 = 0$$

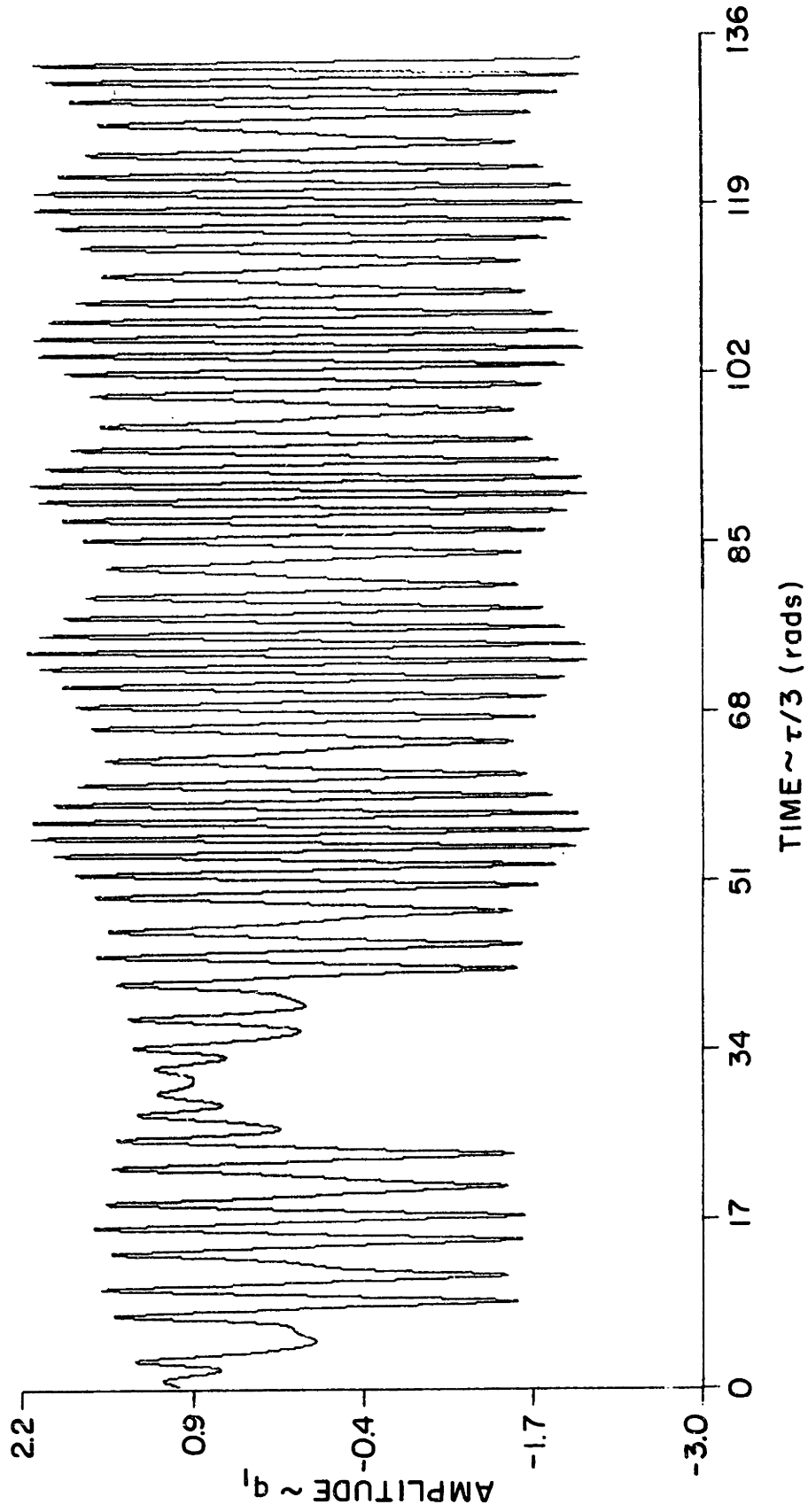


FIG.32 CONTINUOUS SHM SNAP-THROUGH RESPONSE

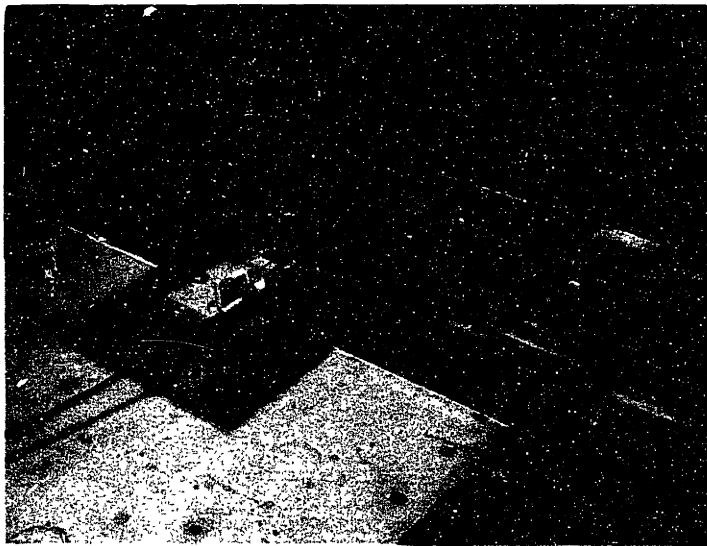
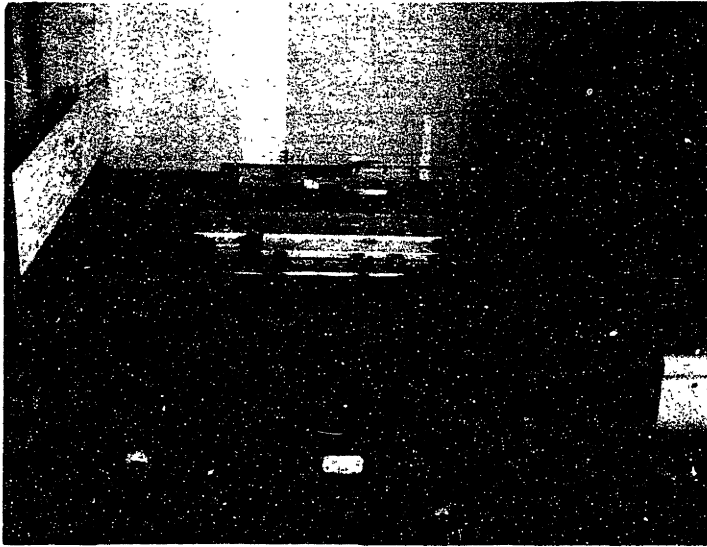
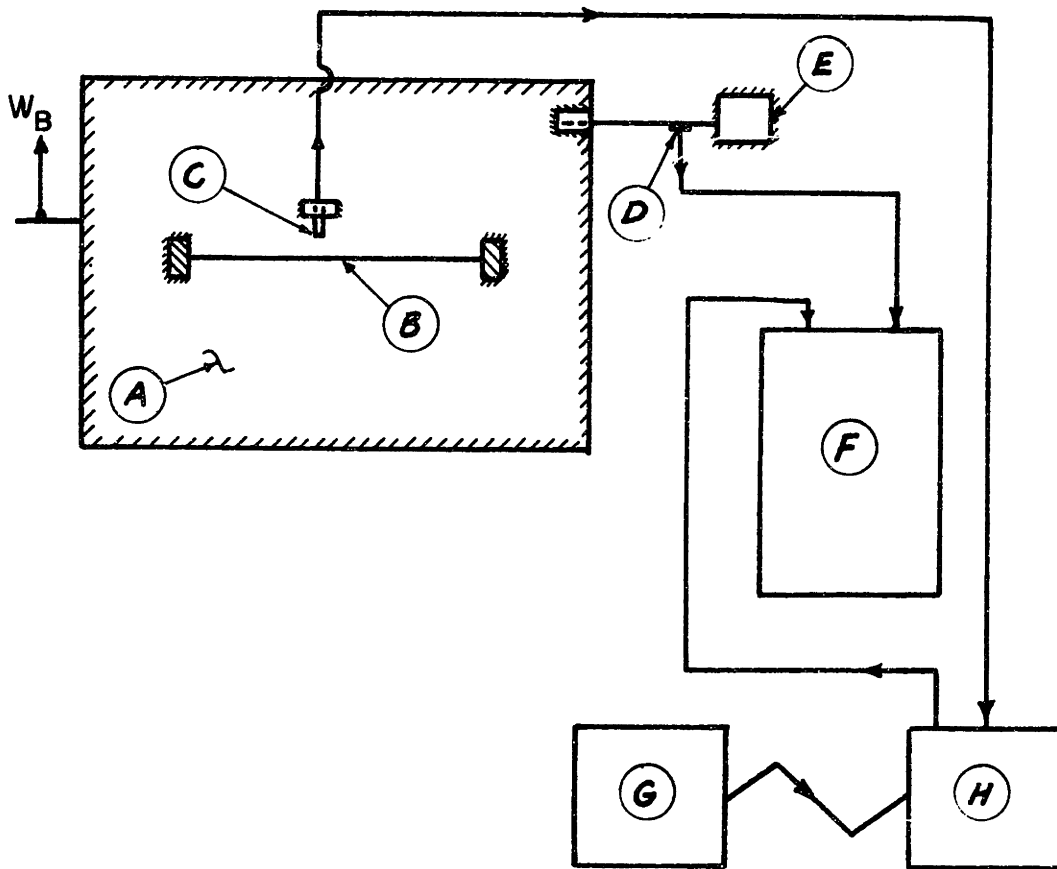


FIG.33 OVERALL EXPERIMENTAL SETUP



- A - shake table
- B - experimental specimen - beam
- C - capacitor probe
- D - strain gages
- E - steel channel bar
- F - Sanborn recorder
- G - power supply unit
- H - capacitance transducer

FIG.34 EXPERIMENTAL SETUP SKETCH

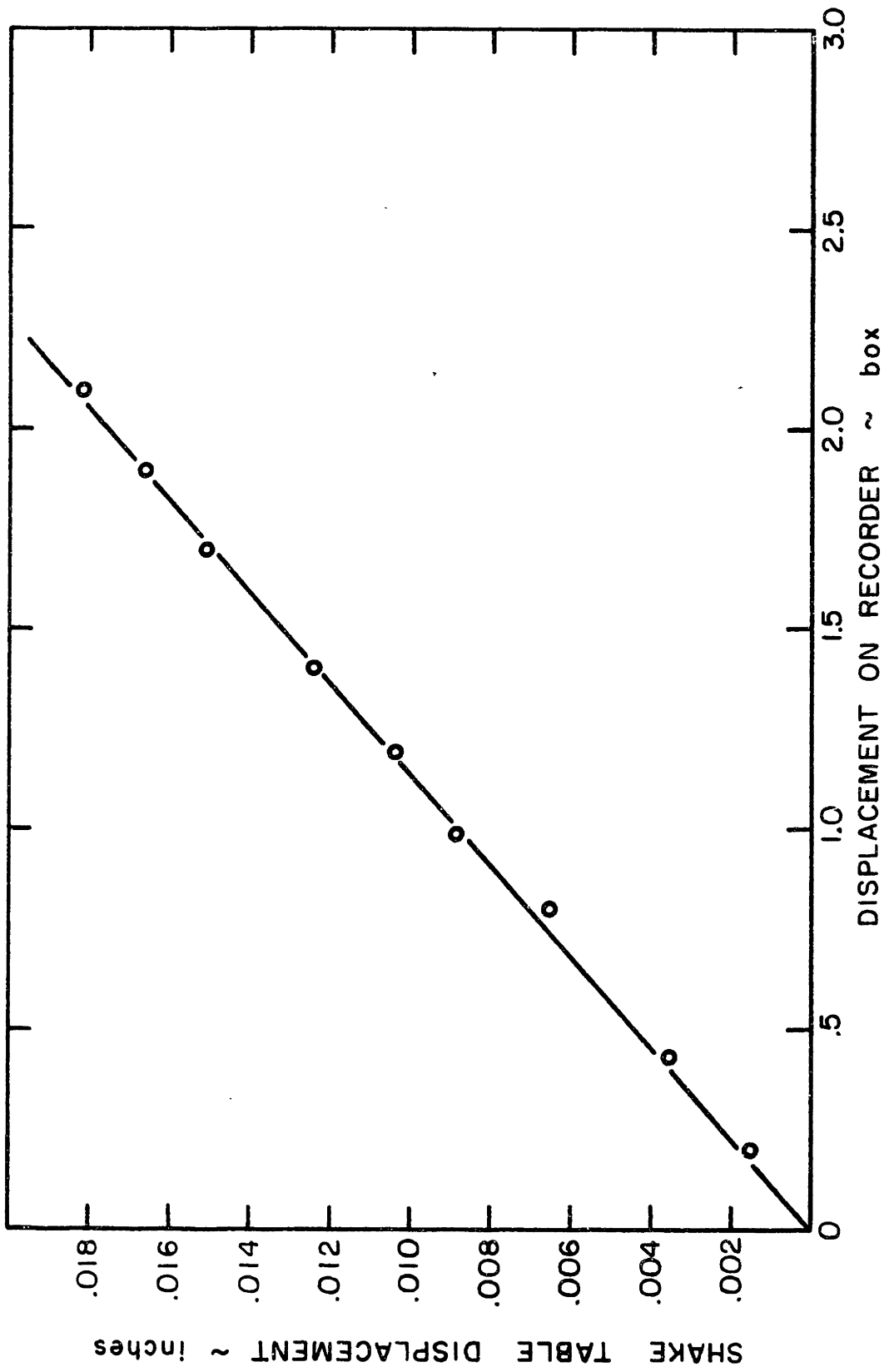


FIG. 35 STRAIN GAGE CALIBRATION

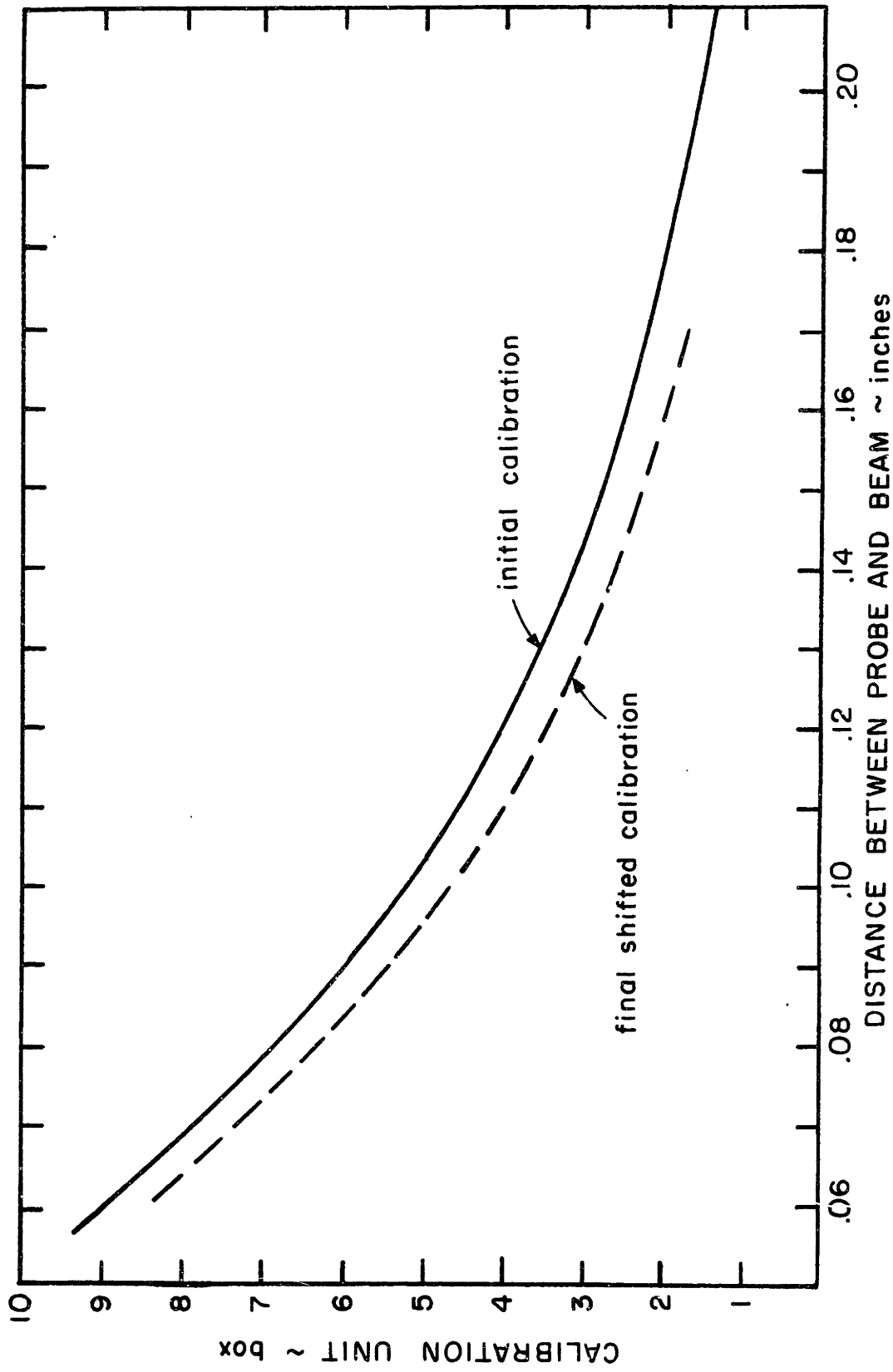


FIG. 36 CAPACITOR PROBE CALIBRATION

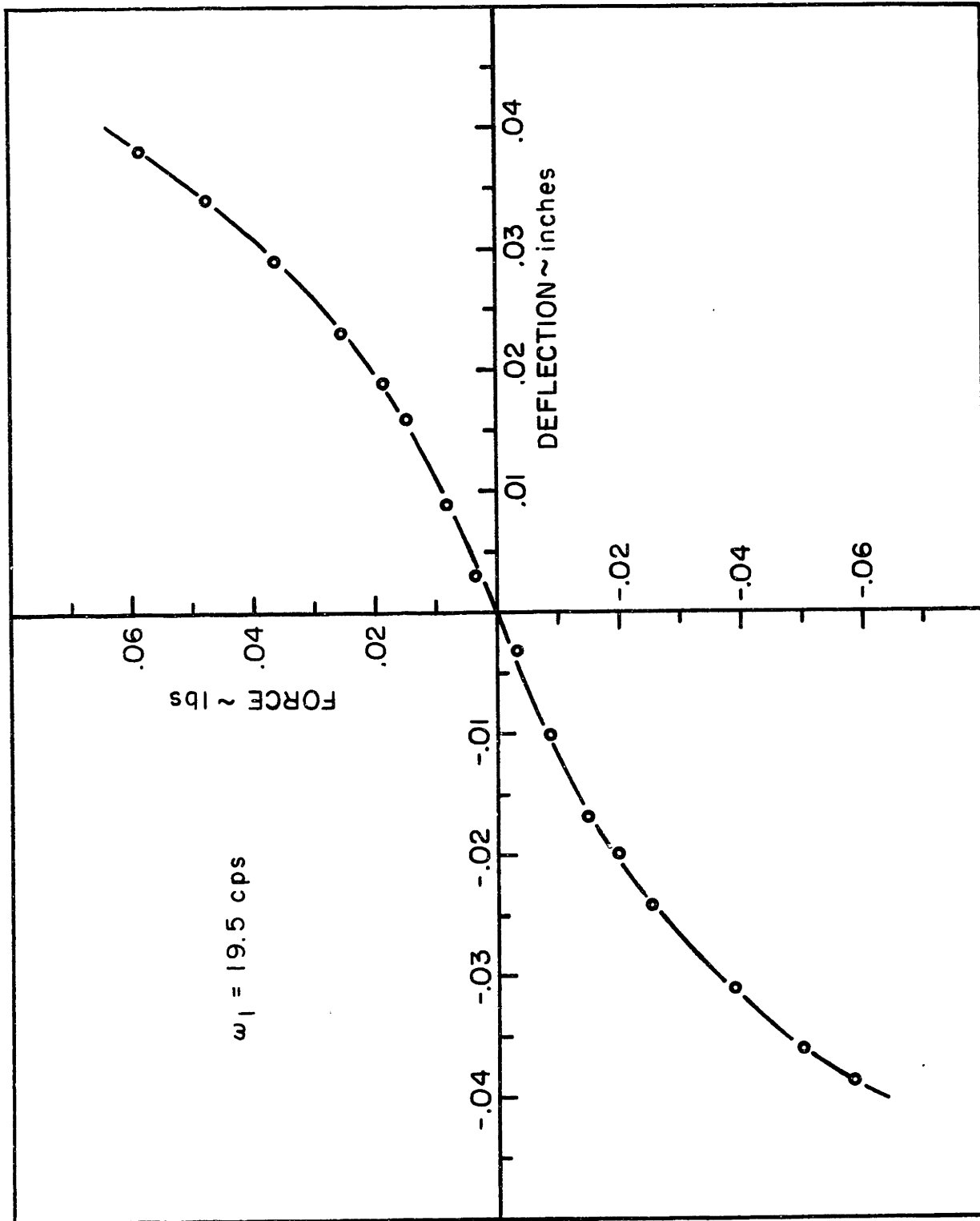


FIG.37 STATIC FORCE ~ DEFLECTION RELATION

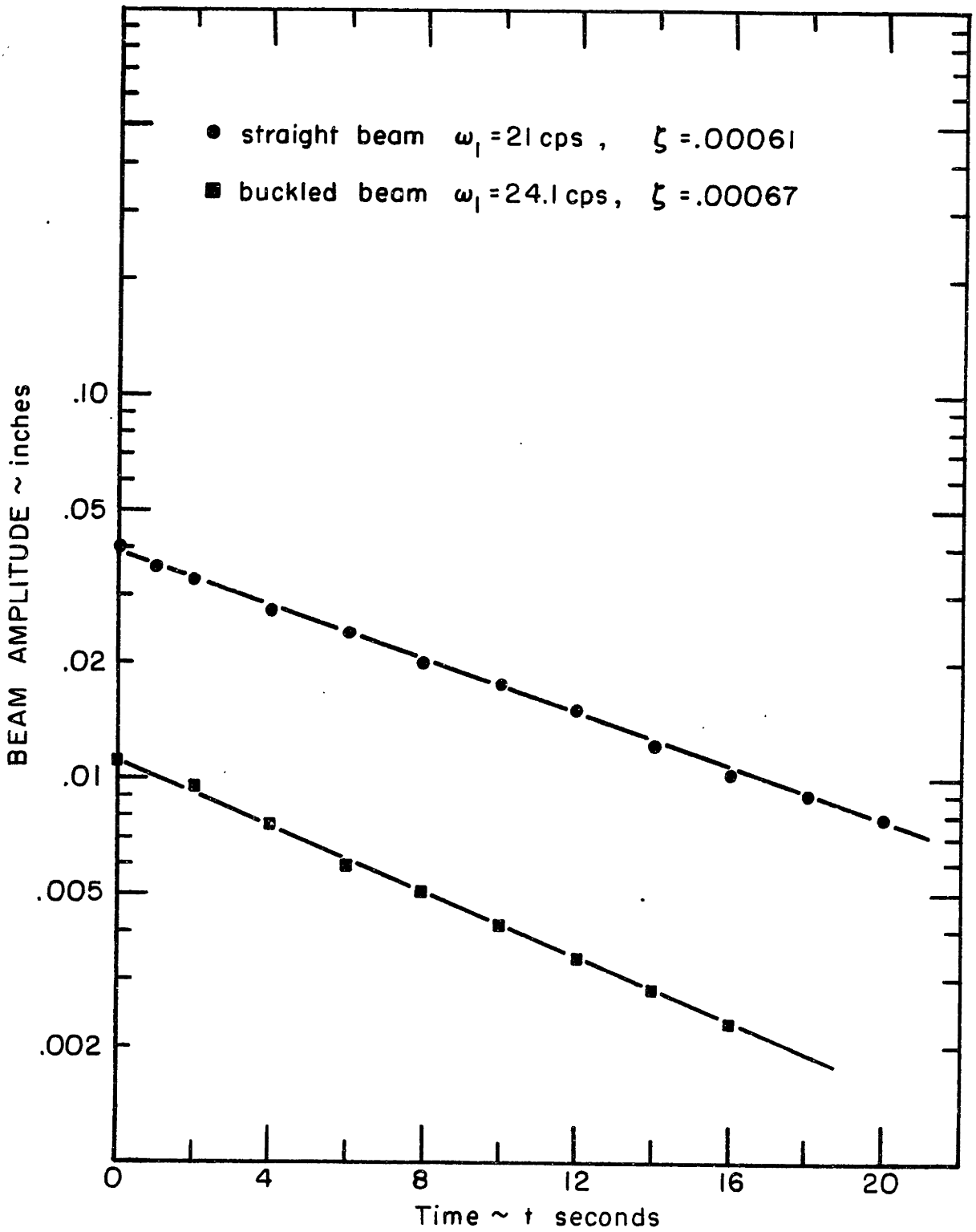
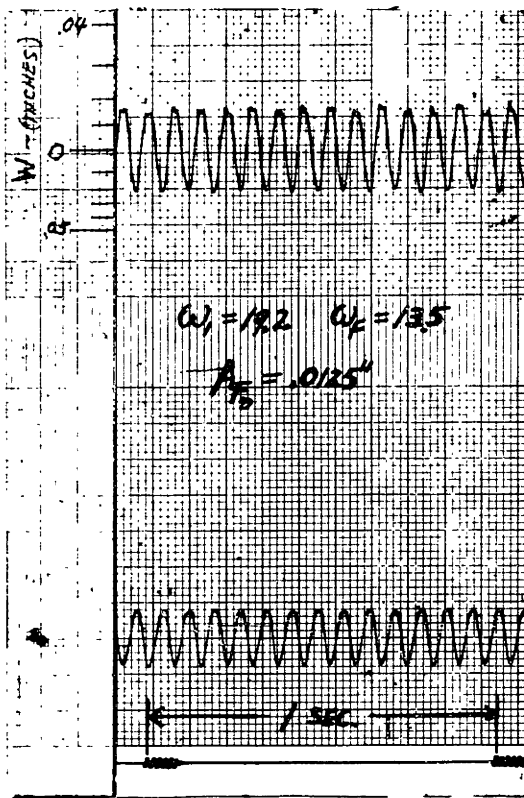
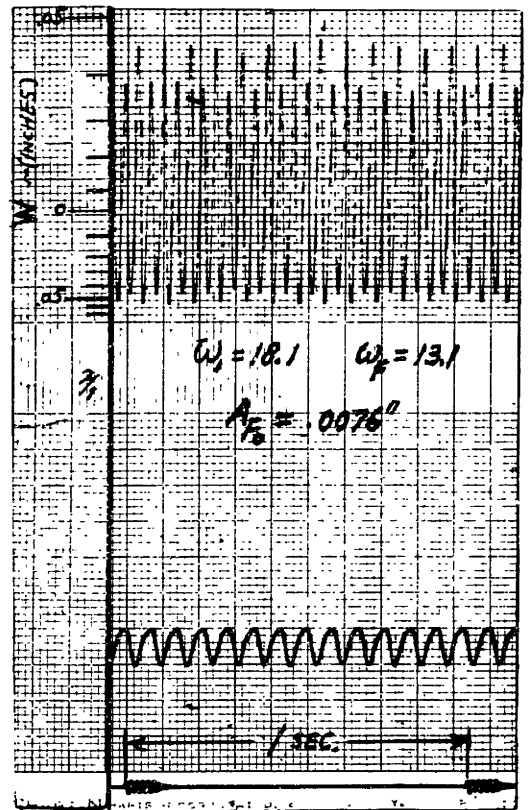


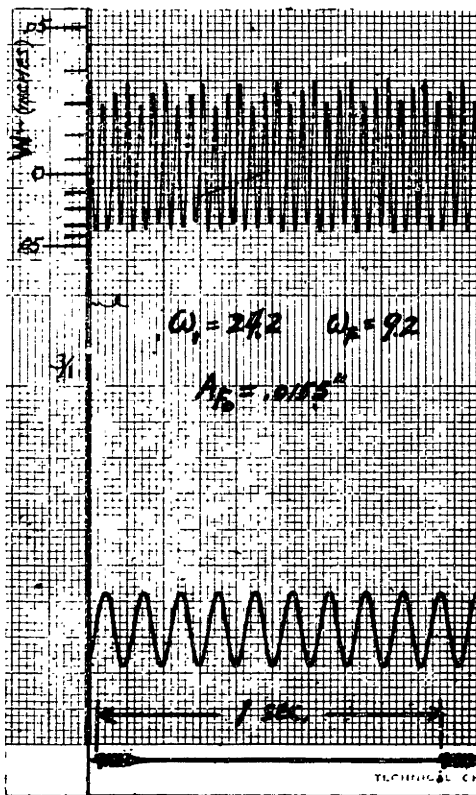
FIG.38 DAMPING COEFFICIENTS



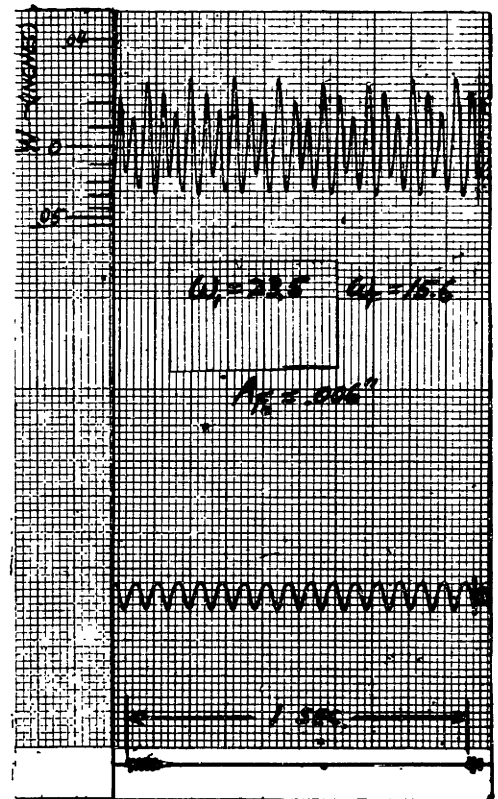
(a) SHM



(b) SPHM order 2

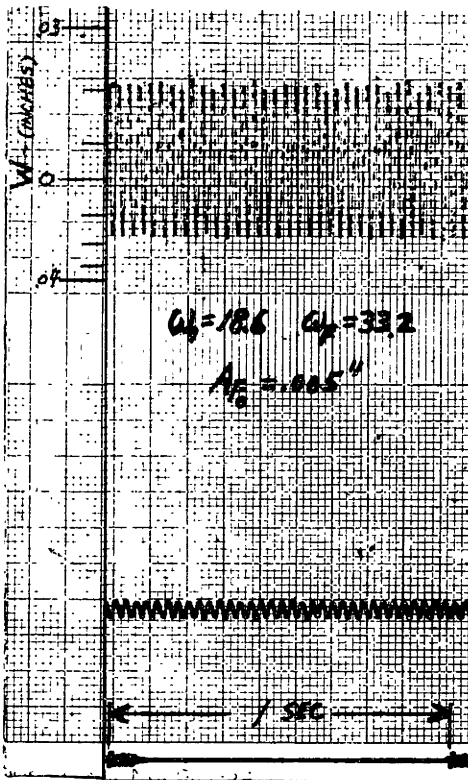


(c) SPHM order 3

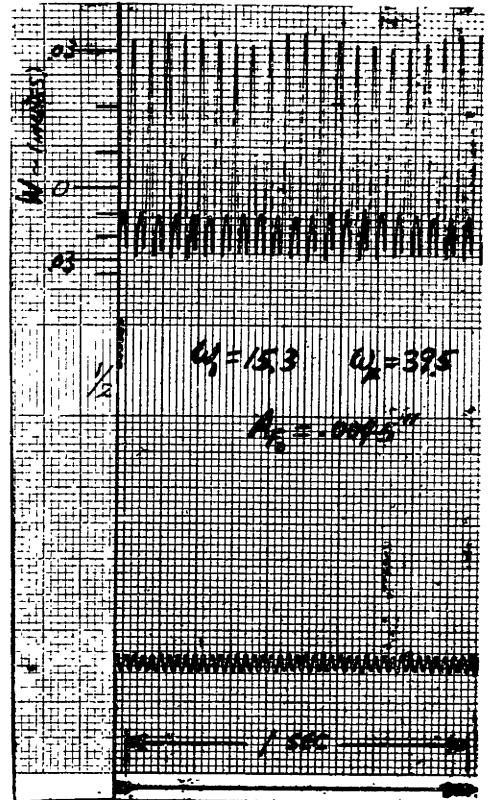


(d) SPHM Order 3/2

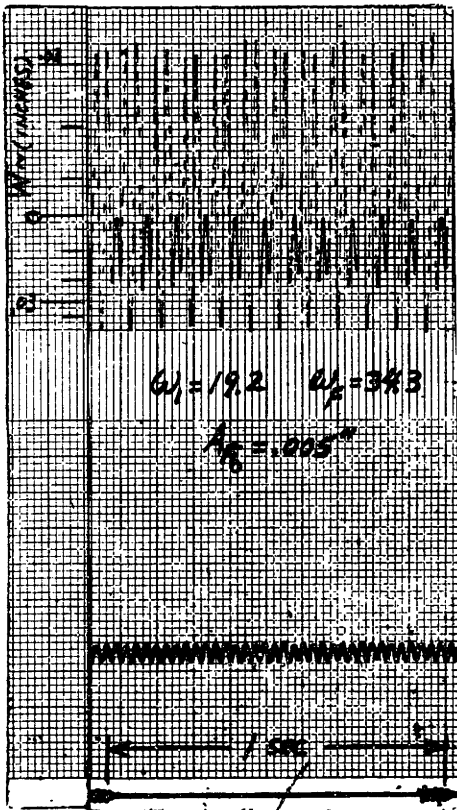
FIG. 39 EXPERIMENTAL SHM, SPHM, SBMH RESPONSE - STRAIGHT BEAM



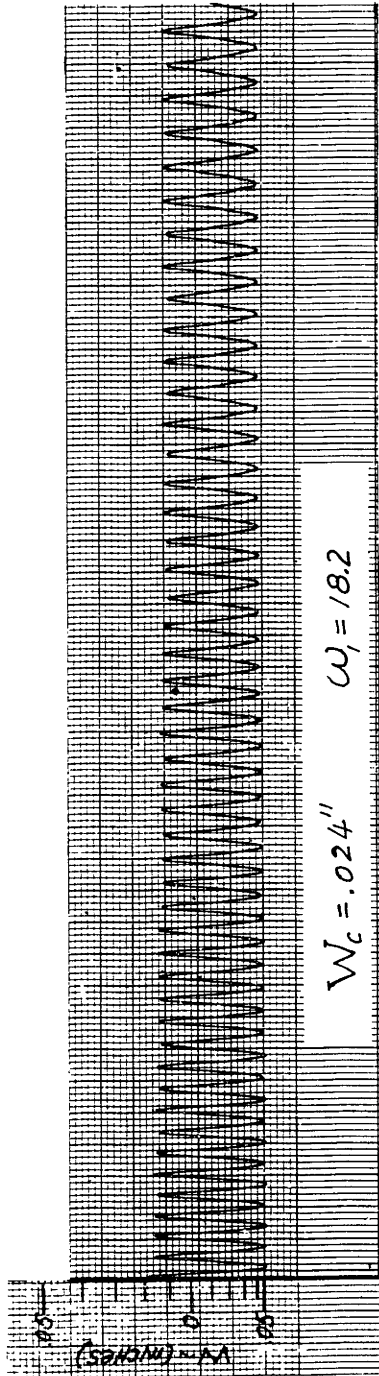
(e) SHM



(f) SBHM order $1/2$



(g) SBHM order $2/3$



(response continued)

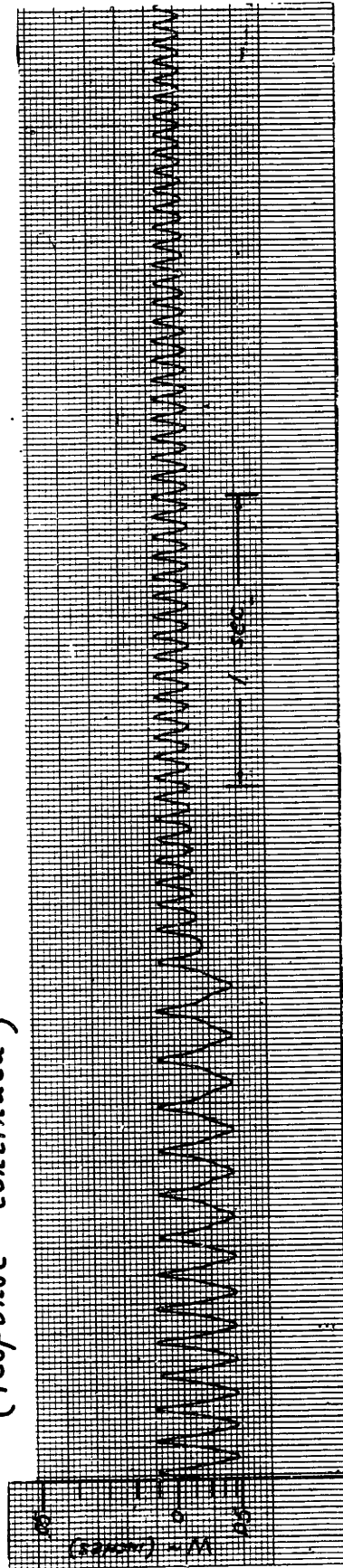
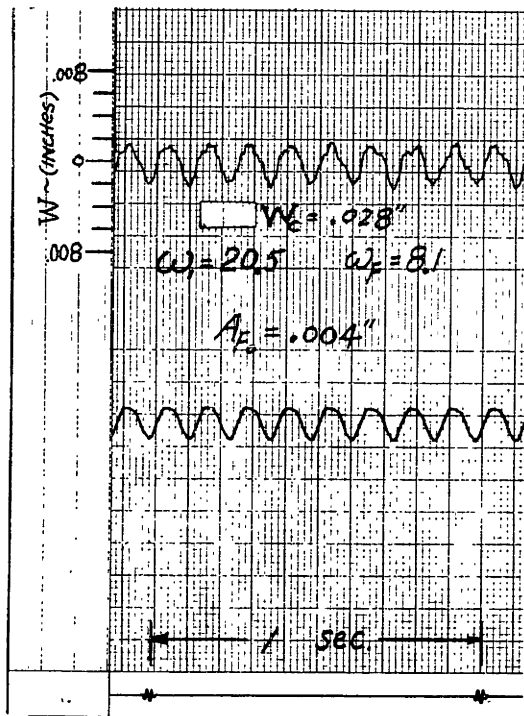
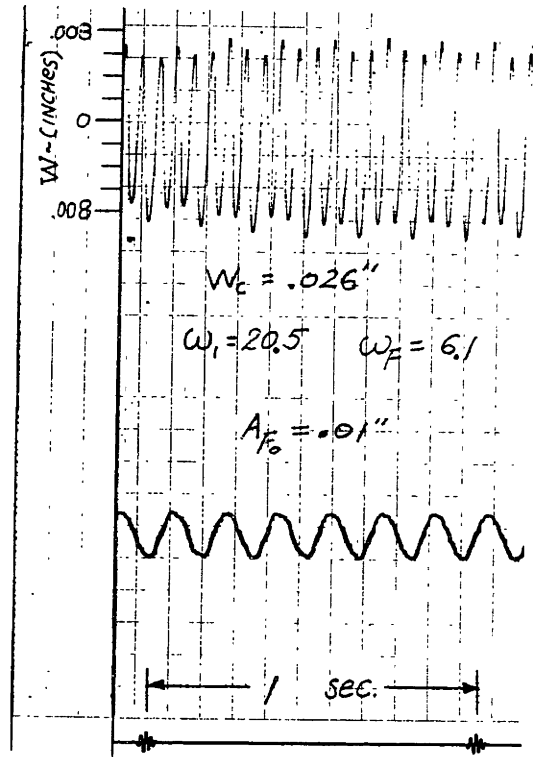


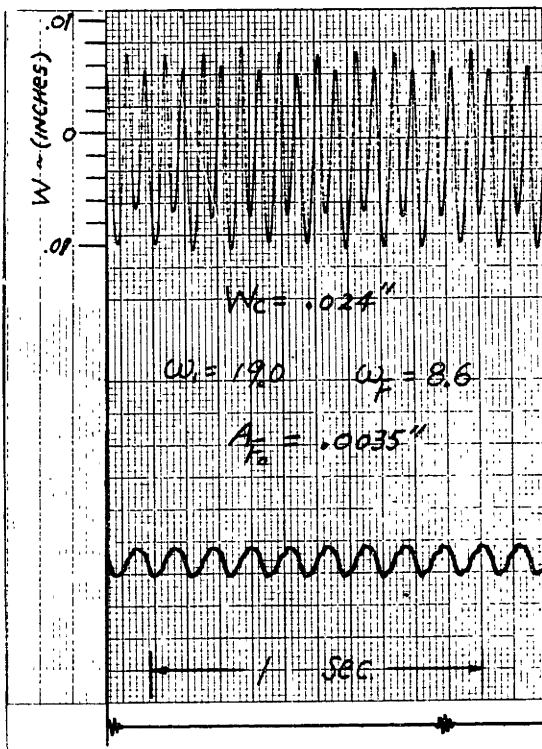
FIG. 40 EXPERIMENTAL FREE VIBRATION RESPONSE—BUCKLED BEAM



(a) SHM



(b) SPHM order 3



(c) SPHM order 2

FIG. 4/ EXPERIMENTAL SHM, SPHM RESPONSE - BUCKLED BEAM

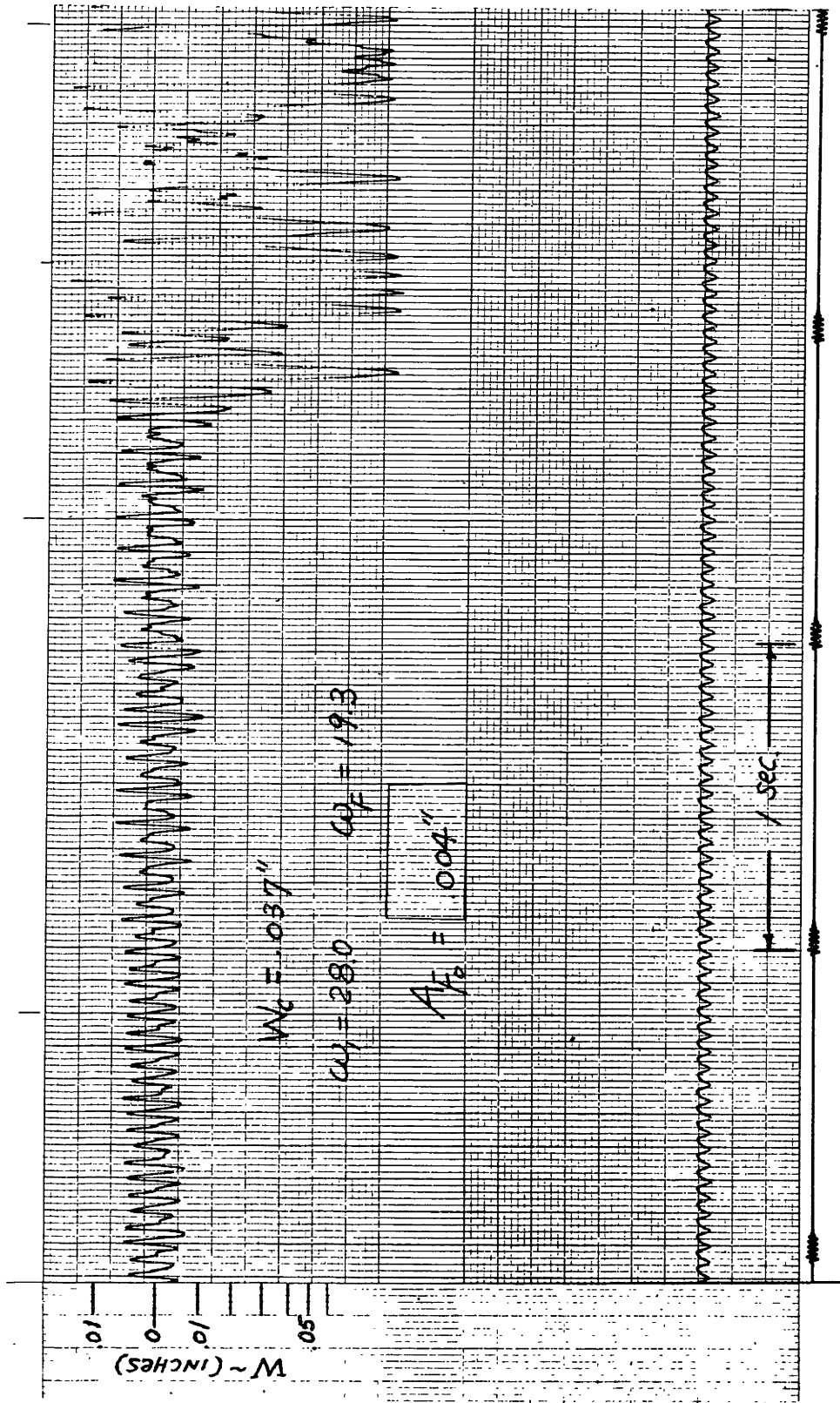


FIG. 42 EXPERIMENTAL SHM SNAP - THROUGH

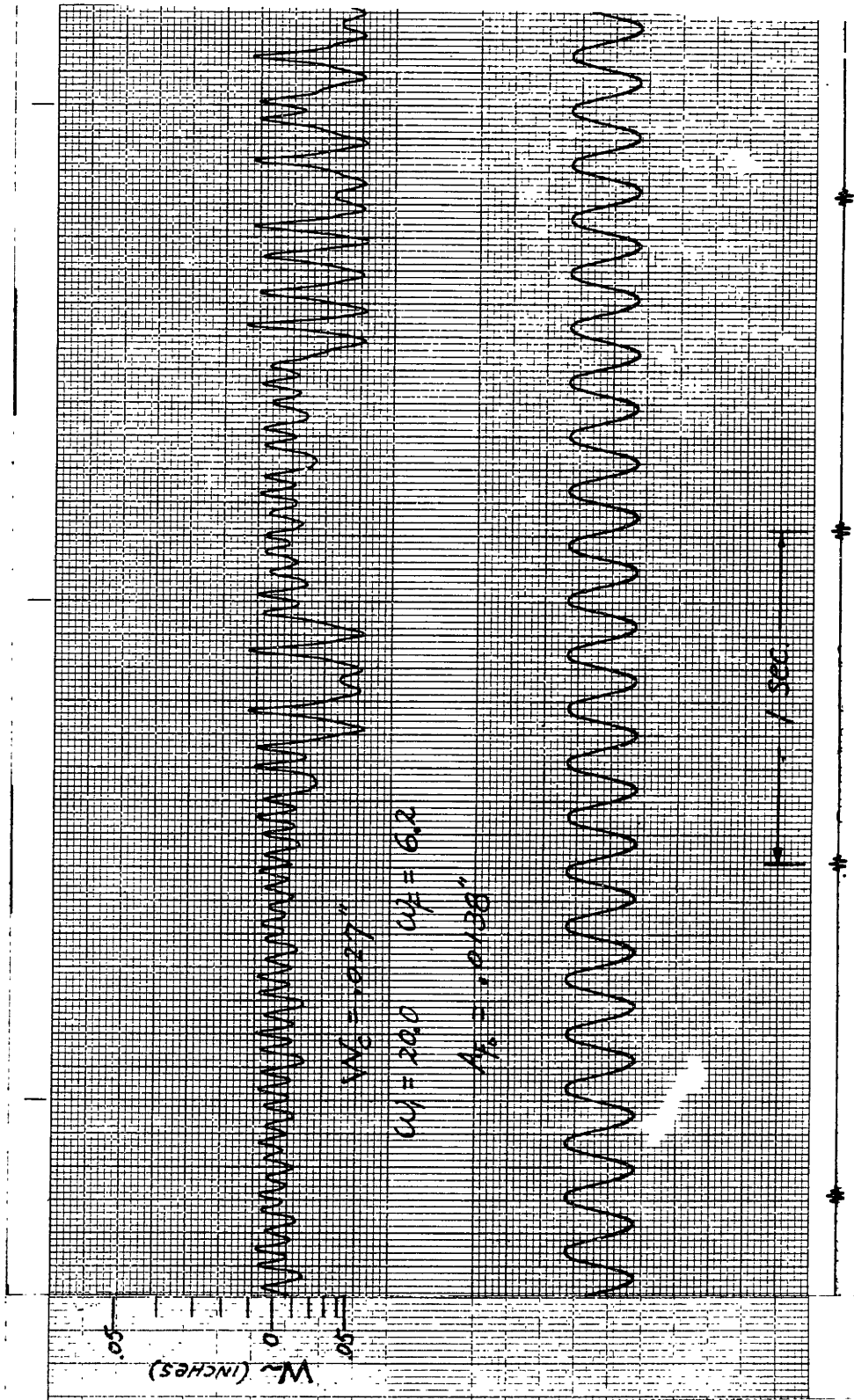


FIG. 43 EXPERIMENTAL SPHM 3 SNAP - THROUGH

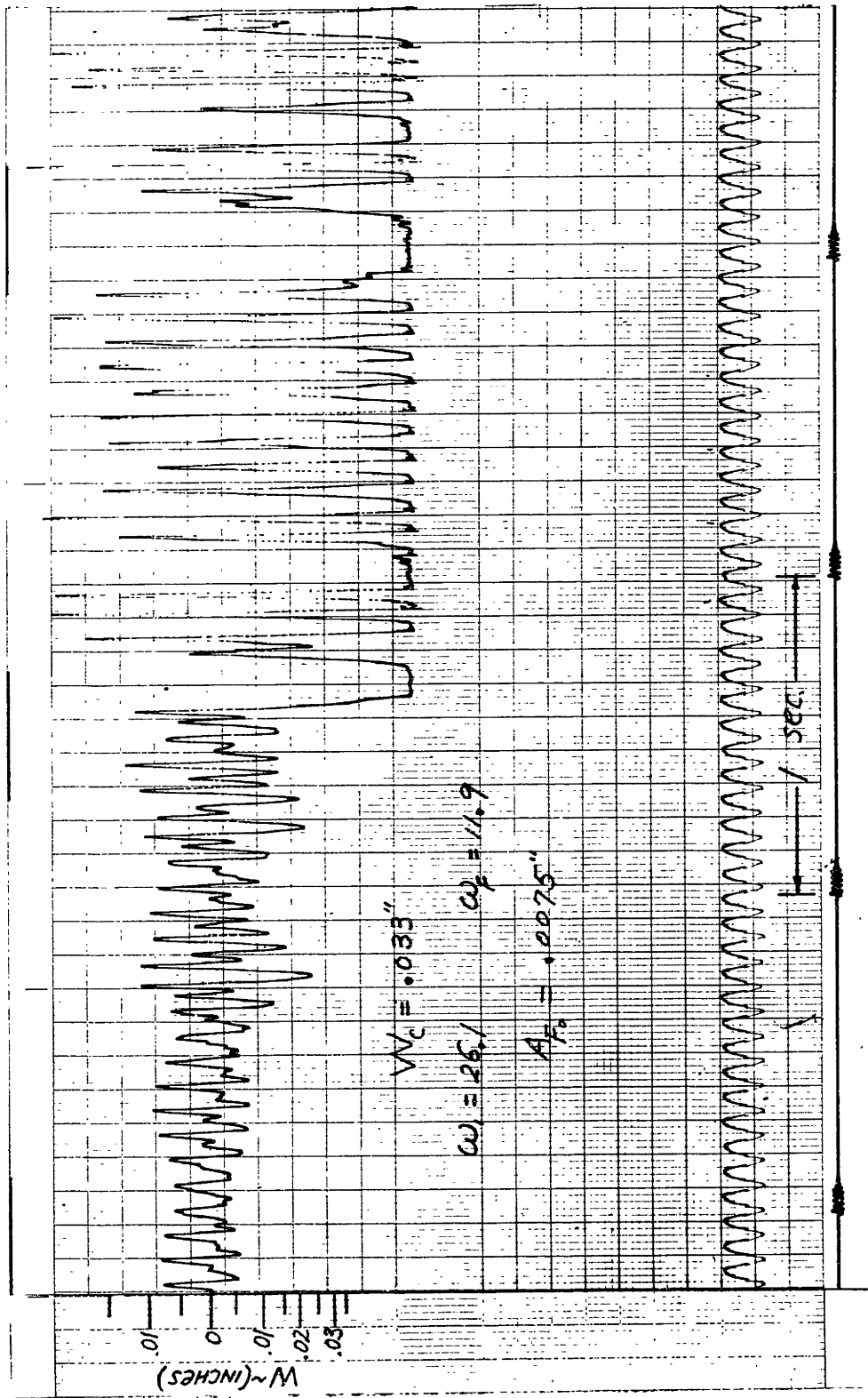


FIG. 44 EXPERIMENTAL SPHM 2 SNAP - THROUGH

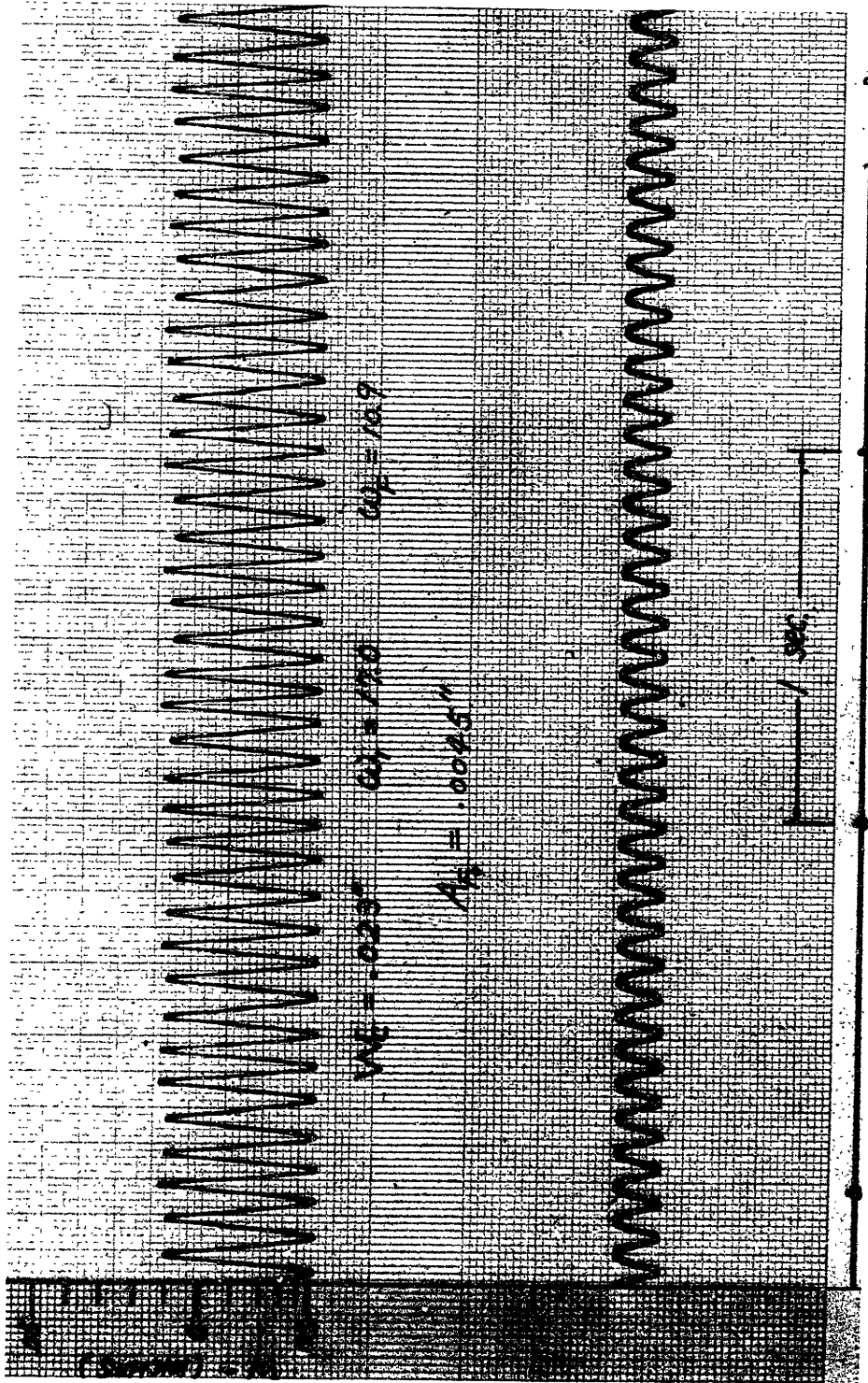


FIG. 45 EXPERIMENTAL CONTINUOUS SHM SNAP-THROUGH RESPONSE

BIOGRAPHY

The author was born in Hsinchu, Taiwan, the Republic of China, on April 11, 1940. He attended the elementary and high schools in that city. In September 1959, he entered the National Taiwan University, and in June 1963 received the degree of Bachelor of Science in Mechanical Engineering. Immediately after his graduation from the University, he served in the Chinese Ordnance Research Institute for a period of one year in fulfillment of his ROTC commitment, and was discharged from military service in July 1964.

The author came to the United States in September 1964 for graduate study at the Virginia Polytechnic Institute, and in September 1965 received the degree of Master of Science in Aerospace Engineering. From September 1965 to June 1966, he attended the Massachusetts Institute of Technology in candidacy for the degree of Doctor of Philosophy in Aeronautics and Astronautics. After that, he worked at the Dynatech Corporation and at the American Science and Engineering Co. He returned to the Massachusetts Institute of Technology to continue his graduate study in the Department of Aeronautics and Astronautics in September 1967.